UNIVERSITY OF HAWAII
LIBRARY
AUG 8 '58

The Philosophical Magazine

FIRST PUBLISHED IN 1798

A Journal of Theoretical Experimental and Applied Physics

Vol. 3 July 1958 No. 31
Eighth Series

£1 5s. 0d., plus postage
Annual Subscription £13 10s. 0d., payable in advance

ALERE FLAMMAM

Printed and Published by
TAYLOR & FRANCIS LTD
RED LION COURT, FLEET STREET, LONDON, E.C.4

THE PHILOSOPHICAL MAGAZINE

Editor

Professor N. F. MOTT, M.A., D.Sc., F.R.S.

Editorial Board

Sir LAWRENCE BRAGG, O.B.E., M.C., M.A., D.Sc., F.R.S.
Sir GEORGE THOMSON, M.A., D.Sc., F.R.S.
Professor A. M. TYNDALL, C.B.E., D.Sc., F.R.S.

AUTHORS wishing to submit papers for publication in the Journal should send manuscripts directly to the Publishers.

Manuscripts should be typed in *double* spacing on one side of quarto (8 × 10 in.) paper, and authors are urged to aim at absolute clarity of meaning and an attractive presentation of their texts.

References should be listed at the end in alphabetical order of authors and should be cited in the text in terms of author's name and date. Diagrams should normally be in Indian ink on white card, with lettering in soft pencil, the captions being typed on a separate sheet.

A leaflet giving detailed instructions to authors on the preparation of papers is available on request from the Publishers.

Authors are entitled to receive 25 offprints of a paper in the Journal free of charge, and additional offprints can be obtained from the Publishers.

The *Philosophical Magazine* and its companion journal, *Advances in Physics*, will accept papers for publication in experimental and theoretical physics. The *Philosophical Magazine* publishes contributions describing new results, letters to the editor and book reviews. *Advances in Physics* publishes articles surveying the present state of knowledge in any branch of the science in which recent progress has been made. The editors welcome contributions from overseas as well as from the United Kingdom, and papers may be published in English, French and German.

Thermal Expansion of Lead at Low Temperatures[†]

By P. N. Dheer[‡] and S. L. Surange[‡]
National Physical Laboratory, New Delhi

[Received March 25, 1958]

Abstract

Changes of length of a lead rod due to thermal expansion have been measured between 4·2°K and 10°K by a heterodyne-beat method in which the changes modify the capacity of a condenser in a resonant circuit. The variation with temperature of the Grüneisen constant γ was deduced; the accuracy was just insufficient to show up the jump in thermal expansion coefficient at the superconducting transition.

§ 1. Introduction

Little work has been done on the measurement of thermal expansion of solids at low temperatures in spite of the importance of such measurements in the study of the equation of state of solids. Most of the existing measurements are based on the use of optical interference, but because of the difficulty of using this principle at low temperatures and the small magnitude of the thermal expansion at low temperatures, large temperature intervals have usually been necessary to produce measurable changes of length. Thus expansion coefficients obtained in this way are averages and cannot exhibit the true temperature variation of this property. To obtain significant results at low temperatures it is necessary to use a technique capable of higher sensitivity than that of most of the previous methods so that relatively smaller temperature intervals can be used.

This paper describes a method in which the change in the length of the specimen caused by heating modifies the capacity of a parallel plate condenser and this in turn produces a measurable change in the resonant frequency of a high frequency circuit from which the change of length can be deduced. A similar method has been used by Bijl and Pullan (1954, 1955) for measuring thermal expansion of copper and aluminium. The present method has been used for measuring the thermal expansion of lead in the range 4–10°K. Lead was chosen because it has a low Debye temperature and is therefore expected to have a fairly high coefficient of expansion in this range. Also it is superconducting below 7·22°K and it was hoped that the measurements might show the small discontinuity in the expansion coefficient at the transition and the small volume changes when the transition occurs in a magnetic field, as predicted by thermodynamics. Unfortunately, the sensitivity did not prove adequate to show up the former effect and technical difficulties prevented any reliable measurements of the latter effect.

[†] Communicated by Dr. D. Shoenberg, F.R.S.

[‡] Now at the Royal Society Mond Laboratory, University of Cambridge.

A brief report of this work has already been published (Dheer and Surange 1957).

§ 2. Experimental Details

2.1. *The Cryostat Assembly*

The cryostat used in the measurements is shown in fig. 1. The fixed plate P_2 of the parallel plate condenser is rigidly attached to the top of a hermetically sealed brass can A through a glass metal seal G, which insulates it electrically from A. The specimen S, a cylinder 4·87 cm long and 0·7 cm diameter of spectroscopically pure lead (Johnson Matthey Ltd.) carries the other (earthed) condenser plate P_1, and is mounted on a copper base B supported in the can A by three thick tubes W of low thermal conductance (cupronickel). The two plates are adjusted to be in contact at room temperature and a gap of about $\frac{1}{3}$ mm is automatically obtained by the differential contraction of the specimen and the brass can A when the cryostat is cooled to liquid helium temperature. The electrical lead from P_2 is taken out of the cryostat through a shielding tube T_1 and a glass metal seal at the top of the cryostat.

Fig. 1

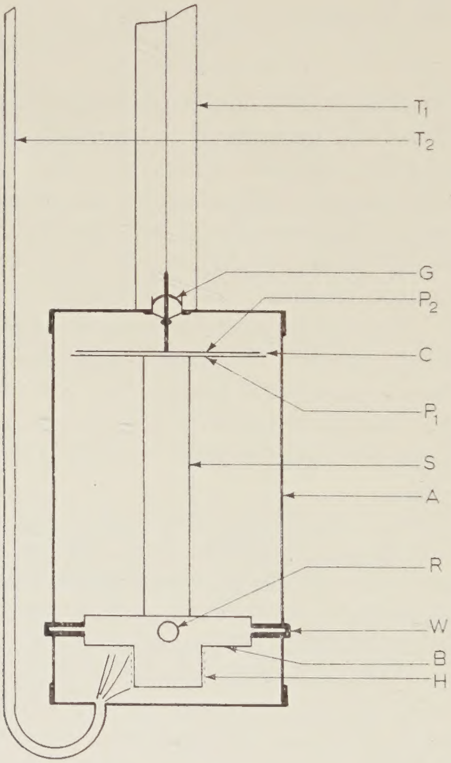

The Cryostat.

A carbon resistor R (Allen Bradley 12 ohm, $\frac{1}{2}$ watt) cemented inside a hole in the copper base B is used for measuring the temperature of the specimen. A search coil is wound on the specimen and serves to reveal the appearance of the superconducting state at the transition temperature by the abrupt fall in the magnetic permeability of the metal at this temperature. The electrical leads to the search coil, thermometer and heater are maintained in thermal contact with the helium bath by filling the metal capillary T_2 with beeswax over part of its length; the exit of the tube is sealed off with picein.

On filling the cryostat with liquid helium the air inside the can freezes out and the specimen cools in about an hour from its initial temperature (80°K) to 4·2°K by conduction through the tubes W. By passing current through the heater H, the specimen can be maintained at a temperature above the bath temperature, determined by the power input and the effective conductance between the specimen and the helium bath; the main contribution to this conductance comes from the tubes W. The time for attaining thermal equilibrium is of the order of a minute between 4°K and 10°K. The power required to raise the temperature from 4°K to 10°K was about 20 mw, which is not excessive from the point of view of evaporating liquid helium (an extra 5 cm^3/hour). There would probably be little difficulty in raising the temperature to about 50°K but the present experiments did not go above 10°K because of the rapidly falling sensitivity of the carbon thermometer used.

2.2. *Determination of Temperature*

For the measurement of the temperature of the specimen the resistance R of the carbon thermometer was measured by a Wheatstone bridge, and was assumed to vary with temperature according to the empirical equation of Clement and Quinnell (1952 a)

$$\log R + K/\log R = A + B/T \quad . \quad . \quad . \quad . \quad . \quad . \quad . \quad (1)$$

where K, A and B are constants, which were determined by calibration between 2·4°K and 4·2°K against the vapour pressure of liquid helium and at 7·22°K by noting the resistance at the superconducting transition temperature of lead. It may be mentioned that the superconducting transition in the measuring field of about 4 gauss was sharp (width of order 0·02°K), thus indicating that the lead was of good quality as regards superconductivity. Subsequently, it was verified by direct calibration against a gas thermometer that the temperatures determined in this way did not differ by more than 0·2° from the actual temperatures, in the range 4–10°K. The sensitivity of the bridge was such that temperature changes of order 10^{-3} degrees could be detected at about 10°K; at lower temperatures the sensitivity was greater.

2.3. *The Oscillator*

The frequency f of the oscillator was 7·5 Mc/sec; the Franklin oscillator circuit (see Ladner and Stoner 1950) was used for two reasons. First because it requires a very loose coupling between the resonant circuit and the valve maintaining circuit. This reduces the effect of valve capacitances, anode voltage, etc., on the oscillation frequency which is therefore determined almost entirely by the constants of the resonant circuit alone so that a high degree of frequency stability can be attained. Secondly, one side of the resonant circuit can be earthed and the design of the low temperature part of the apparatus is thereby much simplified. Also by earthing the plate P_1 of the condenser any possible radio-frequency coupling of the thermometer and heater with the oscillator circuit was eliminated.

To measure the change Δf in the frequency of the oscillator associated with the expansion of the specimen, the oscillator was allowed to beat against a similar oscillator of fixed frequency and the frequency of the audible beat note was determined by observing Lissajous figures produced by combining the beat note with an audiofrequency note from a calibrated oscillator. Changes in f were then read directly on the dial of the audio-oscillator. A typical measurement is illustrated in fig. 2 showing the variation of the audiofrequency as the specimen is heated from 4·2°K to 5·54°K. The heating current was switched on at B and the specimen attained a steady temperature at P (as indicated by the carbon thermometer) beyond which the oscillator is seen to follow its natural drift. At R the heating current was switched off and the specimen cooled to the bath temperature as is shown by the portion CD of the curve. The parts AB and CD were joined by a smooth curve and the mean change $\Delta f = XY$ was estimated from the graph. At least three such measurements were made for each temperature T; each point plotted in fig. 3 is the average of such measurements.

Figure 2 also illustrates the performance of the oscillator; it can be seen that the drift is of order 3 c/s per minute which may vary appreciably over several minutes, and the scatter of the points is presumably due to irregular changes of frequency of order 5 c/s. It is estimated that Δf can be determined to within about 10 c/s.

2.4. *Measurement of Changes of Length* Δl

The change of length Δl of the specimen is related to Δf by the relation

$$\Delta l = \frac{A}{2\pi f}\,\frac{C+C_0}{C^2}\,\Delta f \qquad . \; . \; . \; . \; . \; . \; . \; . \quad (2)$$

where A is the area and C the capacity of the parallel plate condenser and C_0 the rest of the capacity in the resonant circuit (capacities in E.S.U.). Calculation of Δl thus requires a knowledge not only of A and f which present no difficulty, but also of C and C_0. The capacity C_0 consists of C_1 (of order 15 cm), the capacity of the lead from the plate P_2 (fig. 1) of the condenser C with respect to the shielding tube T_1; C_2 (of order 10 cm) the capacity of a small calibrated condenser and C_3 (of order 18 cm) the self capacity of the coil which serves as the inductance of the resonant circuit together with the capacities introduced by the connecting wires.

The condenser C_2 is introduced deliberately to permit easy adjustment of the resonant frequency and for calibrating purposes. The various unknown capacities are measured as follows.

The capacity $C+C_1$ is determined by disconnecting the cryostat from the oscillator circuit and then measuring the amount by which the capacity of the variable condenser C_2 has to be increased in order to bring the oscillator frequency to its original value. Now without disturbing the condenser lead the can A is opened and assembled again after removing the specimen S and the plate P_1 so that C is removed from the resonant circuit. C_1 is now determined in the same way with the help of the variable condenser, and the difference of the two determinations gives C. The total capacity $C+C_0$ is determined by introducing a small change δC (about 0·5 cm) in it by varying C_2, and measuring the corresponding change δf in the oscillator frequency; it is easily seen that

Fig. 2

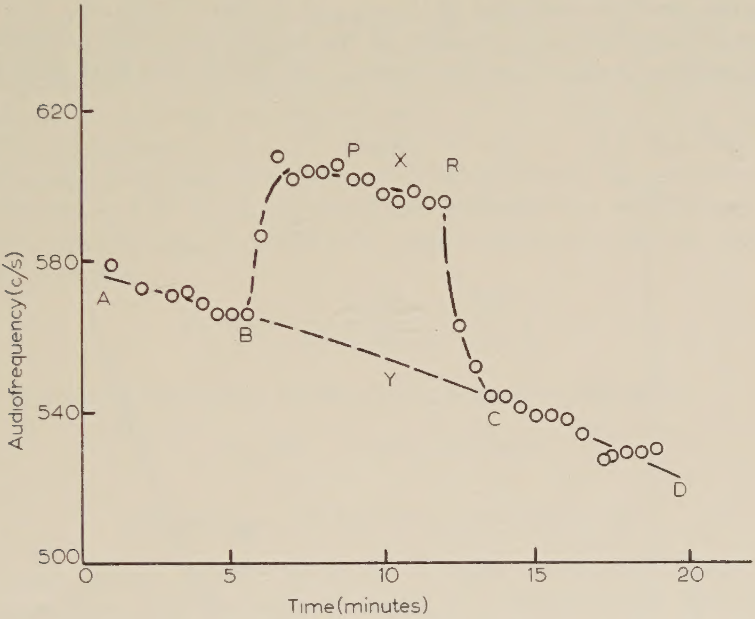

A typical measurement of Δf. The temperature at P is 5·54°K; $\Delta f = 47$ c/s which corresponds to $\Delta l/l = 0{\cdot}3\times 10^{-6}$.

$$C+C_0=\tfrac{1}{2}(\delta C/\delta f)f. \qquad (3)$$

Combining (2) and (3) we get

$$\Delta l=(A/4\pi C^2)(\delta C/\delta f)\Delta f. \qquad (4)$$

Substitution of the values of A(5·06 cm^2), C(15 cm) and $\delta C/\delta f$(1·6 × 10^{-5} cm sec) gives $\Delta l/l = 6{\cdot}5\times 10^{-9}\,\Delta f$. As already mentioned, Δf can be measured to within about 10 c/s so that the accuracy of our measurements of $\Delta l/l$ is about $0{\cdot}07 \times 10^{-6}$. This is comparable to that attained by Rubin *et al.* (1954) in their optical interference method.

The error introduced in the expansion measurements due to thermal strains in the supporting tubes W, produced by heating, was ascertained by a special experiment in which the can A was made much shorter, S was removed and P_2 was supported very close to P_1 which was attached directly to B. The total change in length produced by heating the base B up to 10°K was found to be 3×10^{-7} cm which is less than 1% of the expansion of the specimen from 4·2 to 10°K.

§ 3. Results

The temperature variation of $(l_T - l_{4{\cdot}20})/l$ is shown in fig. 3. For comparison the corresponding readings of McLennan *et al.* (1931) obtained by an optical lever method are also shown. It can be seen that their points

Fig. 3

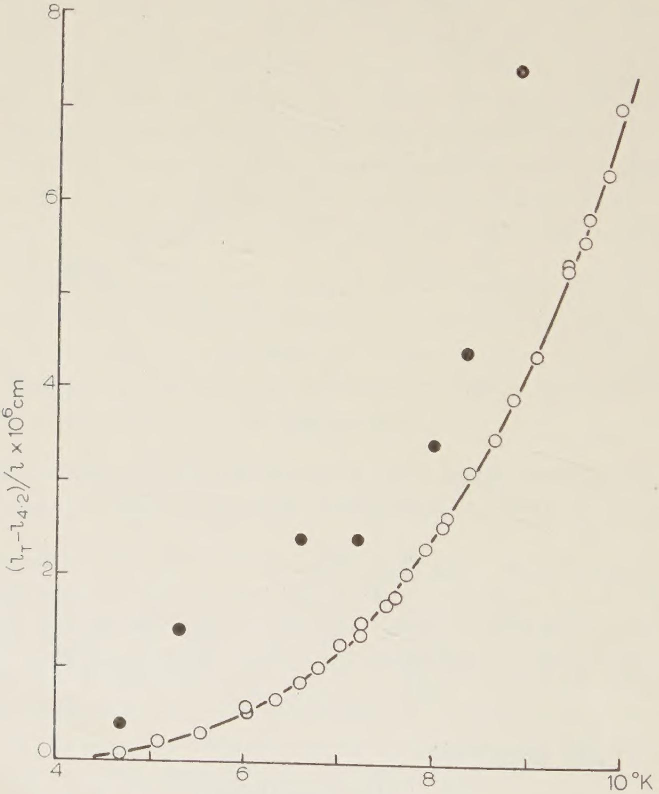

Temperature variation of $(l_T - l_{4{\cdot}20})/l$.

○ Our observations.
● McLennan *et al.*

show a greater scatter and lie rather above ours; the latter fact may perhaps be due to a negative expansion coefficient of the quartz supports used in their apparatus (see Bijl and Pullan 1955, p. 290).

An attempt was made to find out if the results show any discontinuity in the coefficient of linear thermal expansion β, at the superconducting transition temperature 7·22°K. Two cubic equations of the form

$$(l_T - l_{7\cdot 22})/l = A(T-7\cdot 22) + B(T-7\cdot 22)^2 + C(T-7\cdot 22)^3$$

were fitted separately to the data for $T < 7\cdot 22$°K and $T > 7\cdot 22$°K; $(l_T - l_{7\cdot 22})/l$ was determined by reading $(l_{7\cdot 22} - l_{4\cdot 20})/l$ from fig. 3 and subtracting it from the measured value $(l_T - l_{4\cdot 20})/l$. The difference in the two values of the coefficients A thus obtained gives the value of any possible discontinuity $\beta_n - \beta_s$ at 7·22°K. This procedure suggested a value $2\cdot 6 \times 10^{-7}$ deg^{-1}. Since, however, the value of $(l_{7\cdot 22} - l_{4\cdot 20})/l$ determined from the graph is subject to experimental error, it was desirable to check the reliability of the procedure and the above analysis was repeated for each of two extreme possible estimates of the value of $(l_{7\cdot 22} - l_{4\cdot 20})/l$; this led to estimates of -2×10^{-7} and 7×10^{-7} deg^{-1}. It is clear then that the data are not precise enough to establish definitely the existence of a discontinuity in β at T_c, though they are evidently not inconsistent with the discontinuity $\beta_n - \beta_s = 0\cdot 66 \times 10^{-7}$ deg^{-1} predicted by the thermodynamic formula

$$\beta_n - \beta_s = \frac{1}{12\pi}\left(\frac{\partial H_c}{\partial T}\right)_{T_c}\left(\frac{\partial H_c}{\partial p}\right)_{T_c}.$$

In the numerical evaluation of this formula we have assumed

$$(\partial H_c/\partial T)_{T_c} = 223 \text{ gauss deg}^{-1}$$

and

$$(\partial H_c/\partial p)_{T_c} = -11\cdot 1 \times 10^{-9} \text{ gauss dyne}^{-1}\text{ cm}^2$$

(Olsen and Rohrer 1957). Recently we have learnt that Lasarev and Sudovstov have reported measurements of a discontinuity in β to the Moscow Low Temperature conference (July 1957).

An attempt was also made to measure the changes of length when superconductivity is destroyed by a magnetic field. This could not be done directly because the frequency of the oscillator proved to be appreciably modified by the presence of a magnetic field, perhaps due to dimensional changes of magnetostrictive origin. To eliminate these effects the following indirect procedure was tried. First the change Δl_1 in the length of the specimen produced by heating it from a temperature T_1 below T_c to a temperature T_2 just above T_c was measured. The magnetic field was then switched on and the corresponding change Δl_2 was measured when the specimen is heated from T_1 to T_2; $(\Delta l_2 - \Delta l_1)/l$ gives the relative change of length $(l_s - l_n)/l$ associated with the transition at T_1. A few measurements made between 3 and 7°K agreed qualitatively with those of Olsen and Rohrer (1957) but showed a considerable scatter (up to a factor 2 in $\Delta l/l$ at any one temperature). Further investigation suggested that the results could not be regarded as reliable because different values of Δl_1 and Δl_2 were obtained even for $T_1 > T_c$; this indicated that the dimensional changes produced by the magnetic field do not remain constant as the temperature is varied. Evidently then the apparatus in its present form is not very suitable for magnetic measurements.

It is of interest to compare the results on thermal expansion with the Grüneisen relation. At low temperatures the electronic contribution to thermal expansion might be expected to be appreciable and the Grüneisen's formula can be expressed as (see, for instance, Bijl and Pullan 1955)

$$3\beta/\chi = \gamma_l C_l + \gamma_e C_e \quad . \quad . \quad . \quad . \quad . \quad . \quad . \quad . \quad . \quad (5)$$

where χ is the compressibility and C_l and C_e the lattice and electronic specific heats per unit volume respectively. In order to avoid complications due to the superconducting state, the measured values of $l_T - l_{4\cdot20s}$ were converted to $l_{Tn} - l_{4\cdot20n}$ by using Olsen and Rohrer's (1957) data on $l_s - l_n$; the subscripts s and n denote the superconducting and normal state respectively. The correction was 2% at 10°K and about 10% below 7°K. The method of least squares was then used to fit an equation of the form

$$(l_{Tn} - l_{4\cdot20n})/l = a(T - 4\cdot20) + b(T - 4\cdot20)^2 + c(T - 4\cdot20)^3 \quad . \quad . \quad (6)$$

to the data; the values $a = 16\cdot2 \times 10^{-8}$, $b = 4\cdot2 \times 10^{-8}$ and $c = 2\cdot4 \times 10^{-8}$ were found. The observed values departed from the relation (6) by at most 2×10^{-7} but were mostly within $0\cdot7 \times 10^{-7}$. Differentation of eqn. (6) gives

$$\beta \times 10^8 = 108\cdot5 - 52\cdot3T + 7\cdot2T^2. \quad . \quad . \quad . \quad . \quad . \quad (7)$$

This formula is of course valid only as an interpolation formula for the actual data and cannot be used reliably for extrapolation far outside the range 5–9°K. In order to assess the reliability of the method of determining β, a formula similar to (6) but containing an extra term in $(T - 4\cdot20)^4$ was also fitted to the data. Differentation gave

$$\beta \times 10^8 = -82\cdot3 + 41\cdot3T - 7\cdot6T^2 + 0\cdot76T^3 \quad . \quad . \quad . \quad . \quad (8)$$

which departs from (7) by at most about 3% except at the ends of the range (5°K and 10°K) where the departure reaches 7%. Thus (7) which is used in the discussion below is unlikely to be in error by more than a few per cent in the relevant range.

The second term on the right-hand side of eqn. (5) was estimated using the value $\gamma_e = 1\cdot7$ determined by Olsen and Rohrer (1957) and the value $C_e = 4\cdot20 \times 10^{-5}\,T$ cal deg^{-1} cm^{-3} as determined by Horowitz *et al.* (1952). We then have $\gamma_e C_e = 0\cdot71 \times 10^{-4}\,T$ cal deg^{-1} cm^{-3}; this is about 1% of $\gamma_l C_l$ at 10°K and becomes 5% at 4·5°K. C_l was determined by combining the measurements of Horowitz *et al.* in the liquid helium and liquid hydrogen range of temperatures and those of Clement and Quinnell (1952 b) near 7·22°K. Since there seem to be no reliable measurements of specific heat other than those mentioned it is rather difficult to assess the reliability of the estimate of C_l. This uncertainty is likely to be greatest (~5%) at 10°K because of the large range of interpolation involved (7° to 14°K). Values of γ_l calculated by taking the room temperature value of χ are plotted against T/θ in fig. 4; $\theta=96{\cdot}3$ is the Debye characteristic temperature of lead. Owing to the various uncertainties the values of γ_l are probably not reliable to better than 0·1 near 10°K and are quite uncertain

Fig. 4

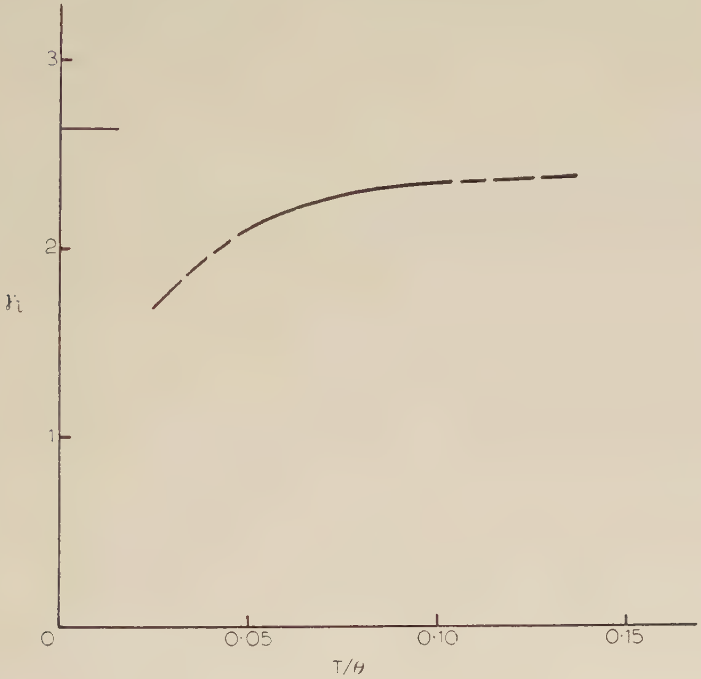

Variation of γ_l with T/θ. The room temperature value of $\gamma=2{\cdot}64$ is shown by a line on the axis of ordinates.

below 5°K where both β and C_l are becoming small and unreliable. It is satisfactory that γ_l seems to flatten off reasonably well towards the high temperature value of 2·64 but there is no evidence for a flattening off at very low temperatures such as might be expected in the region where the specific heat begins to follow a T^3 law (this is probably below 4·2°K). The fall off in γ_l from its high temperature value is similar for lead to that found by Bijl and Pullan (1955) for copper and aluminium but occurs at an appreciably lower value of T/θ.

ACKNOWLEDGMENTS

We wish to thank Dr. D. Shoenberg, F.R.S., who suggested this problem, for his advice and suggestions, Dr. K. G. Ramanathan for his advice and supervision during the course of this work and Dr. K. S. Krishnan, F.R.S., for his stimulating interest. We are also grateful to Mr. T. M. Srinivasan for his assistance with the measurements and Mr. B. S. Bhatnagar and Mr. R. K. Malhotra for regularly supplying us with liquid helium.

REFERENCES

BIJL, D., and PULLAN, H., 1954, *Phil. Mag.*, **45,** 290 ; 1955, *Physica*, **21,** 285.
CLEMENT, J. R., and QUINNELL, E. H., 1952 a, *Rev. sci. Instrum.*, **23,** 213 ; 1952 b, *Phys. Rev.*, **85,** 502.
DHEER, P. N., and SURANGE, S. L., 1957, *Proc. 5th Int. Conf. Low Temp. Phys. and Chem. Cof., Madison.*
HOROWITZ, M., SILVIDI, A. A., MALAKER, S. F., and DAUNT, J. G., 1952, *Phys. Rev.*, **88,** 1182.
LADNER, A. W., and STONER, C. R., 1950, *Short Wave Wireless Communication* (London : Chapman and Hall).
LASAREV, B. G., and SUDOVSOTV, A. I., 1957, *Proc. Low Temp. Conf., Moscow.*
McLENNAN, J. C., ALLEN, J. F., and WILHELM, J. O., 1931, *Trans. roy. Soc. Canad.*, **25,** III, 1.
OLSEN, J. L., and ROHRER, H., 1957, *Helv. Phys. Acta*, **30,** 49.
RUBIN, T., ALTMAN, H. W., and JOHNSTON, H. L., 1954, *J. Amer. chem. Soc.*, **76,** 5289.

On the Occurrence of Slip in Diamond†

By S. Tolansky, A. Halperin‡ and S. H. Emara
Royal Holloway College, Englefield Green, Surrey

[Received March 29, 1958]

Abstract

Linear discontinuities strictly in (1, 1, 1) planes have been observed on the natural octahedral faces of a diamond. The lines are studied optically. The characteristics of the lines suggest that they originate in slip which could well have occurred while the diamond was still growing and presumably hot. The slip hypothesis is the only reasonable one which accounts for the observed characteristics of the lines.

§ 1. Introduction

Diamonds are known to give good cleavages in octahedral planes. It is, however, not possible to induce slip in diamond by application of shearing stresses, at least not at room temperature.

Not much is known about the behaviour of diamond at high temperatures. Silicon and germanium crystals which have the diamond structure are also brittle at room temperatures. At higher temperatures, however, both silicon and germanium become ductile. Slip bands have been observed on germanium crystals deformed at temperatures about 500°c and for silicon about 900°c (Gallagher 1952, Maddin and Chen 1954). These temperatures are about two-thirds of the way to the melting points of the corresponding crystals. Diamond therefore might possibly be expected to slip at high temperatures, which in this case might well be above 2000°c. Experiments with diamonds at such high temperatures would be formidably difficult, and in any case diamond is not stable at ordinary pressures at these temperatures (Robertson *et al.* 1934, 1936).

In the present paper observations are reported on some growth features on diamond faces which seem to imply that the diamond concerned might well have been deformed plastically, presumably then at a high temperature.

§ 2. Observations

The type of linear discontinuity observed here appears to be relatively rare in diamond. Nevertheless we have observed it on six diamonds out of many hundreds investigated. One diamond showed the linear discontinuities under consideration arranged in such a way that it made their nature fairly clear. Our work has been concentrated mainly on this specimen which was investigated in detail. This stone was an almost perfect octahedron weighing 1·2 carats. Some 50 line markings were observed on 6 of the 8 faces of the octahedron (the other 2 faces did not show any). All the lines were oriented strictly parallel to octahedral planes of the crystal. Moreover, many of the lines could be traced continuously from one face to the neighbouring faces in such a way as to define a plane which in all cases was parallel to octahedral planes. A photograph (×30) of one of the faces of the octahedron is shown in fig. 1, Pl. 28. The discontinuity lines will be shown later with much higher magnifications. Rows of growth trigons are seen and their centres are just on the lines, as if strung on them.

---

† Communicated by the Authors.

‡ While on study leave. Present address: Department of Physics, The Hebrew University, Jerusalem

An overall view on the orientation of the lines in general, and of their interrelation is given by fig. 2, Pl. 29. This shows a photograph of a cardboard model of the crystal made by combining the photomicrographs of all the 8 faces of the octahedron. The octahedral planes defined by the lines continue across the crystal and can clearly be fixed, as seen on the photograph.

Figure 3, Pl. 29 shows part of a line using higher magnification (×600). It shows clearly how smaller trigons are centred on the lines. The dark bold curved lines *below* the row of trigons are edges of growth sheets which emerged from the lower part of the crystal, below the picture spreading upwards, and stopped at the row of trigons. Figure 4, Pl. 30 shows (×600) triple lines with only about 5 microns separating the individual lines. Again the smaller trigons are centred on one or another of the three lines.

The topography of the surface in the neighbourhood of the lines is revealed by fig. 5, Pl. 30 and fig 6, Pl. 31. Figure 5 is a multiple-beam interferogram (×250) taken across one of the lines. Clearly they are regions of discontinuity. On approaching the row of trigons from the lower part of the picture there is a sharp discontinuous drop from the level of the surface. On approaching the line from the upper side, i.e. from the direction which the apexes of the row of trigons are directed, there is a gradual fall until the line is reached when again an abrupt fall occurs. Figure 6 (×350) shows a high-dispersion multiple-beam interferogram. It can again be seen clearly how growth waves, which emerged from below, were stopped by a barricade formed by the bases of the trigons, while the growth waves on the upper part are seen to penetrate *between* the apexes of the trigons, so that a gradual slope is formed. Growth from this direction often crosses the discontinuity itself as can be seen in fig. 6 and in figs. 3 and 4.

2.1. *Step Heights*

These were measured by the methods of light-profile microscopy (Tolansky 1952) and by multiple-beam interferometry, the latter including fringes of equal chromatic order (Tolansky 1948). The results may be summed as follows : (i) The steps across the discontinuity lines range in height from nearly zero up to about 2 microns, and differ not only from line to line, but also *along* the same line. In some cases the step changes progressively along the line. Usually, however, it changes irregularly along a given line. (ii) Without exception, all the steps are directed in such a way that the lower level is towards the bases of the trigons, while the upper level is towards the apexes of the trigons.

In the following discussion it will be shown how the characteristics of the observed discontinuous lines can be accounted for by assuming that the discontinuity lines originate from disturbances in the growth of the crystal as a result of *slip*, which we postulate could have occurred while the crystal was still in the process of growth, and presumably at a fairly high temperature.

§ 3. DISCUSSION

The high concentration of *growth* trigons along the lines implies that the observed discontinuities on the surfaces of the crystal were created whilst it was still growing.

Misfits bound to octahedral planes of the crystal can be one of the following : (*a*) cracks in the crystal, (*b*) twinnings, (*c*) stacking fault surfaces, (*d*) slip in the crystal. We do of course reject outright the unfounded suggestion of Omar and Kenawi (1957) that the growth trigons might be etch figures. We consider (*d*) is the most probable explanation here for the following reasons.

(*a*) *Cracks :* It is most improbable that the crystal could have cracked in so many places, in some cases into slices only a few microns thick (see fig. 4), and then subsequently healed itself to such a perfection, for the crystal as a whole is a good crystal. The possibility of cracks can be discarded in this case.

(*b*) *Twinning :* It is known that the orientation of trigons changes on crossing a twinning boundary. As this does not happen when crossing a discontinuity line on our crystal, it can be concluded that the parts of the crystal on both sides of the discontinuity line are not twinned relative to each other. We have further proved this point by etching experiments. We have already firmly established in this laboratory that a diamond etched lightly in hot potassium nitrate produces small triangular etch pits oriented *opposite* to growth trigons. Such etch pits reverse over a twin boundary. Figure 7, Pl. 31 shows the etch pits (×400) over one of our discontinuity lines. Etching is preferentially stronger on the line itself, but the main issue clearly seen is the identical orientation of the pits on either side. There remains to be considered the possibility that submicroscopic thin twinned slices divide both parts of the crystal. From our microscopic observations it is certain that the thickness of any such postulated twinned regions, if present, is always less than 0·2 microns. It seems most unreasonable to assume that the crystal contains so many twinned regions that for some strange reason are all limited to submicroscopic thicknesses. The only reasonable limit would then be that all of them are monolayer twins, but this is effectively identical with stacking fault surfaces, which are to be discussed now.

(*c*) and (*d*) *Stacking fault surfaces and slip :* It is more difficult to decide between these two possibilities for slip with a slip vector which corresponds to a translation from perfect lattice points to twin-lattice points will leave the crystal with a stacking fault surface. The only difference between (*c*) and (*d*) in this case would be in the process of formation of the stacking fault surface. Under (*c*) we understand the case in which the stacking fault surface was formed during the process of growth on the surface of the growing crystal ; while under (*d*) we consider slip of the growing crystal by the action of shearing forces parallel to its octahedral planes.

On assumption (*c*) the distribution of the stacking fault surfaces in the crystal (some of them pass the crystal near its centre) would imply that some of them were formed in very early stages of growth of the crystal. It would then be very difficult to explain how these stacking fault surfaces extended in such a perfect way right out to the external faces of the crystal. This, further, seems much more improbable when taking into account the excellent crystallographic form of the octahedron shape of the crystal.

Only the assumption of the occurrence of slip remains, and it will be shown now how this assumption accounts for the observed characteristics of the lines in a reasonably satisfactory manner.

We assume that slip occurred when the crystal was still growing, and that the observed discontinuities are the result of *overgrowth* on the surfaces of the already slipped crystal. Nothing can therefore be said as to the original number of slip lines nor about the original amount of slip. On a growing crystal surface, perfect slip in integral lattice multiples would supply perfect steps for rapid advance of growth layers. Slip would soon be overgrown leaving no traces on the surface of the original slip lines.

However, an *imperfect* step due to slip, which is not an integral of the lattice, would form a misfit boundary on the surface, at which growth emerging from either side would be retarded. Trigons should then be expected to be formed along the slip lines where the lattice was disturbed (Halperin 1954).

Once the row of trigons has started to form, an asymetry is introduced with regard to the advance of the oncoming growth layers (from both sides) towards the slip line. On one side, where the bases of the trigons are arranged parallel to the slip line, they form a barricade at which growth is necessarily stopped. On the other side, however, growth layers are free to penetrate between the apexes of the trigons and stop just on the slip line. Thus, no matter what the direction and height of the slip step originally, the side towards the apexes of the trigons will grow much faster and will finally become the higher level of the step, indeed exactly as we find experimentally. Growth, although retarded in rate, might continue across the step, and the final step height at a given point on the slip line will then depend on the degree of perfection of the step at that point as well as on other factors, which will determine the rate of penetration of growth across the slip line. This could account for the irregular changes in the step heights found along a given line. A striking example (×375) is shown in fig. 8, Pl. 32 where a part of the upper slip line is completely covered by growth which penetrated across the slip lines, for the line is partially obliterated over some half of the picture, reappearing at the sides.

It follows from these considerations that the rows of trigons formed along the slip lines actually preserve them by preventing growth on one side from reaching the lines. This is also demonstrated (×160) in fig. 9, Pl. 32. Here, besides the four slip lines with trigons along them, a trace of another appears in the centre. The impression is given of a line obliterated everywhere except where there is a trigon, and here a small part of it has been preserved in the neighbourhood of this trigon. Attention is incidently drawn to the fact that lines of the character analysed here have already long been reported in the literature. Sutton (1928) mentions observations of rows of trigons 'strung' on straight lines and gives a description of such a line in one of his sketches. Williams (1932) also shows microphotographs which also demonstrate this phenomenon.

It seems then that a slip hypothesis is the only one which accounts for the characteristics of the observed lines. This is also in accord with theoretical considerations (Jaswon and Dove 1955) by which potentially glissile dislocations exist in diamond, but are rendered immobile at low temperatures.

We cannot of course even make a guess as to the temperature at which the conjectured slip would have taken place.

ACKNOWLEDGMENTS

One of us (A. H.) wishes to express his thanks to the Hebrew University, Jerusalem, for granting a study leave and to the Humanitarian Trust, London, for a Fellowship which enabled him to carry out the work.

REFERENCES

GALLAGHER, C. J., 1952, *Phys. Rev.*, **88,** 721.

HALPERIN, A., 1954, *Proc. phys. Soc. Lond.* B, **67**, 538.

JASWON, M. A., and DOVE, D. B., 1955, *Acta cryst.*, **8,** 806.

MADDIN, R., and CHEN, N. K., 1954, *Progr. Metal Phys.*, **5,** 91.

OMAR, M., and KENAWI, M., 1957, *Phil. Mag.*, **48,** 859.

ROBERTSON, R., FOX, J. J., and MARTIN, A. E., 1934, *Phil. Trans. roy. Soc.* A, **232**, 453 ; 1936, *Proc. roy. Soc.* A, **157**, 579.

SUTTON, J. R., 1928, *Diamond* (London : Thomas Murry).

TOLANSKY, S., 1948, *Multiple-beam Interferometry of Surfaces and Films* (Oxford : Clarendon Press) ; 1952, *Z. Elektrochem.*, **56**, 263.

WILLIAMS, A. F., 1932, *Genesis of Diamond* (London : Benn).

Suppression Effect of the Ionization Produced by Electron–Positron Pairs of Extremely High Energy†

By JUNJI IWADARE‡
H. H. Wills Physics Laboratory, University of Bristol

[Received April 16, 1958]

ABSTRACT

The ionization produced by 27 electron–positron pairs with energies between 80 and 2000 BeV, recorded in stacks of emulsion, has been studied. The energies were estimated from the development of the soft cascades in an auxiliary experiment. Suppression of the ionization near the origin of the pairs was observed, and the measured effect found to be in satisfactory agreement with theoretical predictions. The observations allow an independent estimate of the energy of the individual pair from the initial ionization, and for pairs with energy ~ 300 BeV most of the values thus obtained were in good accord with those from other methods.

There is a correlation between the suppression effect and the disparity in energy of the two particles of a pair. This suggests that ionization measurements give information similar to that provided by studies of the relative scattering of the two components of a pair.

§ 1. INTRODUCTION

IT was suggested by King (private communication, see Perkins 1955), and later confirmed by Perkins (1955) that the ionization of electron–positron pairs of extremely high energy is reduced near their origin, owing to the destructive interference of the electromagnetic fields of two particles with equal charges opposite in sign.

Roughly speaking, a pair with energy $\geqslant 100$ BeV is created with an opening angle $\leqslant 2\times 10^{-5}$ radians (Borsellino 1953), and travels a few hundred microns before the separation between the electron and positron exceeds the maximum effective impact parameter for the ionization of atoms (10^{-6}–10^{-7} cm). For smaller values of the separation, the ionization is smaller than that for two independent, singly charged, particles, each of minimum ionization.

Although the detailed features of the suppression effect may depend on the actual mechanisms of ionization, and grain-formation in emulsion, an application of the simple theory of energy loss is known to give a fairly satisfactory account of this phenomenon. In addition to its theoretical implications, the phenomenon has some practical importance, for it provides a useful method of determining the energy of pairs of extremely great energy—up to 10^9–10^{10} ev.

---

† Communicated by Professor C. F. Powell, F.R.S.

‡ On leave of absence from Research Institute for Fundamental Physics, Kyoto University, Kyoto, Japan.

There are several established methods of determining the energy of electron pairs. At low energies ($\leqslant 10$ Bev), the measurements either of the multiple scattering, or of opening angle have proved useful. For much higher energies, however ($\geqslant 100$ Bev), it is difficult to obtain reliable information by such measurements. For this energy region, a method of energy determination has been developed by Pinkau, based on measuring the lateral spread of the ensuing soft cascade (Pinkau 1956, 1957). This method has the advantage that several observations can be made at different depths in the cascade, so that errors due to statistical fluctuations are reduced. The disadvantages of the method are that it is laborious; and also that the development of the cascade has to be observed over several radiation units. This imposes certain geometrical restrictions which are important when the original pairs convert near the edge of an emulsion stack. On the other hand, the method based on the decrease of ionization near the origin of a pair requires only simple measurements over the first few millimetres of the track.

At the present time, one of the great difficulties associated with the investigations of interactions of extremely high energy is the rarity of suitable events: it is therefore very important to extract as much information as possible from the limited material available. Because of the importance of the investigations, it seemed desirable to study the ionizations near the origin of pairs in more detail, and to establish a practicable method of energy determination based on this phenomenon.

In the present paper, we shall show that the theory of the effect is in satisfactory agreement with observation, and that ionization measurements near the origin of pairs can be used to make reliable energy estimates on pairs with energy $\geqslant 300$ Bev.

§ 2. THEORY

The effect has been studied theoretically by several authors. The calculation of the ionization produced by a pair has been performed by Cudakov (1955), using a classical treatment. Yekutieli (1957), and Mito and Ezawa (1957), made improvements in the calculations by using a semi-classical treatment, whilst Burkhardt (1957) attempted to elucidate the quantum theoretical aspects of the phenomenon: Burkhardt calculated the ionization produced by a wave-packet representing the motion of the two particles moving with a small angle of divergence. His wave-packet has a spread corresponding to the distribution of the opening angle of the pair produced by a photon of a definite energy. He showed, that a quantum-mechanical calculation of this type, gives the same results as the simple classical treatments. In the following, we shall use the results given by Mito and Ezawa, because it predicts a reasonable asymptotic value of the ionization for large separations of the particles.

Following Mito and Ezawa, the ionization produced by a pair, g_{pair} with a separation b (in cm) may be written

$$g_{\text{pair}} \propto -\frac{dE}{dx} = \frac{4\pi N e^4}{m_e c^2}\left[2Q - 2K_0\left(\nu_p \frac{b}{c}\right)\right], \quad . \quad . \quad . \quad (2.1)$$

where
$$\nu_p=\left[\frac{4\pi Ne^2}{m_e}\right]^{1/2}=7{\cdot}36\times10^{16}\,\mathrm{sec}^{-1}. \quad . \quad . \quad . \quad . \quad (2.2)$$

is the plasma frequency of the emulsion, and $K_0(x)$ the modified Bessel function with imaginary argument, which has the asymptotic form, $K_0(x)\xrightarrow[x\to0]{}0$. Q is a parameter which represents the magnitude of the ionization produced by a single relativistic particle, (g_0). It is defined by the relation
$$Q=\tfrac{1}{2}\log\left(4c^2/\gamma^2\nu_p{}^2r_0{}^2\right),\quad g_0=(4\pi Ne^4/m_ec^2)Q, \quad . \quad . \quad . \quad (2.3)$$

where $\gamma=1{\cdot}781$ (Euler constant). r_0 represents the minimum value of the impact parameter, and is left as a free parameter. The ratio of the ionization produced by a pair, to that of a single charge relativistic particle, is then given by:
$$2R\equiv\frac{g_{\text{pair}}}{g_0}=2\left[1-\frac{1}{Q}K_0\left(\frac{\nu_pb}{c}\right)\right]. \quad . \quad . \quad . \quad . \quad (2.4)$$

To evaluate the magnitude of the suppression effect, we must know the separation, b, between the two components of the pair, which is determined by two principal factors: (i) the initial angle of divergence of the pair at creation: and, (ii) the subsequent multiple scattering of the electron and positron.

The effect of multiple scattering has been evaluated by many authors (Scott 1949). We shall consider two particles of a pair, with energies E_+ and E_- (total energy $E_t=E_++E_-$) respectively, travelling initially parallel from a common origin. Then the distribution of the spatial separation b' between them will be
$$P(b')\,db'\,d\phi'=\frac{1}{\pi\sigma^2}\exp\left(-\frac{b'^2}{\sigma^2}\right)b'\,db'\,d\phi' \quad (\phi':\ \text{azimuthal angle}) \quad (2.5)$$

at distance d from the origin. Here σ is the root mean square separation:
$$\sigma=\sqrt{\langle b'^2\rangle}=\sqrt{\frac{1}{3}}\sqrt{\left(\frac{1}{E_+{}^2}+\frac{1}{E_-{}^2}\right)}\,d^{3/2}\lambda, \quad . \quad . \quad . \quad (2.6)$$

and λ is defined in terms of the conventional scattering constant K for angles between successive chords:
$$\lambda=\sqrt{\frac{3\pi}{2}}\,K. \quad . \quad . \quad . \quad . \quad . \quad . \quad . \quad . \quad . \quad (2.7)$$

We adopt for K a value corresponding to small cell sizes,
$$K=4{\cdot}71\,\text{MeV cm}^{-1/2}. \quad . \quad . \quad . \quad . \quad . \quad . \quad . \quad (2.8)$$

On the other hand, the most probable initial opening angle for the pair is estimated by Borsellino (1953), as
$$\omega_p=\frac{4m_ec^2}{E_t}\,\phi\left(\frac{E_\pm}{E_t}\right). \quad . \quad . \quad . \quad . \quad . \quad . \quad . \quad (2.9)$$

The corresponding separation b'', at a distance d from the origin, due only to the initial opening angle, is then given by

$$b'' = \frac{4m_e c^2}{E_t}\left[d\,\phi\left(\frac{E_\pm}{E_t}\right)\right]. \qquad (2.10)$$

Here $\phi(x)$ is a slowly varying function of x with a minimum $\phi(\tfrac{1}{2}) = 1$.

Comparing the dependence of (2.6) and (2.10) on d, we see that the effect of multiple scattering predominates after a certain distance, $\bar{d}$, given by

$$\bar{d} \sim 6\frac{(m_e c^2)^2}{\lambda^2} \sim 150\,\mu, \qquad (2.11)$$

for the case of the equi-partition of energy ($E_+ = E_- = \tfrac{1}{2}E_t$). If the energy is not equally distributed between the two components, this distance will be reduced by a factor

$$\frac{8\phi^2(E_\pm/E_t)}{(1/E_+^{\,2} + 1/E_-^{\,2})E_t^2}. \qquad (2.12)$$

Therefore, in the cases of practical interest, where the suppression is appreciable over distances $\geqslant 200\,\mu$, both effects contribute almost equal amounts to the relative separation of the pair.

To reduce the expression (2.4) to a more practical form, we note that in the region of appreciable suppression ($K_0 \geqslant 0{\cdot}7$), we can approximate (2·4) by

$$R \sim \left[1 + \frac{1}{Q}\log\frac{\nu_p \gamma b}{2c}\right] = \left[1 + \frac{1}{Q}\log 2{\cdot}18 \times 10^6 b\right] \quad (b \text{ in cm}). \qquad (2.13)$$

Then, substituting the expression

$$b^2 = b''^2 + b'^2 - 2b''b'\cos\phi' \qquad (2.14)$$

for b, and averaging over b' and ϕ' with the distribution (2.5) we obtain the formula

$$R \sim \left[1 + \frac{1}{Q}\log 2{\cdot}18 \times 10^6\, b'' - \frac{1}{2Q}\,Ei\left(-\frac{b''^2}{\sigma^2}\right)\right]. \qquad (2.15)$$

where $Ei(x)$ is the exponential integral. The second term in the bracket is due to the initial opening angle, and the third term represents the additional effect of scattering. In the limit of small and large scattering, (2.15) reduces to:

$$R \sim \left[1 + \frac{1}{Q}\log\frac{\nu_p \gamma b''}{2c}\right] = \left[1 + \frac{1}{Q}\log 2{\cdot}18 \times 10^6\, b''\right], \qquad (2.16)$$

and

$$R \sim \left[1 + \frac{1}{Q}\log\frac{\nu_p \gamma^{1/2}\sigma}{2c}\right] = \left[1 + \frac{1}{Q}\log 1{\cdot}63 \times 10^6 \sigma\right], \qquad (2.17)$$

respectively. It can be seen in the last formula that the effective separation due to the scattering is $\sigma\gamma^{-1/2}$ instead of σ.

So far we have assumed that we know the individual energies of the two electrons of a pair. In most cases, however, we know only the total energy of both electrons as estimated by cascade measurements. We shall therefore next evaluate the average ionization of pairs with a given total energy, taking into account the distribution in values of the disparity. For the distribution we shall use that resulting from the assumption of complete screening given by a conventional theory. The average value of $\log \sigma$ will then be

$$\overline{\log \sigma} = \overline{\log (\text{const. } (1/E_+^{\,2} + 1/E_-^{\,2})^{1/2})} = \log (\text{const. } \sqrt{2}(2/E_{\text{eff}})), \qquad (2.18)$$

where E_{eff} has been calculated by averaging over all values of the disparity up to a minimum value $(E_+/E_t) = 0{\cdot}05$, and is given by

$$E_{\text{eff}} = 0{\cdot}56\, E_t. \qquad . \quad . \quad . \quad . \quad . \quad . \quad . \quad . \qquad (2.19)$$

Concerning the term containing b'', we do not know the precise variation of this quantity with the disparity. For the sake of simplicity, we shall assume that the new effective value of b'' (eqn. (2.10)), can be obtained by replacing E_t by E_{eff} in the factor outside the bracket, and setting ϕ equal to unity.

Thus, in order to take into account the effect of the disparity in energies of the two electrons of the pair, we simply replace E_t in eqn. (2.15) for the equi-partition case, by the quantity $E_{\text{eff}} = 0{\cdot}56 E_t$. In the following we shall call the case as the average partition case.

§ 3. Experimental Procedure

The electron–positron pairs on which measurements were made were found in five large emulsion stacks, in systematic scanning for electromagnetic cascades. The total energy of each pair was determined from the development of the cascade in a separate experiment by Pinkau (private communication). In the present experiment, pairs with energy $\geqslant 80$ Bev and length per emulsion > 1 mm were used. We believe that the selection of the events is unbiased. Twenty-seven pairs were found satisfying the above conditions. The energy region covered by these pairs ranges from 80 to 2000 Bev.

The ionization of each pair was determined by using the gap and blob method of Fowler and Perkins (1956). A gap-length of $4{\cdot}16\,\mu$ was used, and, in addition, to reduce the statistical fluctuations, gap-lengths of $2{\cdot}50\,\mu$ and $5{\cdot}83\,\mu$ were also used on the first $750\,\mu$ of the track of the pair.

The ionization parameter, g, an dits statistical fluctuation were evaluated using the formula

$$g = \frac{1}{l} \log \frac{B}{H_l},$$

$$\frac{\Delta g}{g} = \frac{1}{\sqrt{(N_l)} \log B/H_l},$$

where B is the blob density: H_l is the gap density for gaps $> l$, and N_l is the total number of gaps counted. In those cases where the ionization was determined using two different gap-lengths, the ionization was evaluated for each gap-length, and the weighted mean was adopted with the smaller one of the two statistical errors.

The ionization was compared with the plateau ionization g_0 of a singly charged particle in the region of the emulsion near the origin of the pair. The magnitude of the ionization was normalized in units of g_0, after being corrected for depth effects, when it was necessary.

The mean value of g_0 is $0{\cdot}52\,\mu^{-1}$, and although it varies from stack to stack and from plate to plate, the variation is not by more than a factor 2. There is no indication in the present experiments of any dependence of the suppression effect on the degree of development.

While the total energy of the pair, was commonly obtained from studies of the resulting cascade, significant measurements of relative scattering were also sometimes possible†. In such cases, the correlation between the disparity in energy of the electrons and the magnitude of the suppression effect was investigated.

§ 4. EXPERIMENTAL RESULTS

Since the existence of the suppression effect has been established by the pioneer work of D.H. Perkins, it appears important at the present stage to study its energy dependence, and to test the possibility of using it to determine the energy of electron-pairs.

4.1

Figure 1 shows the plot of the mean ionization against the distance from the pair-origin: the sample has been divided into three energy groups:

Group I	17 pairs	$80 \leqslant E_c \leqslant 200$ Bev,	$\bar{E}_c = 138$ Bev,	$E_{\text{eff}} = 77$ Bev,
Group II	6 pairs	$300 \leqslant E_c \leqslant 500$ Bev,	$\bar{E}_c = 425$ Bev,	$E_{\text{eff}} = 240$ Bev,
Group III	4 pairs	$1000 \leqslant E_c \leqslant 2000$ Bev,	$\bar{E}_c = 1450$ Bev,	$E_{\text{eff}} = 810$ Bev,

E_c is the total energy of the pair determined by cascade measurements; and $\bar{E}_c$ is the geometrical mean of E_c's. The solid and dotted lines in fig. 1 represent the theoretical prediction given by (2.15), calculated for the equipartition case, and the average partition case. It should be noted that the intersection of the asymptotic curve given by (2.15) with the axis $R = 1$ is determined by the value of ν_p, whereas the slope of the curve is determined by the choice of Q. The best overall fit to the data, using the dotted curves is given by choosing the parameter $Q = 6{\cdot}45$, corresponding to a value of $r_0 = 7{\cdot}2 \times 10^{-10}$ cm. The form of the theoretical curves is in qualitative agreement with the observed variation in grain density. There is an obvious dependence of the suppression effect on energy as expected.

Group III is worthy of special consideration, in view of the high energies involved. We have four pairs in this energy group. Three of them (1, 2 and 3) were found in the core of a jet of type 0 + 4p, together with a pair of lower energy, ~ 30 Bev. The total energy of pairs in the jet was found to be 5000 Bev by cascade measurements: considerations of the relative angle of divergence of the pairs give the energy estimates quoted in fig. 1, under the assumption that they have originated from two π^0-mesons in the core of the jet. The fourth pair occurs at the origin of a purely electromagnetic cascade produced by a photon which originates outside the stack. The energy was determined rather unambiguously by cascade measurements. The observed ionization suggests deviations from a monotonic behaviour, but they are nevertheless attributed to statistical fluctuations. It should be emphasized that no appreciable deviation of the asymptotic value of the ionization from twice plateau value was observed.

---

† The author is indebted to Mr. K. Pinkau for his kindness in making the results of his measurements available prior to publication.

Fig. 1

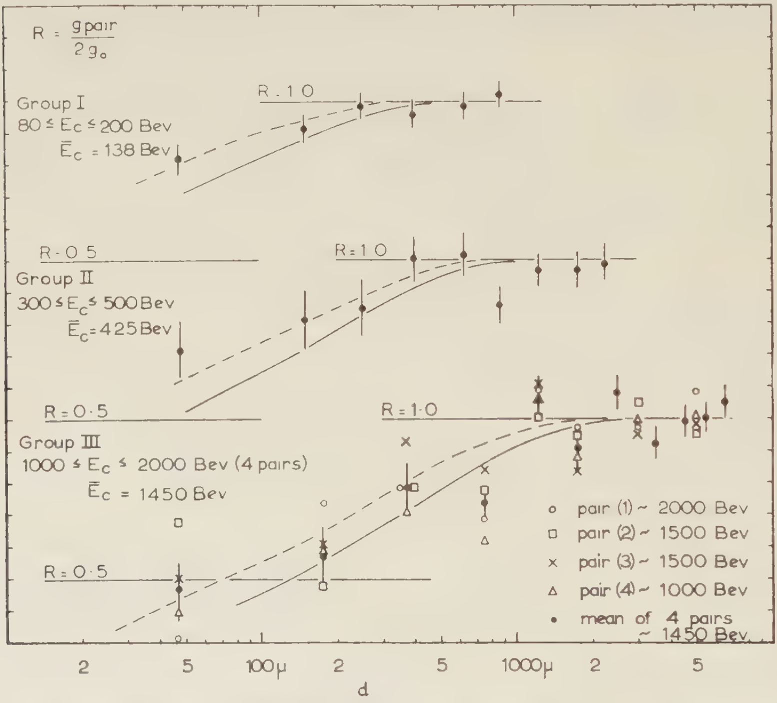

The ionization versus the distance from the pair origin. The solid and dotted lines are evaluated by (2.15) for the cases of the equi-partition and the average partition of the energy, respectively. For Group III the ionizations of the individual pairs are recorded together with the mean values.

4.2

On the basis of the agreement between the observations and theoretical predictions in the last section, it seems worthwhile to try to estimate the energy of pairs by ionization measurements near the origin. To this end, it would be preferable to deal with the average ionization up to certain distances rather than the variation of the ionization over these distances. The average ionization is plotted against total energy of the pairs in figs.

2 (*a*) and 2 (*b*). The solid and dotted curves represent the theoretical values as given by formula (2.15), for the equi-partition case and the average case, respectively. In averaging (2.15) a lower limit of the

Fig. 2 (*a*)

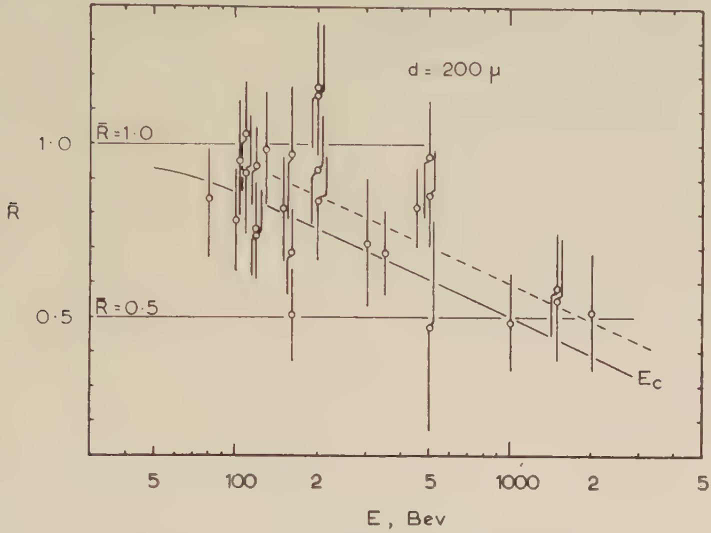

The average ionization up to 200 μ versus the total energy E_c estimated by cascade measurements. The solid and dotted lines are due to the theoretical prediction (2.15) corresponding to the equi-partition and average partition of energy.

Fig. 2 (*b*)

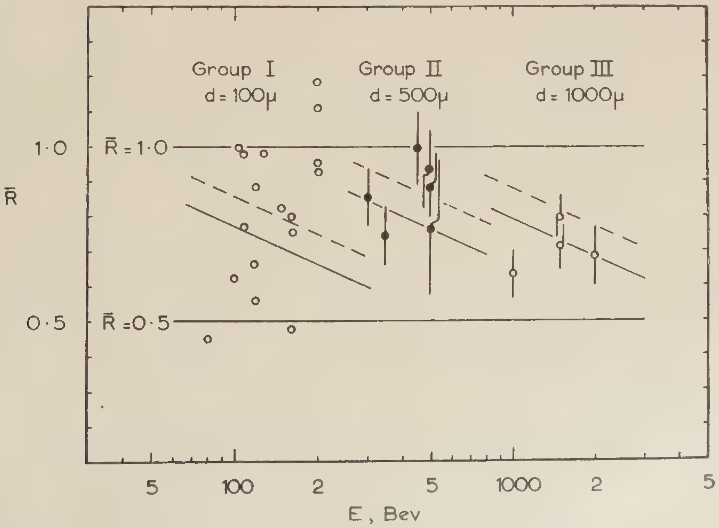

The average ionization up to 100 μ, 500 μ and 1000 μ. The solid and dotted curves represent the theoretical prediction (2.15).

distance was taken at $10\,\mu$ to avoid the false contributions from the portion too near the origin. Figure 2 (*a*) shows the average ionization up to $200\,\mu$ for all the pairs. In fig. 2 (*b*) various lengths are adopted for different energy groups; here also the agreement is satisfactory.

From these figures we can obtain the independent estimates of the energies of individual pairs, using the solid theoretical curves assuming equi-partition.

Fig. 3

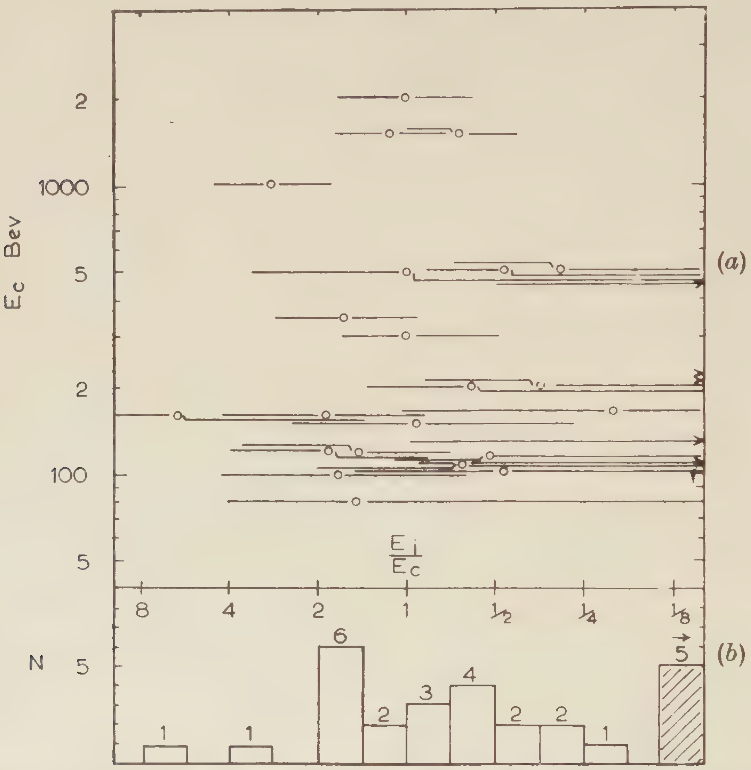

(*a*) The ratio of the energy estimated by ionization (E_i) to that estimated by cascade measurements (E_c) versus E_c. Arrow → means that the most probable estimate of E_i/E_c is outside the scale; > means that its upper limit is also outside the scale.

(*b*) The distribution of E_i/E_c. Five points fall outside the scale.

The energy values E_i estimated in this way are plotted in fig. 3 against the energy values E_c determined by cascade measurements. The average ionization over the distances $200\,\mu$, $500\,\mu$ and $1000\,\mu$ were used for groups I, II and III respectively. For several pairs in group I, no significant decrease of the ionization was observed, this being masked by large statistical fluctuations. For these cases we have shown only the upper limits of the energy estimates. In this figure arrow (→) indicates that the most probable value of E_i/E_c is outside the scale, and (>) means that even its upper limit is outside the scale. The histogram in fig. 3 (*b*) shows the distribution of the values E_i/E_c. E_i coincides with E_c within a factor 3, in 19 cases out of 27. Only one point falls in the region $E_i/E_c > 3$. The distribution has a spread of the order of a factor 3, in either direction, around the median value of $E_i/E_c \sim 0{\cdot}67$. This distribution seems too broad to be explained by statistical fluctuations in gap and blob densities. It suggests that there is some real fluctuation in the suppression effect itself. In fact, there are several conceivable causes of the fluctuation. Multiple scattering results in a distribution of the relative separation given by (2.5). There may also be an effect due to the fluctuation in the initial angle of divergence for a given total energy†. In addition to these there is a fluctuation due to the disparity in the energies of two particles of a pair. In § 2 we considered the average effect of the disparity in energy partition and found that the effective energy of the average pair is $E_{\text{eff}} \equiv 0{\cdot}56E_t$ instead of E_t. However, the disparity in the energy, and

Fig. 4

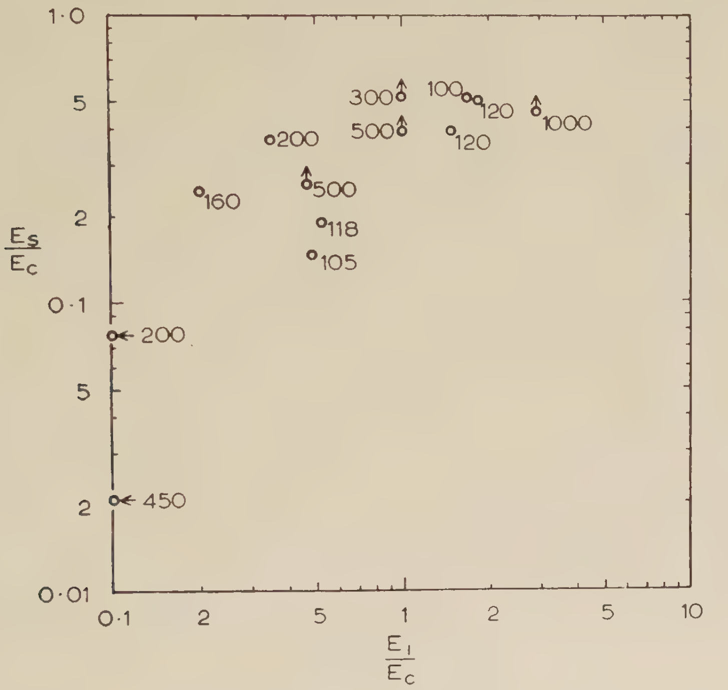

E_i/E_c *vs* E_s/E_c.
E_i = the energy estimated by ionization measurements ;
E_c = the energy estimated by cascade measurements ;
E_s = the energy estimated by relative scattering measurements.

---

† Burkhardt (1957) has given an interesting discussion about this point.

thus the effective energy, should fluctuate from pair to pair, giving a spread in the observed suppression effect for the pairs with a given total energy.

Fortunately, in 13 cases, the results of the measurements of the relative scattering were available, and thus gave an estimate of the degree of energy disparity. For these pairs, we have studied the correlation between the results of relative scattering measurements and ionization measurements. The results are shown in fig. 4. The ordinate shows E_s/E_c, and the abscissa shows E_i/E_c. The 'scattering energy' E_s was deduced from the data of relative scattering, making the fallacious assumption that both the particles were of equal energy ($E_s=2\sqrt{2}K/\bar{\alpha}_{\rm rel}$, where K is scattering constant, $\bar{\alpha}_{\rm rel}$ scattering angle). Each circle represents one pair and the figures show the corresponding value of energy E_c in Bev estimated from cascade measurements. Arrows indicate that the points are only upper or lower limits. Obviously, two quantities E_s/E_c and E_i/E_c correlate strongly. We can also see that the points are along the straight line $E_s=E_i$, which will be expected under the circumstances where the relative separation is determined mainly by multiple scattering. In the present experiment, due to the poor statistics, we cannot decide whether there is an appreciable change in the initial angle of divergences according to the disparity in energy.

However, it is rather clear that in the measurements of the suppression of ionization, one obtains information on a quantity of almost the same physical nature as the relative scattering.

In conclusion, it may be said that the ionization measurements give a fairly good energy estimate for pairs with energy $\geqslant 300$ Bev. On the other hand, this method cannot be expected to give significant results for pairs with energy $\leqslant 200$ Bev, because of the small amount of information to be gained from the ionization over the first few hundred microns of the track.

Among previous experimenters, Perkins (1955) has measured the ionization of six pairs. Their energies were estimated to be between 80 and 400 Bev with a mean ~ 180 Bev. Some of the pairs which are used in these experiments were re-measured and included in the present experiment. Wolter and Miesowicz (1957) have measured the ionization of a single pair with somewhat higher energy ~ 1000 Bev. They gave the mean ionization over the first $260\,\mu$ and the next $1300\,\mu$. Both these results are consistent with those of the present experiment.

§ 5. SUMMARY AND CONCLUSIONS

Summarizing the above discussions, we would like to emphasize the following points:

(1) The theory for the suppression effect of ionization by high energy pairs is in agreement with observations.

(2) It is confirmed that the suppression is energy dependent, a fact which provides the basis for a method of determining the energy of pairs by ionization measurements.

(3) A strong correlation between the suppression effect and the disparity in energy between the particles of a pair has been observed.

(4) The formula (2.15) gives reasonable basis for estimating the energies of pairs, at least for values $\geqslant 300$ BeV. This serves as a simple method for the energy determination, and is expected to be extremely useful in those cases where the available length of the pair in the emulsion stack is very short, or where there are several pairs of which the soft cascades cannot be separated from one another. The method seems to give information of a nature similar to that derived from the relative scattering measurements. At low energies the latter are superior to the former. At higher energies, however, the multiple scattering method is not applicable, because effects due to multiple scattering are easily masked by errors of measurements, and by effects due to the creation of bremsstrahlung by one or both members of a pair before the two component tracks are resolved. Reliable measurements are then difficult to make, and ionization measurements are therefore preferable: they become increasingly useful as the pair energy increases.

It may be remarked that the accumulation of the data on pairs with energy $\geqslant 1000$ BeV is highly desirable, in order to separate the effects of the multiple scattering from those due to the initial angle of divergence. The detailed study of the distance dependence of the suppression for these pairs may contribute to our understanding of the mechanism of grain formation in emulsion. The examination of the suppression in over- and under-developed emulsions may be useful for the same purpose.

ACKNOWLEDGMENTS

The author would like to thank Professor C. F. Powell and Professor M. H. L. Pryce for the facilities in the Laboratory. He also wishes to acknowledge his indebtedness to Dr. D. H. Perkins, who suggested this experiment, and to Mr. K. Pinkau, Dr. G. H. Burkhardt and Professor G. Yekutieli for their stimulating discussions. He is also grateful to Mr. J. Losty who has read carefully through the manuscript and made many important remarks.

REFERENCES

BORSELLINO, A., 1953, *Phys. Rev.*, **89,** 1023.
BURKHARDT, G. H., 1957, *Thesis*, Birmingham University.
CUDAKOV, A. E., 1955, *Izs. Akad. Nauk, U.S.S.R.*, **19,** 650.
FOWLER, P. H., and PERKINS, D. H., 1956, *Phil. Mag.*, **46,** 589.
MITO, I., and EZAWA, H., 1957, *Progr. theor. Phys., Osaka*, **18,** 437.
PERKINS, D. H., 1955, *Phil. Mag.*, **46,** 1146.
PINKAU, K., 1956, *Nuovo Cim.*, **3,** 1285 ; 1957, *Phil. Mag.*, **2,** 1382.
SCOTT, W. D., 1949, *Phys. Rev.*, **76,** 212.
WOLTER, W., and MIESOWICZ, M., 1956, *Nuovo Cim.*, **4,** 648.
YEKUTIELI, G., 1957, *Nuovo Cim.*, **5,** 1381.

Formation of Fatigue Cracks†

By W. A. Wood
Baillieu Laboratory, University of Melbourne

[Received January 25, 1958]

Abstract

The contours of the slip bands produced by fatigue straining of metals are viewed by a process of taper-sectioning and optical microscopy which permits effective magnifications of some 20 000 times. The observations indicate ways in which the slip bands may turn into cracks and start disintegration of the metal surface. They also show that the mechanism of deformation and failure changes as the amplitude of the cyclic straining increases, the general form of the fatigue S/N curve arising from superposition of two distinct mechanisms. The observations support the view that fatigue cracking is primarily a simple geometrical consequence of to-and-fro fine slip movements in the fatigue slip-bands.

§ 1. Introduction

Early investigators, notably Stanton and Bairstow (see Gough 1924). showed that fatigue failure results from fluctuating strains which contain a plastic component of small amplitude. Gough and his co-workers (1933) then showed that this component proceeded by slip, which in cubic metals concentrates in bands, and that failure normally begins as a fine crack in those bands where slip is particularly dense. They concluded that the cracking was due to excessive deformation there. Later workers have amplified these observations. The fine structure of the bands is clearly shown, for instance, in beautiful photographs of aluminium published by Laurent (1952), Bullen (1952), and Forsyth (1952). Localizing of deformation in the bands is proved in a specially interesting manner by the observations of Hanstock (1957) on the over-ageing of fatigue bands in aluminium alloys and of Forsyth and Stubbington (1954) on the extrusion of material from such bands.

However, though the general conclusion of Gough and his co-workers has been established, there are as yet few observations to show exactly how the localized deformation changes a fatigue slip band into a fine crack or to test the theoretical explanations that have been put forward. One experimental difficulty is that normal metallographic methods, while adequate for resolving a fatigue band laterally, as illustrated by fig. 2, Pl. 33, do not so easily show the structure in depth. The present work attempts to overcome the difficulty by observing the slip bands in section.

Preliminary tests (Wood and Segall 1957 a) showed that for this purpose sufficient magnification could be obtained by taper-sectioning a specimen at a very small angle to the surface and then viewing the polished section under high optical magnification. Thus a taper angle of 2° or 3° could magnify a surface disturbance in section by some 20 times, the cosecant of the angle of section. This, multiplied by optical magnifications of 500 to 1000, gave effective magnifications of some 10 000 to 20 000, which appeared likely to show in some detail the disturbances created where a band of slip planes emerged from the surface.

---

† Communicated by the Author.

§ 2. Experimental Procedure

The general procedure was to prepare fatigue test pieces with initially smooth surfaces, protect the slip bands produced in straining by an electrodeposited coating, and then section. In the preliminary tests taper-sectioning was carried out by standard techniques. Part of a test piece was mounted in plastic with its surface inclined at a small angle to the surface of the mount. Parallel grinding of the mount then exposed the required section. This method, however, proved tedious; also it did not lend itself to precise measurement of the very small angles needed for high magnification.

Fig. 1

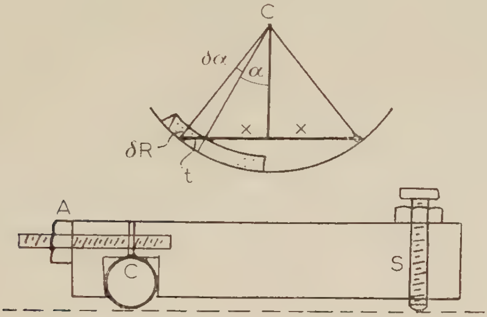

Specimen C is clamped in jig by nut A. Surface disturbance δR is magnified in section to $t = \delta R \operatorname{cosec} \alpha = \delta R \,.\, R/x$. (Not to scale.)

Consequently, for the following tests a simpler technique was devised. The test length of a cylindrical specimen after straining and plating was clamped in a Perspex jig, as shown in fig. 1, and the effect of taper sectioning obtained simply by grinding on the specimen a narrow flat. It will be seen that the plane of the flat is fixed geometrically by its lengthwise direction and by the ball point of the screw S, and that a radial disturbance at the specimen surface is magnified in section by $\operatorname{cosec} \alpha = R/x$. It was found in this way that sections at very small angle could readily be obtained by making x small, and the angle still accurately found, for x could be measured by microscope. The method had also the advantage that several sections could be made on the one specimen merely by turning it in the jig. Also the magnifying factor could be varied along the one section, if desired, by clamping the specimen with its length at a slight angle to the plane of the jig and so grinding a flat with a width $2x$ varying along its length.

The metals used in the experiments described below were annealed OFHC copper and commercially pure alpha-brass containing 70·06% zinc. Specimens were prepared with test length 1·75 in. and diameter 0·2 in., dimensions chosen because of other work on the fatigue properties of these metals, though a larger diameter would have made it easier to obtain a high magnifying factor R/x. The specimens were finished by fine turning and final grinding on 600 grade emery, and after annealing were again smoothed by electropolishing in phosphoric acid. They were then subjected to fatigue straining, protected by a heavy plating of silver, and sectioned by grinding on a 600 emery surface. The sections were prepared for metallographic examinations by standard mechanical polishing with emery, diamond dust, and alumina, and by final etching in 10% ammonium persulphate. In the photographs, later reproduced, the magnifications are written in the form $t \times m$, the first being the theoretical taper magnifications of a surface disturbance and the second the magnifications by microscope.

The fatigue straining was alternating torsion applied in a Chevenard-type testing machine (1942), the straining being chosen to show how the fatigue bands developed during the progressive cycling at typical amplitudes. These details are given below as the metallographic observations are described, the amplitudes being expressed in terms of the angles of twist on the standardized test lengths.

§ 3. INTERNAL FATIGUE BANDS

Examination of the sections was facilitated because etching brought out the internal slip zones. This was to be expected for it is known that zones of heavy deformation can often be etched up in sections of strained metals. Samuels (1955) in this way has recently identified internal slip bands in copper and copper alloys after direct straining, and Kemsley (1956) in ordinary sections of copper after fatigue straining. The effect in the present taper-sections is illustrated by fig. 3, Pl. 33, obtained from brass after 5×10^5 cycles at $\pm 5°$. This photograph is taken at relatively low magnification so as to show several grains and to confirm that the bands have the characteristics of slip, being parallel in one grain and differing in direction from grain to grain.

Some properties of these fatigue bands are described later. The immediate point of interest is the disturbances of surface contour seen at higher magnification where the fatigue bands meet the specimen surface. These are described below.

§ 4. NOTCH AND PEAK EFFECTS

It was found that the fatigue bands caused striking changes in local surface contour. They are conveniently classed as follows.

The first type is formed by fatigue bands which at the surface open into sharp notches. A typical example is provided by fig. 4, Pl. 33, taken from brass after 10^5 cycles at ±5°, only 1/10th of the estimated fatigue life. Further cycling appears to increase the number of fatigue bands and of such notches, rather than increase the depth of each, and to cause final fracture by a linking of these small fissures, the crack jumping from one set to another. Typical linking is shown in fig. 5, Pl. 34, taken from a brass specimen which failed in another part of the specimen after 10^6 cycles at ±5°.

The second type is a converse effect, where relative slip movements in the fatigue band build up a peak or ridge. Figure 6, Pl. 34, taken from brass after 5×10^6 cycles at ±2·5°, just before the fracture stage at the amplitude, shows a typical peak. The effect apparently arises when forward slip movements concentrate on one set of planes in a band and backward movements on a neighbouring set, so that the region in between is left protruding.

The third type is a combination of the foregoing, both notches and peaks forming at the head of the same slip band, so resulting in an irregular contour. A representative example is shown by fig. 7, Pl. 34, taken from copper after 5×10^4 cycles at ±2·5°, approximately 1/20th of the expected life.

The following are special cases of interest. The first occurs when fatigue bands happen to lie almost parallel to the surface. It is found that such bands can open into fissures also parallel to the surface; an example is provided by fig. 8, Pl. 35, taken from brass after 10^5 cycles at ±5°. The second is when a grain is capable of cross-slip. Then fissures can develop along two directions in the grain. This is shown by fig. 9, Pl. 35, taken from the same specimen. It will also be noticed that the two sets of fissures can intersect and thus loosen a block of metal. In fact attention has been drawn to both cases because they illustrate particularly effective methods in which the fatigue bands can disintegrate the metal surface.

The above observations appear to support the view previously put forward (Wood 1955, 1957) that a fatigue band is built up by to-and-fro fine-slip movements that can produce a notch or peak or any intermediate contour according as they become distributed across the band during progressive cycling. Initiation of cracks, particularly at the notches, then becomes simply a geometrical consequence of the to-and-fro fine slip peculiar to fatigue straining. The observations would also support a similar but more detailed process proposed by Mott (1958) in terms of dislocation theory.

§ 5. BLOCK MOVEMENTS BETWEEN SLIP BANDS

It is clear from the above observations that the fatigue bands may divide a grain into blocks and that the boundaries of the blocks are loosened when the bands become fissures. It is to be expected that the blocks in consequence may move relatively to each other. This was found to be a common occurrence, The beginning of such movement in a typical case is shown by fig. 10, Pl. 35, taken from brass after 5×10^5 cycles at ± 5°, approximately half the expected life. Figure 11, Pl. 36, taken from the same specimen, shows the same kind of movement at a more advanced stage. Figure 12, Pl. 36, taken from brass after 10^6 cycles at this amplitude, shows a still more advanced stage, with a crack jumping from one fissure to the next and at the same time undermining surface blocks to such an extent that they can drop out.

If the fatigue bands happen to be very close together then the block movements can build up a pronounced peak. An example is provided by fig. 13, Pl. 36, taken from the same specimen as the last photograph. Breakdown of such a peak evidently becomes a further effective process of surface disintegration.

A special case of interest, which also amounts to relative block movement, frequently occurs at the boundary of neighbouring grains in which the slip movements happen to be inclined to each other at a small angle. Then a fissure forms at the boundary and one grain rears over the other. A typical example is given in fig. 14, Pl. 37, also taken from brass after 10^6 cycles at ± 5° (which caused failure in another part of this specimen).

Thus the relative block movements, though facilitated by the fissure formations, in effect provide a second mechanism whereby disintegration and failure of a specimen may occur. It will again be noticed that these processes again begin at an early stage of the expected specimen life, being usually observed easily at 1/10th the life, although they appeared to accelerate in the final stages.

§ 6. Further Properties of the Fatigue Bands

The following observations are selected because they appear relevant to the general problem of fatigue failure.

(1) First it will have been noticed from the photographs that the etched-up fatigue bands are often limited in length and uneven in strength. This implies that the intensity of deformation is not uniform along the slip planes, so that only portions of the bands respond to etching. The effect was shown clearly in grains which exhibited cross-slip. The heavy deformation could start at one point on the first slip system and then continue on the second system, so creating a pattern of ‘ crazy slip ’ which made the irregular deformation particularly obvious. An example is given by fig. 15, Pl. 37, taken from brass after 7×10^5 cycles at ± 5°.

Though such non-uniformity is to be expected, it is of special interest because of the further observation that *as the amplitude of cyclic strain to which a specimen is subjected is made larger the active lengths of the fatigue bands become smaller, with the result that when the amplitude is large enough no slip bands at all etch up.* (This accounts for an observation by Kemsley (1956) who found that his etching techniques brought out fatigue bands only in specimens tested at what he termed low stresses.) The point is also of interest in confirming suggestions (Wood 1957) that the mechanism of cyclic deformation should change with increasing amplitude and pure fatigue occur only when the plastic component in the cyclic strain is small. Further, it is of interest because the way in which the deformation leads to fracture should also change with increasing amplitude. This change in fact showed itself as follows. Whereas cracks at low amplitudes resulted in effect from the opening up of the fatigue bands, so following regular crystallographic paths, cracks at high amplitudes showed no such regular behaviour. Instead they formed at isolated regions, which could be points to which the fatigue bands had contracted, and at once branched out in quite irregular formations. These features will be clear from figs. 16, Pl. 37, and 17, Pl. 38, taken from brass which failed after 10^4 cycles at ± 15° and 10^3 cycles at ± 20° respectively. The first shows at the surface merely relics of fatigue bands, and cracks which, though beginning among these bands, soon branch out quite irregularly. The second shows the complete absence of the fatigue bands and again the irregularly branching of cracks typical of the large amplitudes. This transition in mechanism of deformation and fracture began at amplitudes of about ± 10° in the brass and ± 7·5° in the copper.

(2) A second group of observations deals with the changes produced when a fatigued specimen is heat-treated before the plating and sectioning. These observations were made to find whether the fatigue bands were zones of deformation of a kind, such as lattice distortions or vacancy concentrations, that could be dispersed by heating.

In a typical experiment two specimens of copper were subjected to 10^5 and 5×10^5 cycles at ± 2·5°, respectively 1/10th and 1/2 of their expected life, and each cut in two. One part was heated *in vacuo* for 1 hour at 800°c, then plated and sectioned in the usual way. The other part was plated and sectioned without heating in order to provide comparisons. The comparison specimens showed the bands and contour disturbances to be expected from the fatigue straining. The heated parts showed the following changes. First the fatigue bands instead of disappearing broke up into links of what appeared to be cavities. This change is illustrated by fig. 18, Pl. 38 from the first specimen. Close examination indicated that a large part of the effect was certainly due to the fact that the bands in many instances must be deeply penetrating fissures which during heat treatment sintered into cavities at intervals along their length. For many examples were found of the kind shown by fig. 19, Pl. 38, taken from the second specimen, where the end of the fissure was rounded off and separated from cavities that clearly seemed initially attached.

The second observation was that though heating rounded off the root of many fissures it never removed them. This is of interest in view of the important finding made first by Sinclair and Dolan (1951) that heating a fatigue test-piece at intervals during cycling does not extend its life, and their conclusion that irreparable damage to the structure is done in the early stages of straining. The present observations that deep persistent fissures are formed early in the life of a specimen would support that conclusion.

(3) A final group of observations confirmed that the intense fatigue bands were lines of weakness at an early stage. A section showing fatigue bands on specimens subjected to 1/10th of their expected life was bent through a small angle along its length in a four-point bending device. It was found that many bands then opened up into obvious cracks. An example from brass before and after bending is clear from figs. 20 and 21, Pl. 39, despite some unavoidable blurring of the latter photograph because of the curvature of the specimen. In general, the bands opening up most were those which before the bending had already formed obvious fissures at the specimen surface.

§ 7. Conclusions

Though observations need still to be obtained on the behaviour of other materials and the effects of other modes of cyclic straining, some initial conclusions may be drawn.

First, the mechanism of deformation and fracture by cyclic straining depends on amplitude. The higher amplitudes, producing few internal fatigue bands and therefore few bands of localized high distortion, are those corresponding to the early part of an S/N curve where the curve falls sharply towards the N-axis. The low amplitudes producing intense fatigue bands are those corresponding to the later part of the S/N curve where it tends to parallelism with the N-axis. Accordingly, the special shape of the S/N curve results from the superposition of two distinct mechanism. This accords with other work on these materials (Wood, 1957, 1958, Wood and Segall 1957 b).

A second conclusion is possible in view of the other work referred to, which showed that the larger amplitudes produced progressive strain-hardening. It would appear then that the mechanism of failure at large amplitudes is akin to that of failure in static deformation, being started by stress-concentrations at a point where dislocations are piled up. The previous work also showed that small amplitudes in contrast produced relatively little strain-hardening, and therefore permitted totals of plastic deformation that would amount to some thousands per cent. The mechanism of failure in this case can scarcely be due to high stress-concentrations. At the same time it cannot primarily be due to high concentrations of vacancies or interstitials, for these would disperse on heat treatment. It appears therefore that the prime cause must lie in the notches and peaks built up by the geometry of the alternating slip movements in the heavily deformed fatigue bands; although concentrations of vacancies or other non-hardening point defects could well be a secondary cause, for they would allow the surface fissures to penetrate rapidly into such weakened zones.

Finally it appears from the observations that numerous small but sharp notches are formed by at least one-tenth of the estimated life of a specimen.

Macroscopic failure is evidently a matter of time, occurring when the fissures become numerous enough to form the basis for a large-scale crack†.

ACKNOWLEDGMENTS

The author is greatly indebted to Mr. P. B. Nantes for much help in the preparation of specimens.

REFERENCES

BULLEN, F. P., 1952, *M.Sc. Thesis*, Melbourne University.

CHEVENARD, P., 1942, *Rev. Métall.*, **39,** 40.

FORSYTH, P. J. E., 1952, *J. Inst. Met.*, **80,** 181.

FORSYTH, P. J. E., and STUBBINGTON, C. A., 1954, *J. Inst. Met.*, **83,** 395.

GOUGH, H. J., 1924, *Fatigue of Metals* (London: Benn).

GOUGH, H. J., 1933, *A.S.T.M.*, Marburg Lecture.

HANSTOCK, R. F., 1957, *Conference on Fatigue, Columbia* (New York : Academic Press).

KEMSLEY, D. S., 1956, *J. Inst. Met.*, **85,** 153.

LAURENT, P., 1952, *Publ. sci. Minist. Air*, No. 256.

MOTT, N. F., 1958, *Acta Metallurgica* (in the press), the author being indebted to Professor Mott for preview.

SAMUELS, L. E., 1955, *J. Inst. Met.*, **83,** 359.

SINCLAIR, G. M., and DOLAN, T. J., June 1951, *Proc. U.S. Nat. Congress of Appl. Mech.*, **647.**

WOOD, W. A., 1955, *Bull. Inst. Met.*, **3,** 5; 1957, *Conference on Fatigue, Columbia* (New York : Academic Press); 1958, *J. Inst. Met.* (in the press).

WOOD, W. A., and SEGALL, R. L., 1957 a, *Bull. Inst. Met.*, 3 (19) 160; 1957 b, *Proc. roy, Soc.* A, **242,** 180.

---

† Since the above paper was written, interesting work by Cottrell and Hull (1957) has come to hand (*Proc. roy. Soc.* A, **242,** 211). This also demonstrates extrusion and intrusion effects in copper and proposes a mechanism by which they might originate. The observations appear to be in general agreement with the above.

The Initial Magnetization of Alpha-Iron at High Temperatures†

By L. ALBERTS and B. J. SHEPSTONE
Physics Department, University of the Orange Free State

[Received February 14th, 1958]

ABSTRACT

As the inherent crystal anisotropy of iron tends to zero above 600°C the initial magnetization above this temperature is considered in terms of purely rotational movements of the domain vectors from preferential directions determined by applied and internal stresses. Experimental results on the influence of applied stress on the initial permeability are described. It is shown that the results are in fair agreement with the theoretical predictions.

§ 1. INTRODUCTION

THE initial magnetization in iron at ordinary temperatures is ascribed to domain boundary movements essentially. The reason for this is the existence of high crystal anisotropy which results in negligibly small rotational movements of the domain vectors in low fields (Becker and Döring 1943). As the temperature of iron is raised the anisotropy constants decrease and tend to approach zero above 600°C (see e.g. Kittel 1949). This should lead one to expect that at temperatures between 600°C and the Curie point the initial magnetization process should be of a rotational type similar to the case of nickel at room temperature (Becker and Döring 1943). Moreover, with the decrease of anisotropy energy as the temperature is raised one would expect an associated increase of initial permeability—a well known phenomenon.

In order to test how far the magnetic behaviour in low fields can be accounted for in terms of rotational movements above 600°C a tensile stress was applied to an iron specimen and the resulting effect on initial permeability observed. It so happens that the (111) magnetostriction in iron also disappears above 600°C (Takaki 1937, Lee 1955), and with the remaining single magnetostriction value the calculation of stress effects on initial permeability becomes possible for a polycrystalline specimen. At room temperature, for instance, the two magnetostrictions of opposite sign, together with the high anisotropy energy, result in such complicated stress effects that no clear conclusions could be drawn from such measurements.

§ 2. EXPERIMENTAL METHOD

The specimen (Johnson and Matthey specpure iron) was in the form of a wire 1 mm in diameter and 30 cm long. After annealing for 30 hours in an atmosphere of wet hydrogen it was mounted vertically in a specially designed tubular oven which provided the necessary elevated temperatures. Throughout the experiment the specimen was kept in an atmosphere of purified hydrogen to prevent oxidation. Weights from the lower end provided the tensile stress. The magnetic measurements were carried out by ballistic galvanometer. A typical B–H curve at an elevated temperature is shown in fig. 1. As the galvanometer arrangement was extremely sensitive (9 maxwell per mm of deflection) the initial linear portion of the curve could be determined accurately and a reliable value obtained for the initial permeability. After the application of a stress the specimen was first thoroughly demagnetized by a continuously decreasing alternating field and then the d.c. magnetizing field applied.

---

† Communicated by the Authors.

Fig. 1

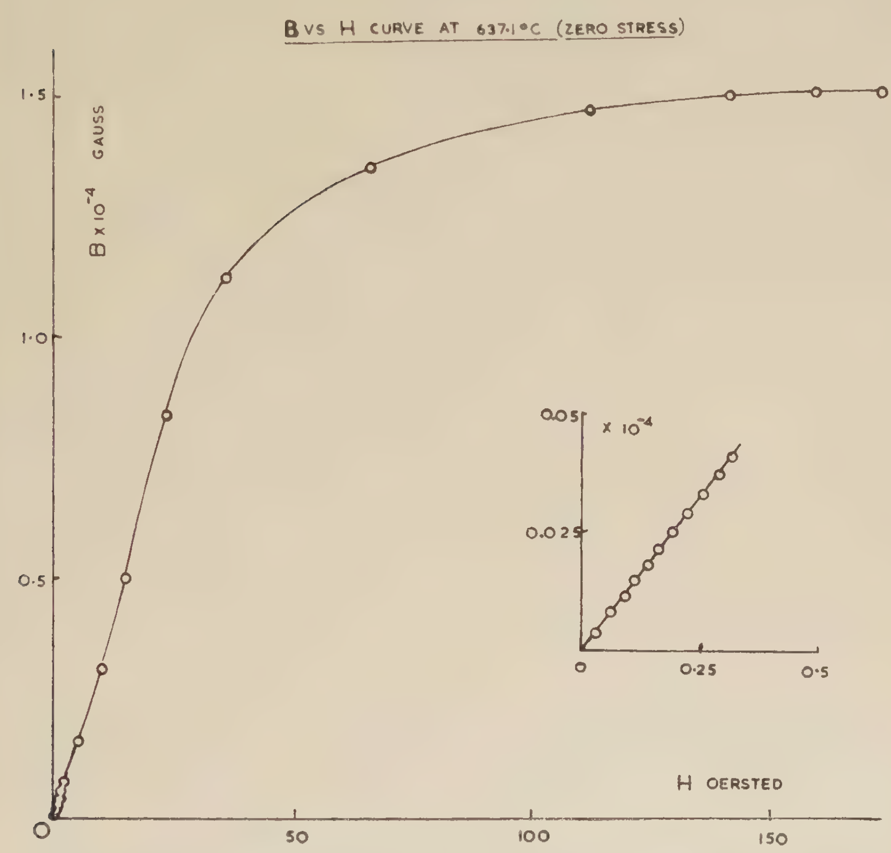

Insert indicates that the linearity of the initial portion lends itself to an accurate determination of the initial permeability.

From the dimensions of the specimen one sees that end effects can be neglected.

A typical curve illustrating the increase of initial permeability with applied stress is shown in fig. 2.

Fig. 2

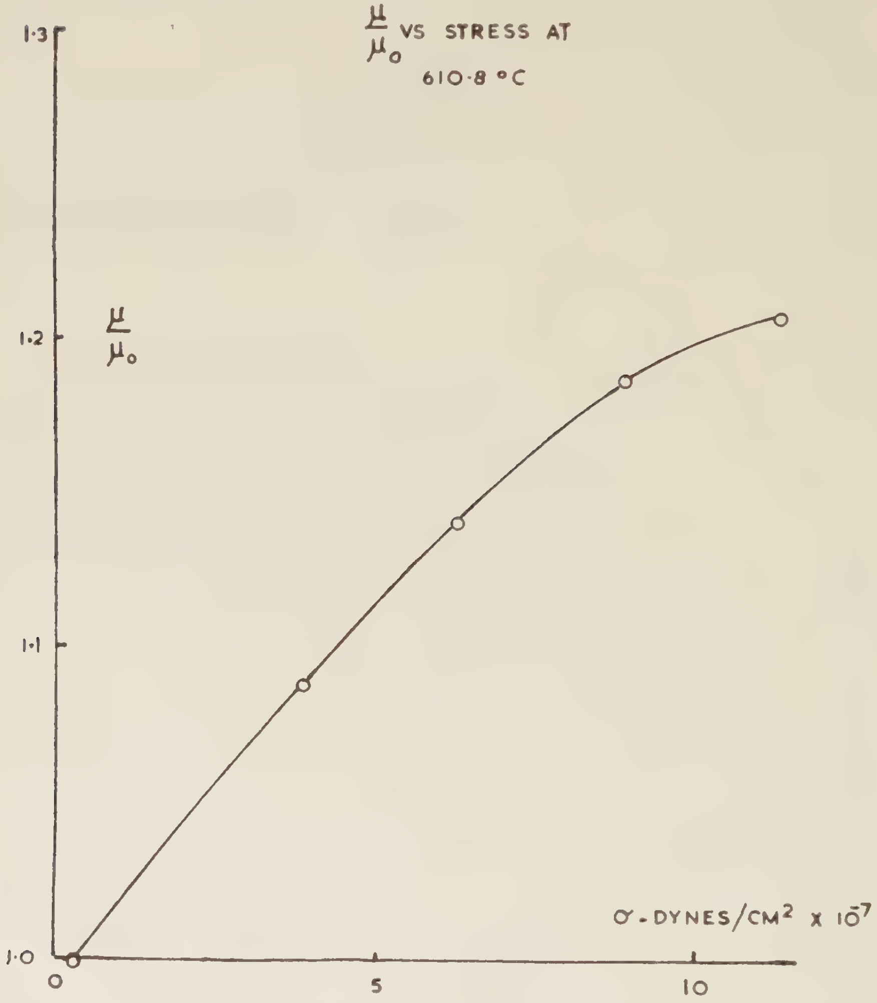

Curve showing variation of initial permeability with applied stress at 610·8°c. $\mu_0=1227$ c.g.s. units is the value at zero stress.

§ 3. Theory

With no applied tension or field we picture the magnetization of a domain as being held by weak internal stresses due to magnetostriction, lattice imperfections, etc. See fig. 3 (*a*). On applying a magnetic field the spins will tend to swing into the direction of the field giving an overall magnetizing effect. If a tension is applied first, the spins will tend to set themselves in the direction of the applied stress, because at this temperature there exists only a single positive magnetostriction. The effect of an applied stress will thus be to increase the initial permeability.

One can see that the influence of stress will be limited, because when all the spins are parallel to the stress axis as a result of stress, the magnetization will proceed as a result of 180° Bloch wall movements. The inhibitions offered to this movement by traces of impurities, lattice imperfections, etc., will not be decreased by stress. The decreasing effect of stress as the latter is increased is borne out by the flattening out of the curve as seen in fig. 2.

Fig. 3

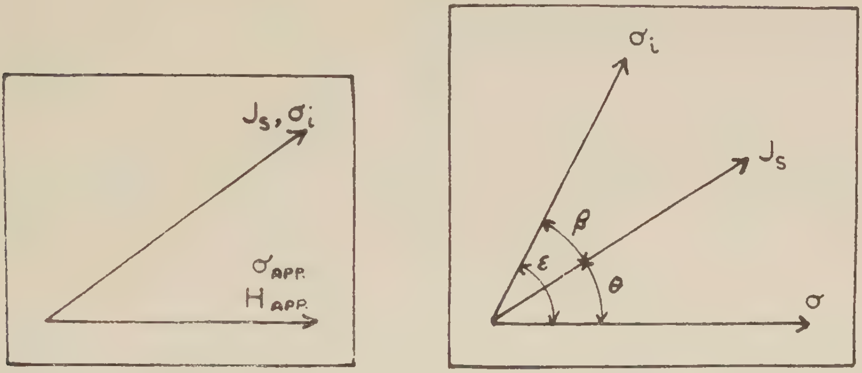

(*a*) (*b*)

Schematic presentation for iron above 600°c.

Referring to fig. 3 (*b*) for calculation purposes : The total energy due to magnetic field H, internal stress σ_i and applied external stress σ, is given by

$$F = \tfrac{3}{2}\lambda\sigma_i \sin^2\beta + \tfrac{3}{2}\lambda\sigma \sin^2\theta - HJ_s \cos\theta \quad . \quad . \quad . \quad (1)$$

where λ, the (100) magnetostriction, is now treated as an isotropic magnetostriction for the polycrystalline specimen. As explained before, the anisotropy energy is negligible. Equation (1) must be minimized to establish the equilibrium condition and hence the expression for the permeability is obtained. We follow a mathematical technique employed by Rathenau and Fast (1955). The contributions of field energy and external strain energy are considered to be small compared with that due to the internal strains. This assumption is justified if the applied magnetic field and external stress approach zero.

Equation (1) leads, with $\frac{3}{2}\lambda\sigma \ll \frac{3}{2}\lambda\sigma_i$ and $HJ_s \ll \frac{3}{2}\lambda\sigma_i$, neglecting quantities of the fourth order, to

$$\begin{aligned} F = \tfrac{3}{2}\lambda\sigma \sin^2 \epsilon - HJ_s \cos \epsilon + \tfrac{3}{2}\lambda\sigma_i\beta^2 \\ - \tfrac{3}{2}\lambda\sigma(\beta \sin 2\epsilon - \beta^2 \cos 2\epsilon) \\ - HJ_s[\beta \sin \epsilon - (\tfrac{1}{2}\beta^2) \cos \epsilon]. \end{aligned}$$

The equilibrium angle follows from $\partial F/\partial B = 0$, giving

$$\beta = \frac{(\frac{3}{2}\lambda\sigma \sin 2\epsilon + HJ_s \sin \epsilon)}{(3\lambda\sigma_i + 3\lambda\sigma \cos 2\epsilon + HJ_s \cos \epsilon)}. \quad . \quad . \quad . \quad . \quad (2)$$

We consider a domain in which the direction of the spins, in the absence of field and stress, is given by angle ϵ. Upon application of stress and field unit volume contributes $J_s \cos \theta$ to the magnetization along the direction of H. To the intial susceptibility it contributes.

$$\begin{aligned} \kappa(\epsilon) &= \left[\frac{\partial}{\partial H}\{J_s \cos (\epsilon - \beta)\}\right]_{H\to 0} \\ &= \left[J_s \sin (\epsilon - \beta) \frac{\partial \beta}{\partial H}\right]_{H\to 0} \end{aligned}$$

which, bearing in mind that we are dealing with initial susceptibility. for small β is

$$\kappa(\epsilon) = J_s\left[(\sin \epsilon - \beta \cos \epsilon) \frac{\partial \beta}{\partial H}\right]_{H\to 0}. \quad . \quad . \quad . \quad (3)$$

Substituting $(\beta)_{H\to 0}$ and $(\partial\beta/\partial H)_{H\to 0}$ from (2) one obtains

$$\kappa(\epsilon) = \frac{J_s^2 \sin^2 \epsilon}{3\lambda\sigma_i}\left(1 - \frac{\frac{3}{2}\lambda\sigma \cos^2 \epsilon}{\frac{3}{2}\lambda\sigma_i + \frac{3}{2}\lambda\sigma \cos 2\epsilon}\right)\frac{[1 - (\sigma/\sigma_i) \sin^2 \epsilon]}{[1 + (\sigma/\sigma_i) \cos 2\epsilon]^2}$$

which for small σ/σ_i reduces to

$$\kappa(\epsilon) = \frac{J_s^2 \sin^2 \epsilon}{3\lambda\sigma_i}[1 + (\sigma/\sigma_i)(1 - 4 \cos^2 \epsilon)]. \quad . \quad . \quad . \quad . \quad (4)$$

Assuming $\frac{3}{2}\lambda\sigma$ independent of ϵ and for an isotropic distribution of ϵ:

$$\begin{aligned} \kappa(\epsilon) &= \tfrac{1}{2}\int_0^{\pi} \kappa(\epsilon) \sin \epsilon \, d\epsilon \\ &= \frac{2J_s^2}{9\sigma_i\lambda}\left\{1 + \frac{1}{5}\left(\frac{\sigma}{\sigma_i}\right)\right\} = \kappa_0\left\{1 + \frac{1}{5}\left(\frac{\sigma}{\sigma_i}\right)\right\}. \quad . \quad . \quad . \quad (5) \end{aligned}$$

Substitute the expression $\kappa_0 = 2J_s^2/9\lambda\sigma_i$. which is obtained from the above if $\sigma = 0$.

Thus we can write

$$\frac{\kappa}{\kappa_0} = 1 + \frac{9\lambda\kappa_0\sigma}{10J_s^2}$$

and for permeabilities, since $\mu = 4\pi\kappa + 1$, $\mu \gg 1$

$$\frac{\mu}{\mu_0} = 1 + \frac{9\lambda\mu_0\sigma}{40\pi J_s^2}$$
$$\equiv 1 + k\sigma \quad . \quad . \quad . \quad . \quad . \quad . \quad . \quad . \quad (6)$$

and the graph of μ/μ_0 *vs* σ (for small values of σ) should be a straight line, with slope k, cutting the ordinate at unity.

§ 4. Results and Discussion

Using the values of Takaki (1937) to plot a curve of magnetostriction versus temperature and reading off values corresponding to our temperatures, the values for k were calculated from eqn. (6) and compared with the measured values taken from curves such as in fig. 2. The results are given in the table below:

$t-{}^\circ$C	μ_0	λ_{100} $\times 10^6$	k Measured $\times 10^9$	k Calc. $\times 10^9$
610·8	1227	28	2·432	2·014
637·1	1338	26·6	3·183	2·412
672·3	1590	23	4·050	3·239
686·5	1770	22·4	4·999	3·821
716·7	2525	19	3·841	5·363
740·5	2895	14·5	3·913	6·531

The fair agreement between theory and experiment in the region 600°c to 700°c indicates that the major part of the initial magnetization process in this region is accounted for. As the Curie point is approached the deviation between theory and experiment becomes more marked. This is not entirely unexpected as we have no adequate knowledge of the value and behaviour in this region of the magnetic constants involved.

If, instead of being caused by spin rotation, we consider the magnetization as being due to reversible wall displacement, we must fit the readings with formulae of the type.

$$\kappa = \kappa_0\{1 + \tfrac{4}{5}(\sigma/\sigma_i)\}$$

due to Rathenau and Fast (1955) or

$$\kappa = \kappa_0\{1 + 3{\cdot}2(\sigma/\sigma_i)\}$$

as found by Bozorth and Williams (1945) for 45 Permalloy. Both of these formulae give very much bigger differences between theory and experiment. Thus the original picture of spin rotation seems to fit the facts far better than that of wall movement.

The formula for the initial permeability without zero stress, as obtained from eqn. (5) is $\mu_0 = (8\pi J_s^2/9\lambda\sigma_i) + 1$. It is the same as that of Becker and Döring (1943) obtained from direct derivation for rotational processes. Using the value of μ_0 at 610·8°c the calculated value for $\sigma_i = 12{\cdot}4 \times 10^7$ dynes/cm^2. Taking an estimated value for Young's modulus of $1{\cdot}4 \times 10^{12}$ dynes/cm^2 at this temperature (e.g. see Smithels 1955), the value of the magnetostrictive stress is approximately 4×10^7 dynes/cm^2. This indicates that the order of magnitude obtained for the internal stress is reasonable if we assume that the residual stresses normally present in a metal have been mostly relieved at the high temperature.

Concerning the steady rise of initial permeability with temperature and the rather rapid increase as the Curie point is reached, Fahlenbrach (1948) proposes that the randomness of domain vector orientation increases with temperature and causes the observed rise. In the light of the foregoing discussion such a permeability rise can be pictured quite simply. With zero crystal anisotropy and the diminishing of internal magnetostrictive strain as the Curie point is approached less and less resistance is offered to reorientation of the domains by an applied magnetic field and consequently a rise in the initial permeability.

ACKNOWLEDGMENTS

It is a pleasure to acknowledge financial support from the South African Council for Scientific and Industrial Research for equipment and a study grant to one of us (B. J. S.).

REFERENCES

BECKER, R., and DÖRING, W., 1943, *Ferromagnetismus* (Berlin: Springer; Ann Arbor Impression).
BOZORTH, R. M., and WILLIAMS, H. J., 1945, *Rev. mod. Phys.*, **17,** 72.
FAHLENBRACH, H., 1948, *Ann. Phys. Lpz.*, **2,** 355.
KITTEL, C., 1949, *Rev. mod. Phys.*, **21,** 541.
LEE, E. W., 1955, *Reports Progr. Phys.*, **18,** 184.
RATHENAU, G. W., and FAST, J. F., 1955, *Physica*, **21,** 954.
SMITHELS, C. J., 1955, *Metals Reference Book* (Butterworth Scientific Publications).
TAKAKI, H., 1937, *Z. Phys.*, **105,** 92.

A New Function in the Theory of Fluids and an Equation of State for Liquids and Gases†

By A. G. McLellan
University of Canterbury, Christchurch, New Zealand

[Received February 17, 1958]

Abstract

A hole theory of fluids is described in which the potential of a molecule in a cell is not assumed to be spherically symmetric about the cell centre. Although this theory is incomplete in several respects, it has lead to the discovery of a function of pressure, density and temperature which when evaluated for real fluids, such as argon and krypton, appears to be a function of density only, and independent of the state, liquid or gas. It is shown how this property would lead to an equation of state valid for liquid and gas, and the results of a first attempt in this direction are given, which are in better agreement with experiment than those of other lattice or hole theories.

§ 1. Introduction

This paper describes a simple but as yet incomplete hole theory of fluids, in which the potential energy of the molecule in a cell is not assumed to be spherically symmetric about the centre of the cell. The cell dimension is obtained by minimizing the free energy. In the course of the development of this theory, a parameter was introduced, whose value as a consequence of the theory could be obtained from the experimental values of pressure, density and temperature. The value of this parameter was evaluated in this way for argon, and it was found to have the important property of being a function of density only, independent of the state, liquid or gas. That such a function of pressure, density and temperature should be a function of the density only for a real fluid should have important consequences in the theory of fluids. A knowledge of its dependence on density, for example, leads immediately to an equation of state valid for liquid and gas and consequently to the evaluation of other thermodynamic functions. A first attempt at such an equation of state is described, and represents an improvement in experimental agreement over others obtained from cell or hole theories.

The present theory differs from previous hole theories (Cernuschi and Eyring 1939, Ono 1947, Peek and Hill 1950, Rowlinson and Curtiss 1951) in the expression used for the generalized free volume per cell (see e.g. Hirschfelder *et al.* 1954, p. 313) and in the manner in which this quantity is introduced. In these earlier theories the logarithm of the generalized

---

† Communicated by the Author.

free volume is taken to be linearly dependent on ω, the fraction of nearest neighbour sites about the central site which are vacant (see Hirschfelder *et al.* 1954, p. 314, or Rowlinson and Curtiss 1951) ; in the present work the generalized free volume, not its logarithm, is taken to be a power series in ω. Further this quantity is introduced by means of a simple modification of the expression for the free energy used in the cell theory of Lennard-Jones and Devonshire (1937).

The theory is incomplete in that it does not yet provide an explicit form for the above-mentioned function of density, and in that it lacks a completely rigorous deduction from the fundamental equations of statistical mechanics. The principal purpose in publishing this work is to describe the properties of the above parameter in the hope that more interest will be stimulated in hole theories of fluids, and in particular, that a rigorous development of the behaviour of this parameter for real fluids will result.

§ 2. THE THEORY

In studying the radial distribution functions for argon obtained from x-ray diffraction experiments (Eisenstein and Gingrich 1942), one is impressed by two facts—that the position of the first coordination peak is practically independent of the density, and that the number of nearest neighbours (proportional to the area under the first coordination peak) varies almost as does the density. Referring these results to a lattice theory where the molecules are to be assumed to lie on or near lattice sites, such a theory should produce a lattice dimension which varies very little with density, the change in the density to be accompanied by a corresponding change in the number of vacant sites. The early theory of Lennard-Jones and Devonshire was unrealistic in these respects.

In taking account of vacant sites, the hole theories mentioned in § 1 obtained a free-volume per cell whose logarithm was linearly dependent on ω. In some cases this was a result of assuming a spherically symmetric potential in each cell, as if the nearest neighbours were smeared out uniformly over a spherical surface ; and in others this dependence was assumed. It is probable that such an assumption is related to a spherically symmetric potential. Such a smearing out of nearest neighbours is possible related to a physical picture of a fluid in which the molecular motions are sufficiently large and random so that a central molecule is always prevented from approaching its cell wall. This is very well illustrated by the cellular potential of Lennard-Jones and Devonshire which becomes infinite on an arbitrarily defined spherical surface which plays the part of a cell wall, and also by any theoretical modification which simply reduced this potential everywhere by the fraction of occupied sites. An equally plausible physical picture, justified by the high degree of short-range order at high densities, as exhibited by x-ray diffraction experiments, is one in which the emphasis is placed on the lattice structure, whereby this structure is preserved, at least locally, even when vacant sites are produced ; that is, when a nearest neighbour site is vacant, the other nearest neighbours are to a certain extent excluded from this vacant site on account of the tight packing. On the same reasoning the central molecule will also be excluded, but nevertheless its free volume in the cell will have been increased in the neighbourhood of this vacant site. Such a picture represents the extent to which this present theory departs from the concept of spherical symmetry in the cell. The above idea thus leads naturally to a free volume which is linearly dependent on ω, and it was assumed at first that the free volume of the cell was the cell volume multiplied by ω. When all sites are occupied the free volume could be taken as that of Lennard-Jones and Devonshire, but this is such a relatively small quantity that it was neglected, though in principle there would be no difficulty in including it. The potential at the centre of the cell is taken to be proportional to $1-\omega$, the fraction of occupied sites.

The Helmholtz free energy per molecule, f, was taken to be

$$f=(1-\omega)\psi(x)-kT\ln(\omega/\gamma x), \quad . \quad . \quad . \quad . \quad . \quad (1)$$

here the terms in f depending on temperature only are not included as they play no part in the minimizing process and in the calculation of the pressure ; ω is the fraction of unoccupied sites ; $x=1/a^3$, where a is the lattice constant ; γx is the reciprocal of the cell volume (for argon the lattice structure is taken as face-centred cubic for which $\gamma=\sqrt{2}$); $(1-\omega)\psi(x)$ is the potential at the cell-centre assumed to be proportional to the fraction, $1-\omega$, of occupied sites. The number density, n_1, is clearly given by

$$n_1=(1-\omega)\gamma x, \quad . \quad . \quad . \quad . \quad . \quad . \quad . \quad . \quad . \quad (2)$$

enabling (1) to be written

$$f=(n_1/\gamma x)\psi(x)-kT\ln\{(\gamma x-n_1)/(\gamma x)^2\}. \quad . \quad . \quad . \quad . \quad (3)$$

This expression enables x to be determined by minimizing f with respect to x. For argon, $\psi(x)$ was taken to be a Lennard-Jones type of potential, corrected for the attraction of more distant neighbours than the nearest (Lennard-Jones and Devonshire 1937), i.e.

$$\psi(x)=6\epsilon\{(r_0/a)^{12}-2{\cdot}4(r_0/a)^6\}. \quad . \quad . \quad . \quad . \quad . \quad (4)$$

The results were promising in that a was always close to r_0, and the number of nearest neighbours, $12(1-\omega)$, agreed reasonably well with those obtained experimentally by Eisenstein and Gingrich (1942). An equation of state was evaluated and the correct behaviour was observed. However the liquid densities at saturation vapour pressure were too near the crystal density for good experimental agreement. It was then that an expression for the free volume which is quadratic in ω was introduced, purely as an assumption. The following expression is now taken as a starting point

$$f=(1-\omega)\psi(x)-kT\ln\{(\alpha\omega+\omega^2)/\gamma x\}, \quad . \quad . \quad . \quad . \quad (5)$$

the coefficient of ω^2 being taken as unity, while for convenience the arbitrarily introduced parameter α was taken as the coefficient of ω. It was hoped that α might be a function of temperature only, and that therefore any necessary constant of proportionality in the expression for the free volume would also be temperature dependent only, and therefore in the minimizing process and in the evaluation of the pressure it would be superfluous. This proved to be wrong, but it will be shown later how the procedure may be made consistent. Thus, assuming α to be dependent on temperature alone, f may be minimized with respect to x, using (2), and an expression for the pressure obtained, resulting in the following two equations finally,

Fig. 1

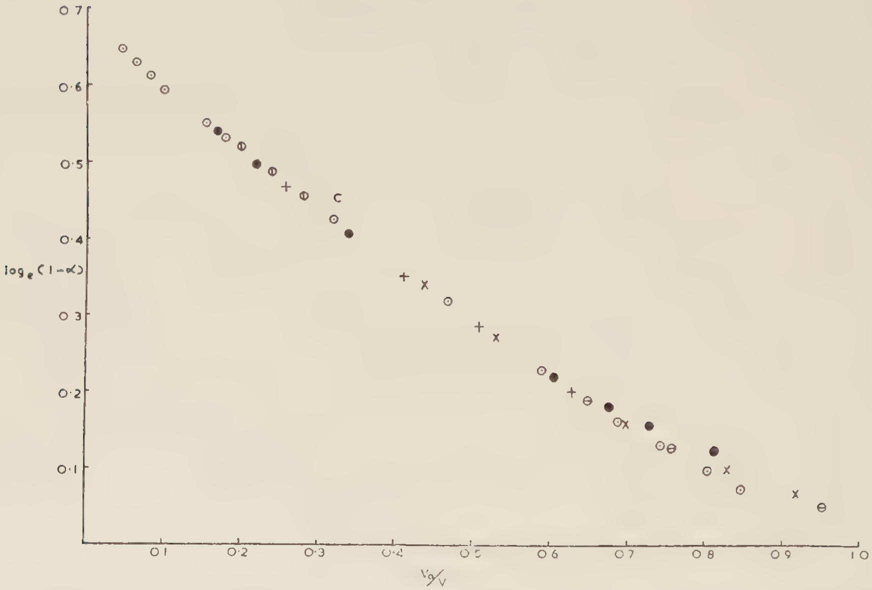

○ Argon, liquid or vapour at saturation vapour pressure ; ⊖ argon, $T_0=1{\cdot}083$, liquid ; × argon, $T_0=1{\cdot}25$, liquid ; ● argon, $T_0=2{\cdot}276$, gas ; + argon, $T_0=4{\cdot}167$, gas. C is the critical point for argon. ⦶ krypton, $T_0=1{\cdot}597$ and $2{\cdot}767$, gas.

$$\frac{pv}{kT}-1=\left(\frac{n_1}{\gamma x}\right)\{[x\psi'(x)]/kT\} \quad . \quad . \quad . \quad . \quad . \quad . \quad (6)$$

$$\left(\frac{n_1}{\gamma x}\right)\frac{1}{(\alpha+1)}\equiv 1-1\bigg/\left\{3-\frac{\gamma x}{\gamma x-n_1}+\left(\frac{n_1}{\gamma x}\right)\frac{[x\psi'(x)-\psi(x)]}{kT}\right\}. \quad . \quad (7)$$

This pair of equations enables α to be evaluated by eliminating x and using experimental values of pressure, density and temperature. For argon (Michels *et al.* 1949, Din 1956) the values of $\ln(1-\alpha)$ thus obtained are shown in fig. 1, plotted against V_0/V, where $V_0=r_0^3/\sqrt{2}$, and V is the reciprocal of the number density ; ϵ was taken to be $120k$, and r_0 3·83 Å, Lennard-Jones (1924). Also shown in this figure are a few points for krypton, derived from the experimental data of Beattie *et al.* (1952). The table gives some numerical values. The reduced temperature $T_0 = kT/\epsilon$ is used.

State	(v_0/v)	T_0	$\ln(1-\alpha)$
Gas	0·051	2·276	0·65
,,	0·051	3·526	0·65
Saturated vapour	0·103	1·159	0·60
Gas	0·103	2·276	0·60
,,	0·103	3·526	0·60
,,	0·112	4·167	0·60
,,	0·340	2·276	0·41
,,	0·340	3·526	0·41
Liquid	0·468	1·233	0·32
Gas	0·473	2·276	0·31
,,	0·608	2·276	0·22
,,	0·608	3·526	0·23
Liquid	0·649	1·083	0·191
,,	0·647	1·25	0·195
Gas	0·677	2·276	0·182
,,	0·677	3·526	0·191

Although the original assumption is not borne out, fig. 1 shows that α definitely appears to be a function of the density only, and to be independent of the state. It should be emphasized that this behaviour of α is an experimental fact, however eqns. (6) and (7) may have been derived. A way of removing the inconsistency that in deriving (6) and (7), α was assumed dependent on T only, and proves to be a function of density only, will be indicated later.

If the functional dependence of α on the density were known, and assumed to hold everywhere, an immediate application would be to the derivation of an equation of state valid for both liquid and gas. A first attempt in this direction has been made by determining empirically from fig. 1 the expression for $\ln(1-\alpha)$. An obvious method would be to use a 'least squares', method, but it was decided not to do this as the experimental errors appear to be greatest in the high density region. The expression

$$\ln(1-\alpha) = \ln 2\{(1-v_0/v) + b(1-v_0/v)^2\}/(1+b) \quad . \quad . \quad . \quad (8)$$

was used, as it is clear from eqns. (6) and (7) that $\alpha \to -1$ as $n_1 \to 0$; also from fig. 1 it appears highly probable that $\alpha \to 0$ as $v \to v_0$. b was chosen equal to 0·4 so that the curve of (8) would pass through the value of $\ln(1-\alpha)$ at the critical point. The equation of state was then derived by assuming (8) solving (7) for x at a given density and temperature, and finally by substituting this value of x in (1). Figure 2 shows several isotherms thus obtained. The critical isotherm, $T_0 = 1·3$ (1·256 experimental for argon) is compared with experimental points. The agreement is very good for such a simple expression for $\ln(1-\alpha)$. The isotherm $T_0 = 1$, yields $v_0/v = 0·670$ (experimental 0·708) for the liquid and 0·04 (experimental 0·04) for the vapour at a saturation vapour pressure of 14 atmospheres (experimental 12 atm); the compressibility of the

Fig. 2

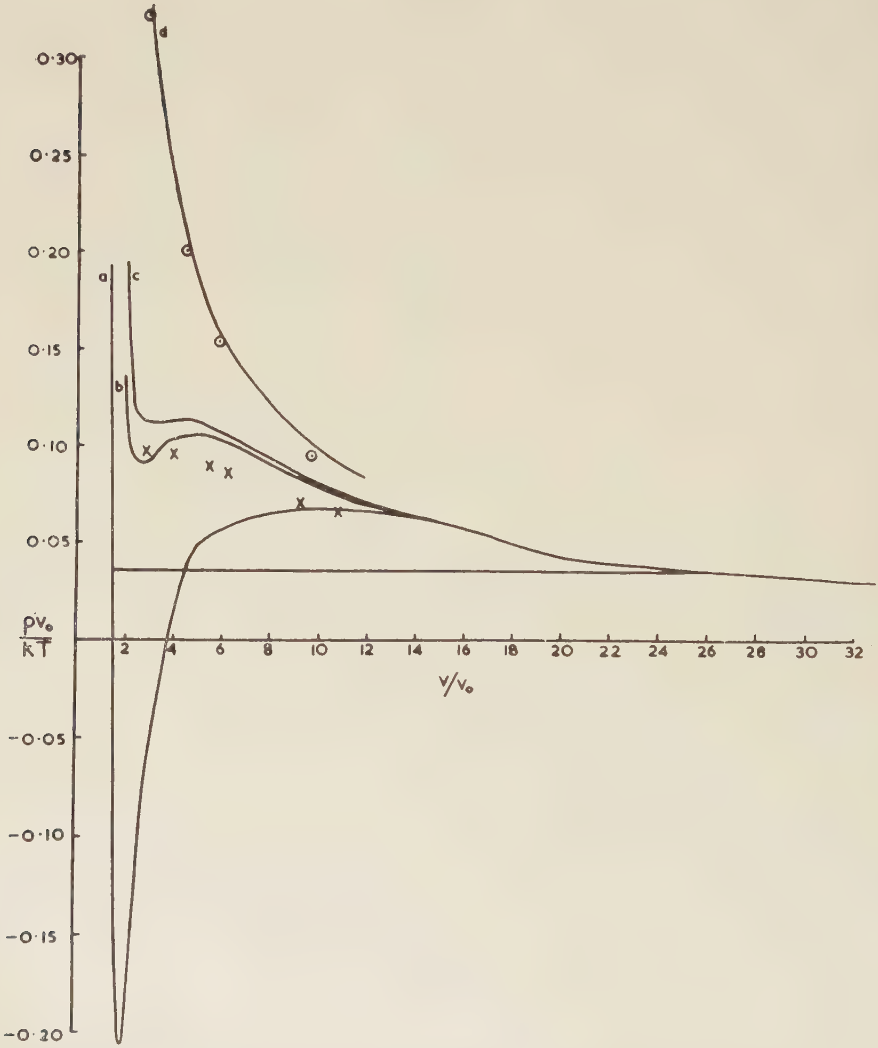

a, *b*, *c* and *d* are isotherms for $T_0 = 1$, 1·258, 1·3, and 2·276 respectively. For *a* the horizontal line giving the saturation vapour pressure, according to Maxwell's law of equal areas, is shown. × denotes experimental points for the critical isotherm of argon at 151·9°K; ⊙ denotes experimental points for argon at 0°C ($T_0 = 2·276$).

liquid at s.v.p. is calculated to be 0·0009 per atmosphere (experimental 0·0006). An isotherm at $T_0=2{\cdot}276$ (for argon, 0°c) is shown to be in excellent agreement with experiment.

It should also be mentioned that the number of nearest neighbours, calculated from (2), taking the value of x obtained when solving (7) using (8), is in good agreement with the values obtained by Eisenstein and Gingrich (1942), from x-ray diffraction patterns. The corresponding value of a, the lattice constant, always differs from r_0 by less than about 8%, a result which is consistent with experiment.

§ 3. Improvement of the Theory

The difficulty mentioned, that α is a function of the density, raises the question as to the consistency of the theory. To avoid this it must be assumed that α is a parameter which, analogously to ω, must be evaluated by minimizing the free energy. To make this possible the free volume should have another factor, such that its complete expression is

$$m(\alpha,T)(\alpha\omega+\omega^2)/(\gamma x), \qquad . \quad . \quad . \quad . \quad . \quad . \quad . \quad (9)$$

the nature of the function m not being known at present. If it is assumed that α must be determined by minimizing the free energy with respect to α, then as $\partial f/\partial\alpha$ is zero, α contributes nothing to the pressure.

The physical significance of α is not known, but it may be that it is a sort of structure factor like ω, such that it determines the arrangement of pairs of vacancies. It is possible, for instance, that in an arrangement where two contiguous nearest neighbour sites are vacant the local structure tends to break down, leading to a smearing out of nearest neighbours and making a free volume, similar to that of Lennard-Jones and Devonshire, the appropriate one. Work is proceeding on this aspect. It is worth mentioning that the free energy of the fluid could be calculated by integrating the equation of state from zero density, where the free energy is know, to any desired point on an isotherm, and thus the value of m could be obtained.

§ 4. Conclusion

A relatively crude theory has been described, whose main virtues are that it indicates a new approach to a hole theory, and that it has been the avenue for the discovery of an important property of real fluids, leading to a useful equation of state depending on one constant (b of (8)) over and above those of the Lennard-Jones potential. Further empirical work is indicated in endeavouring to find central cell potentials, $\psi(x)$, for more complicated fluids such as carbon dioxide, nitrogen etc., and in determining a more satisfactory empirical form for $\ln(1-\alpha)$, which would probably improve the agreement on the compressibility of liquid argon. On the theoretical side, much remains to be done in elucidating the physical significance of the hypothecated expression for the free volume stated in (9).

REFERENCES

BEATTIE, J. A., BRIERLEY, J. S., and BARRIAULT, R. J., 1952, *J. chem. Phys.*, **20,** 1613.

CERNUSCHI, F., and EYRING, H., 1939, *J. chem. Phys.*, **7,** 547.

DIN, F., 1956, *Thermodynamic functions of gases*, Vol. 2 (London : Butterworths Scientific Publications).

EISENSTEIN, A., and GINGRICH, N. S., 1942, *Phys. Rev.*, **62,** 261.

HIRSCHFELDER, J. O., CURTISS, C. F., and BIRD, R. B., 1954, *The Molecular Theory of Gases and Liquids* (New York : John Wiley & Sons).

LENNARD-JONES, J. E., 1924, *Proc. roy. Soc.* A, **106,** 463.

LENNARD-JONES, J. E., and DEVONSHIRE, A. F., 1937, *Proc. roy. Soc.* A, **163,** 53.

MICHELS, A., WIJKER HUB., and WIJKER, HK., 1949, *Physica*, **15,** 627.

ONO, S., 1947, *Mem. Fac. Engng Kyushu*, **10,** 190.

PEEK, H. M., and HILL, T. L., 1950, *J. chem. Phys.*, **18,** 1252.

ROWLINSON, J. S., and CURTISS, C. F., 1951, *J. chem. Phys.*, **19,** 1519.

Nuclear Particle Track Photography in Electric Fields†

By I. E. Bock
Clarendon Laboratory, Oxford

[Received May 2, 1958]

Abstract

A method is proposed whereby the light emitted by liquid scintillators may be increased by application of a suitable a.c. field. It is calculated that by this means the light output may be increased amply to allow minimum ionizing tracks to be recorded photographically without the possibility of instability arising.

§ 1. Introduction

Various drawbacks in the bubble chamber method of obtaining photographs of nuclear particle tracks make a consideration of other methods desirable. In this investigation two main points are considered: firstly, techniques to increase the ionization along the track of a nuclear particle; secondly, methods of observing ionization.

§ 2. Increase of Ionization along the Track of a Nuclear Particle

Two distinct thresholds occur in a dielectric as the a.c. field potential is increased: the lower threshold is at about 42% of the breakdown voltage when ionization commences in the dielectric; the higher threshold is when breakdown of the dielectric occurs (Bute *et al.* 1954). For high frequencies this ionization does not occur randomly in the dielectric but occurs along the tracks of ionizing particles and indeed breakdown streamers develop from these (Prowse and Lane 1956).

Although for gases, consideration of negative ion mobilities indicates that fields of microwave frequency are required to confine the increase in ionization to a 10^{-3} cm diameter track; for liquefied gases, fields of frequencies of a few Mc/s should be satisfactory.

§ 3. Photography of Ionization

For the observation of the ionization direct photography of the ‘scintillation’ light, emitted during decay of excitation and recombination of ionization, is possible. The liquefied noble gases are known to be good scintillators having scintillation efficiencies comparable with NaI-Tl (Northrop and Nobles 1956). For liquid argon it is estimated that the ionization along the track must be increased by about 10^5 in order to obtain photographs of minimum ionization. Using fields greater than the breakdown threshold, inception of breakdown occurs when the number of ions have increased by about 10^8 (Gould and Roberts 1956). Hence the above required magnification can be obtained without breakdown of the dielectric and will occur in about 9 cycles of the high frequency electric field. Alternatively, using field strengths less than the breakdown strength, but in excess of the ionization threshold, a slower, but completely stable method of magnifying the light output may be obtained.

---

† Communicated by Mr. R. B. Owen.

§ 4. PRACTICAL ASPECTS

Ionizations occur in liquid argon and liquid hydrocarbons in fields of 100 kv/cm and 400 kv/cm respectively (Williams and Stacey 1957, Bute *et al.* 1954). Large chambers will be possible since Tesla coils and resonance transformers have been developed which are capable of producing radio frequency fields at several million volts (Craggs and Meek 1954).

Heating of the dielectric volume is expected due to the presence of the electric field. However, comparison with dynamic losses of liquid hydrogen bubble chambers indicated that the loss expected for the electrical method is 10^{-2} that obtained with bubble chambers.

The velocity of the particles can be determined from the degree of ionization. The initial ionization produced by the nuclear particle will be magnified by a factor 2^n where n is the number of ionizing collisions, related to the number of cycles of the field. If the field is uniform, then throughout the chamber n will be the same, and the intensity of light emitted along a track will be nearly proportional to the initial number of electrons.

§ 5. ADVANTAGES OF THE METHOD AS COMPARED TO BUBBLE CHAMBERS

The method proposed has certain definite advantages over the use of bubble chambers:

(*a*) Counter control is possible.

(*b*) Cycling rate can be very high.

(*c*) No illumination or mirror system is required.

(*d*) Experimentally the method is adaptable for the use of various liquids in one chamber.

(*e*) Comparatively low dynamic loss is a definite advantage when large chambers are required.

(*f*) Thermal gradients of the liquid only affect stopping power through density, unlike in bubble chambers where they also affect bubble nucleation.

ACKNOWLEDGMENT

This investigation has been conducted in the development of a thesis subject by the author, who wishes to acknowledge the tenure of a Rhodes Scholarship.

REFERENCES

BUTE, C. J., SOMMERMAN, C. M. L., and LARSON, E. L. C., 1954, *Commun. Electron.*, **12,** 147.

CRAGGS, J. D., and MEEK, T. M., 1954, *High Voltage Laboratory Technique* (London: Butterworth).

GOULD, L., and ROBERTS, L. W., 1956, *J. appl. Phys.*, **27,** 1162.

NORTHROP, J. A., and NOBLES, R., 1956, *Nucleonic*, Vol. 14, No. 4, p. 36.

PROWSE, W. A., and LANE, P. E., 1956, *Proc. phys. Soc. Lond.* B, **69,** 33.

WILLIAMS, R. L., and STACEY, F. D., 1957, *Can. J. Phys.*, **35,** 928.

Crack Formation in Magnesium Oxide Single Crystals†

By R. J. Stokes, T. L. Johnston, and C. H. Li
Minneapolis-Honeywell Research Center, Hopkins, Minnesota, U.S.A.

[Received April 2, 1958]

Abstract

Experimental evidence is presented which lends direct support to the Stroh mechanism for crack formation. After a magnesium oxide crystal was compressed about 3%, it was observed that minute cracks had been formed in the region of a kink band generated by non-homogeneous plastic strain. These cracks lay on conjugate {110} slip planes and not on the usual {100} cleavage planes. They extended in the form of [001] direction slits running right through the crystal.

§ 1. Introduction

Stroh (1954, 1955, 1957) has analysed the nucleation of a crack in terms of the stresses associated with edge dislocations piled up against a barrier. On the basis of this analysis it is to be expected that there will be three factors which govern the formation of cracks in a solid. First, the density and distribution of the obstacles responsible for pile-up which are already present in the material; second, the ease with which new barriers can be formed during plastic deformation; and finally, the ability of the material to relieve the stress field due to a pile-up by further local plastic flow.

That grain boundaries in polycrystalline materials can be effective barriers has been demonstrated by Gilman (1957) using zinc bicrystals. As far as single crystals are concerned, however, little is understood of the nature of the barriers. Sessile dislocations formed as a result of dislocation interaction are not sufficiently stable to support a large pile-up (Stroh 1957). Also, Stokes (1957) has shown that a fixed array of small angle boundaries (formed by annealing a dimple in a zinc single crystal (Washburn 1956) will not support a sufficient pile-up of dislocations to produce a crack during simple shear fatigue.

On the basis of the Stroh theory, it is the shear stress forcing dislocations into the head of the piled-up group which leads to crack nucleation. So far as crack growth in a single crystal is concerned, there are then two possibilities depending upon the nature of the external stress field. In a tensile stress field, providing the Griffith energy and the crack velocity criteria (Mott 1948, Gilman 1956) are satisfied, microcracks will extend and cleavage failure will occur catastrophically. In a compressive stress field the microcrack will remain stable. For this reason it seems advisable to study the problem of crack formation in single crystals during compression.

---

† Communicated by Dr. A. H. Cottrell, F.R.S.

In the work reported here, cracks have been found to originate in kink bands, produced as a result of non-homogeneous compression, in single crystals of magnesium oxide. Crystals of this material have the advantage of being transparent and exhibit stress birefringence under polarized illumination, thereby enabling the internal stress pattern to be examined following plastic strain.

§ 2. EXPERIMENTAL TECHNIQUES

The specimens used in this investigation were cleaved from commercial purity (96–99% MgO) magnorite crystals purchased from the Norton Company. The bulk crystals were slightly amber in colour, and contained a number of small boundaries, otherwise there were no microscopic flaws.

Specimens, having approximate dimensions 10 mm × 2 mm × 2 mm, were deformed in a conventional hard testing machine arranged for compression, after which they were examined on the metallograph.

A successful etching solution was developed for revealing individual dislocations in this material. The solution consisted of: 5 parts of saturated ammonium chloride, 1 part of concentrated sulphuric acid, and 1 part of distilled water. When the crystals were immersed in this solution for $\frac{1}{4}$-hour at room temperature, conical etch pits were produced. Etch pits on two crystal surfaces exposed by cleavage matched one another exactly as shown in fig. 1, Pl. 40, thus confirming the selectivity of the re-agent.

§ 3. EXPERIMENTAL OBSERVATIONS

3.1. *Plastic Flow in Magnesium Oxide at Room Temperature*

By combining metallographic and etch pit techniques, the slip system in magnesium oxide at room temperature has been confirmed to be over $\{110\}$ slip planes in $\langle 110 \rangle$ slip directions, as previously quoted by Schmid and Boas (1935). This is a typical slip mode for crystals having the rock salt structure.

Residual stresses within these transparent cubic crystals could be detected with polarized illumination, so that the slip surfaces were delineated when viewed edge on (Nye 1949). The etch pit distribution pattern confirmed that the stress birefringence resulted from concentrations of edge dislocations on the active slip planes.

Deformation at room temperature led to the appearance of many slip bands of widely varying band width. These slip bands were characterized by being exceptionally straight, similar to those produced on sodium chloride for example. Only at very high magnifications (× 1000) could individual slip lines be resolved within them. At this magnification there was a complete absence of cross slip.

The inherent plasticity of magnesium oxide was readily demonstrated by the following experiment. Particles of 46 mesh silicon carbide were sprinkled from a height of only three inches. Rosettes, of the kind studied by Gilman and Johnston (1957) on lithium fluoride crystals, appeared on etching in the ammonium chloride solution. These rosettes are due to slip dislocations generated under the impact of the tiny carborundum particles (of approximate weight $3{\cdot}6 \times 10^{-4}$ g). Loading a crystal which had been previously sprinkled in this way resulted in the expansion of the dislocation half loops, and as fig. 2, Pl. 40 shows, each slip line passes through a rosette. A more detailed study of the behaviour of individual dislocations in magnesium oxide will be published at a later date.

Recent observations indicate that the mechanical properties of magnesium oxide crystals are sensitive to their surface condition (Lad *et al.* 1958, Gorum *et al.* 1957). In particular, workers at the University of California and elsewhere have shown that freshly cleaved crystals are more ductile than those which have been standing in air for a length of time. In a study of crack formation under a three-point bending load carried out in our laboratories, it was found that specimens *always* plastically deform to a certain extent prior to fracture, irrespective of the time for which the surfaces had been exposed to the atmosphere. While the plastic strain cannot necessarily be detected macroscopically, it is readily visible under the microscope.

Although it is recognized that the state of the surface is an important variable in the fracture behaviour of magnesium oxide, in the work reported below the surface condition was essentially constant. Specimens were allowed to stand in air for six days following cleavage from the bulk crystal before being deformed.

3.2. *Crack Formation*

Figures 3 and 4, Pls. 41 and 42, are photomicrographs taken with polarized illumination on a specimen after compression in the testing machine†. It will be noticed that according to the stress birefringence striations in fig. 3 the crystal lattice was kinked in this region about an [001] axis of rotation, with the plane of the kink parallel to the (110) plane.

Careful examination of the external surface in this kinked region enabled two kinds of cracks to be distinguished. One type was characterized by its short length and the fact that it was situated at the boundary of the kink band. It lay parallel to the [110] direction and thus to the trace of the kink band, as indicated by the arrows in fig. 4 (*e*). This type of crack, for reasons to be given in the discussion (§ 4), will be referred to as a 'Stroh-crack' to distinguish it from the other type, which will be called a

---

† This particular specimen had buckled during compression so that the strain was distinctly non-homogeneous. These photomicrographs were taken in the *most severely compressed* region of the specimen. The crosshead movement was equivalent to an overall strain of 3%.

'secondary crack'. Secondary cracks lay for the most part parallel to the [110] direction and were situated *within* the kink band, as shown in fig. 3. Most of the secondary cracks also had a short segment parallel to and in line with the Stroh-cracks, all delineating the boundary (A–B) of the kink band. It is significant that neither the Stroh-cracks nor the secondary cracks lay along the normal (100) cleavage planes, instead they were formed on the conjugate (110) and (110) slip planes. One of the secondary cracks in fig. 3 (top, right) however, had extended a short distance along the (010) plane at one tip.

A most interesting observation was made when the metallograph was focused beneath the surface of the crystal. It was found that the cracks did not exist merely on the surface but continued right through the specimen. They were, in fact, *tiny slits* extending along the [001] direction normal to the crystal surface, as illustrated in fig. 5. The series of photomicrographs in fig. 4 were taken at different levels beneath the surface using polarized illumination. These show that the two Stroh-cracks extended all the way from one surface to the other. On the other hand, the secondary crack did not, it was tapered and stopped within 20 μ of the far surface.

Fig. 5

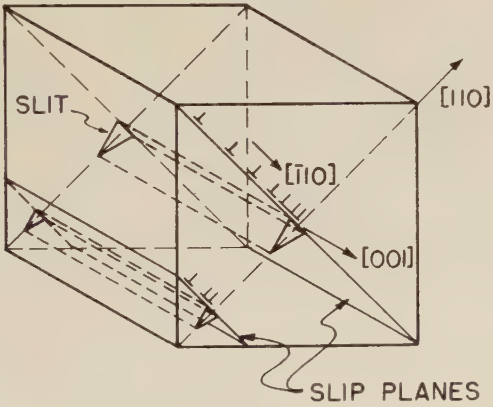

Crystallographic configuration of the slits in fig. 4.

The formation of these slits in compression offered a rare opportunity to observe this phenomenon, for once having formed in a region where the local stresses were tensile there was no tendency for the crack length to increase beyond this region, since the macroscopic stress was compressive. However, if Stroh-cracks nucleate under a macroscopic tensile stress in this material brittle failure may be catastrophic and such tiny slits will be difficult to observe.

A survey of the whole crystal surface indicated that not all of the cracks extended beneath the surface. The one shown in fig. 6 (*a*), Pl. 43, for example, was only a surface crack. This photomicrograph was taken on a region quite separate from that of figs. 3 and 4. Figure 6 (*b*), Pl. 43, was taken on the same area as fig. 6 (*a*) after an attempt had been made to reveal the dislocation distribution near the kink band using the etching solution referred to in § 2. In the case of the severely strained crystal used here, however, the dislocation density was so high that individual etch pits could not be distinguished, instead a uniform stain resulted. Nevertheless, in regions of extremely high residual stress a localized attack did occur giving rise to the 'cracks' shown in fig. 6 (*b*). The interesting fact was that each 'crack' coincided exactly with the region of stress concentration revealed using polarized light in fig. 6 (*a*). Presumably they were the result of a form of stress-corrosion and indicated the position and orientation of Stroh-cracks which would have formed next had loading been continued. Furthermore, they all lay on a straight line as did the Stroh-cracks of figs. 3 and 4, and this line, which presumably delineated the length of the associated kink band, was perpendicular to the 'slip' lines running into the 'cracks'.

§ 4. Discussion

There can be little doubt that the cracks discussed in connection with figs. 3 and 4 all form as a result of the piling up of dislocations associated with one slip system only. An important question then arises, which of the two possible slip systems is actually responsible, the one with its slip planes parallel to the cracks in fig. 3 (having a slip direction $[\bar{1}10]$) or perpendicular to them (having a slip direction [110]) ? In other words, are the cracks the result of slip on a number of planes meeting a common crystallographic barrier (the kink band) or slip on a single plane meeting a number of well-spaced barriers ? Although we have no direct evidence on this point, the most self-consistent picture evolves when the first of these two slip systems is considered responsible. Indeed it is difficult to understand how slip confined to a single plane could develop a number of independent cracks, since as soon as one crack forms, further shear across the plane would preferably enlarge the existing crack rather than generate new ones. Assuming the former case to be correct the configuration of the cracks and the directions of the slits with respect to the planes of crystalline slip represents a direct confirmation of the Stroh analysis. When edge dislocations are forced together at the head of a pile-up, the incipient crack so formed lies perpendicular to the slip plane concerned, this is illustrated diagrammatically in fig. 7. The Stroh-cracks of fig. 4 have an orientation in exact agreement with this mechanism.

It is interesting to consider the nature of the barrier and the eventual crack development. In our opinion, dislocation pile-ups were caused by the kink bands. These kink bands were geometrically necessary for the specimen to conform to the grip constraints and were a direct result of the non-homogeneous strain. Mott (1951) has considered the development of kink bands within a crystal. Initially dislocations of opposite sign pile against a common barrier. This barrier may be the effect of their own stress field interaction or due to imperfections created previously as a result of dislocation interaction on intersecting slip planes. Once a localized lattice curvature has started, its influence spreads to neighbouring planes causing further dislocation pile-up. The end result is a kinked region, shown in fig. 8 (*a*), across which dislocation pile-ups of opposite sign face one another. Further deformation forces more dislocations into this region which becomes more severely kinked and thereby more effective as a barrier.

Fig. 7

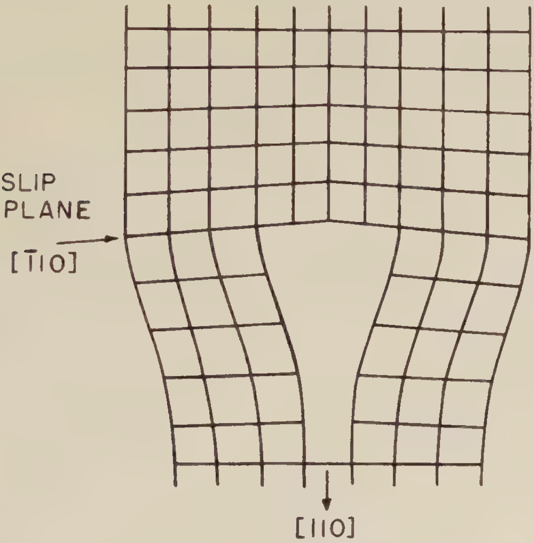

Formation of a Stroh-crack by the coalescence of edge dislocations (after Stroh 1957).

Referring to figs. 3 and 4, we have seen that the Stroh-cracks and the tips of the secondary cracks are all situated accurately on a straight line. This line marks one boundary of the kink band (see fig. 8) which was the crystallographic barrier responsible for dislocation pile-up.

Stroh (1955) has already considered the case of crack nucleation due to piled-up groups on several slip planes. He shows that the equation for nucleation of a stable microcrack is:

$$n\mathbf{b}\sigma_0 = 12\gamma$$

where σ_0 is the applied shear stress over the slip plane; $\mathbf{b}$ is the Burgers vector; γ is the surface energy; and n is the total number of edge dislocations involved. It must be emphasized that it is not necessary for the n dislocations to be concentrated on a single slip plane; they can be distributed over a number of different slip planes. In his calculation the shear stress field around each piled-up group acts on the adjacent ones to assist the applied shear stress in forcing the leading dislocations against the barrier.

By a similar analysis it can be shown that pile-ups of opposite signs distributed as in fig. 8 (*a*) around a kink band will also assist the applied shear stress in nucleating cracks. Indeed the analysis applies for all pile-up distributions formed as the result of an applied shear stress of a given sign. It is for this reason that the kink band is a preferred site, since fewer dislocations per slip band are required for crack nucleation.

Fig. 8

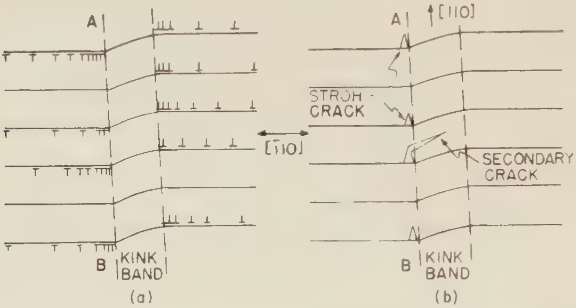

(*a*) The distribution of dislocations around a kink band. (*b*) The position and orientation of the Stroh and secondary cracks around the kink band.

Once the Stroh-cracks have formed perpendicular to their associated slip plane, they then run into the compression stress field of the dislocation pile-up immediately below (see fig. 8 (*b*)) and can extend no further in this direction. This accounts for the comparatively short length ($\sim 5\ \mu$) of the stable Stroh-crack component. They can, however, spread rapidly along the length of the edge dislocation lines, thereby forming a [001] direction slit. A slit is most likely to start from the surface where less surface energy is required for nucleation. Such was the case for the crack illustrated in fig. 6 (*a*).

The Stroh-cracks also increase their length by switching through 90° and advancing into the region within the kink band, as was demonstrated in fig. 3. This can be explained in terms of the normal stresses around the pile-ups. In between two pile-ups of opposite sign tensile stresses may assist one another and cause the Stroh-crack to run into the kink band to form a secondary crack as in fig. 8 (*b*). There is, however, the additional possibility that the cracks may open up due to the residual stresses in the crystal when the compressive load is released.

In terms of these observations, if a single crystal could be deformed homogeneously, deformation bands would not form and fracture would be delayed. Preliminary observations indicate that this may be the case.

Specimens, where particular care was taken in the alignment, were uniaxially compressed by 5%. These specimens were examined carefully for surface cracks but none were detected. It is possible, of course, that a much more severe uniaxial compression would eventually lead to kinking and thence to cracking. Following this line of approach in the future it is hoped to learn more of the mechanism whereby kink bands are developed and thence cracks are formed in these materials.

ACKNOWLEDGMENTS

The authors wish to acknowledge the assistance of Mr. K. H. Olsen throughout this investigation. They are also grateful to Dr. J. J. Harwood of the O.N.R. and to Dr. F. J. Larsen, Director of Research, for continued interest and permission to publish these results. The authors wish to thank the Office of Naval Research for sponsoring the work on which this paper is based.

REFERENCES

GILMAN, J. J., 1956, *J. appl. Phys.*, **27,** 1262 ; 1957, Fall Meeting A.I.M.E., Chicago.

GILMAN, J. J., and JOHNSTON, W. G., 1957, *Dislocations and Mechanical Properties of Crystals* (Lake Placid Conference Report), p. 116.

GORUM, A. E., PARKER, E. R., and PASK, J. A., 1957, Paper presented at Fall Meeting, American Ceramic Society (Basic Science Div.).

LAD, R. A., STEARNS, C. A., and DEL DUCA, M. G., 1958, Acta Metall. (to be published).

MOTT, N. F., 1948, *Engineering*, **165,** 16 ; 1951, *Proc. phys. Soc. Lond.* B, **64,** 729.

NYE, J. F., 1949, *Proc. roy. Soc.* A, **198,** 190.

SCHMID, E., and BOAS, W., 1935, *Kristallplastizitat* (Berlin : Springer).

STOKES, R. J., 1957, *O.N.R. Report*, University of California (to be published).

STROH, A. N., 1954, *Proc. roy. Soc.* A, **223,** 404 ; 1955, *Ibid.*, **232,** 548 ; 1957, *Advance Phys.*, **6,** 418.

WASHBURN, J., 1956, *J. of Metals,* **8,** 189.

Polarization Measurements of Gamma Radiation from Sulphur-34[†]

By G. G. SHUTE[‡] and P. S. FISHER[§]
Department of Physics, University of Birmingham

[Received April 21, 1958]

ABSTRACT

Polarization measurements have been made on the gamma cascade in ^{34}S. The experimental results are consistent with a spin sequence 2^+, 2^+, 0^+ with a mixture of M1 and 1·5% of E2 in the first transition. The theoretical analysis of polarization–direction correlations with mixing included is discussed in some detail. Shell model assignments for the gamma cascade are given with possible explanations of the mixing ratio value obtained.

§ 1. INTRODUCTION

THE angular correlation of the gamma cascade in ^{34}S has been studied by Handler and Richardson (1956) and by Fisher and Shute[||] (1957). Both these measurements assigned spins and parities 2^+, 2^+, 0^+ to the levels shown in fig. 1, the first transition being an M1, E2 mixture. The theoretical and experimental values of the A_4 coefficient (see I) were, however, only just within acceptable statistical limits and the polarization measurements reported in this paper were made to check the spin sequence and mixing previously found. The general techniques used in polarization correlation experiments are well known but special problems arise in the study of ^{34}S because of the short half-life of the parent ^{34}Cl ($32\frac{1}{2}$ min) and because of the presence of abundant annihilation radiation.

§ 2. POLARIZATION–DIRECTION CORRELATION MEASUREMENTS

The polarization correlation for a gamma-ray cascade is given by Biedenharn and Rose (1953) in the form

$$W(\theta, \phi) = \eta_1 W_1(\theta, \phi) + \eta_2 W_2(\theta, \phi).$$

Here θ is the angle between the direction of emission of the cascade gamma-rays and ϕ is the angle between the electric vector of the gamma-ray entering the polarimeter and the normal to the plane contained by the gamma-rays of the cascade. η_1 is the efficiency for detecting one gamma-ray in the polarimeter and measuring the direction of the other. $W_1(\theta, \phi)$ is the corresponding correlation function. η_2 and $W_2(\theta, \phi)$ are the corresponding quantities for the reverse measurement.

[†] Communicated by the Authors.

[‡] 1956 Travelling scholar from the University of Melbourne.

[§] Now at Palmer Physical Laboratory, Princeton University, New Jersey.

[||] Referred to as I in the following paper.

Fig. 1

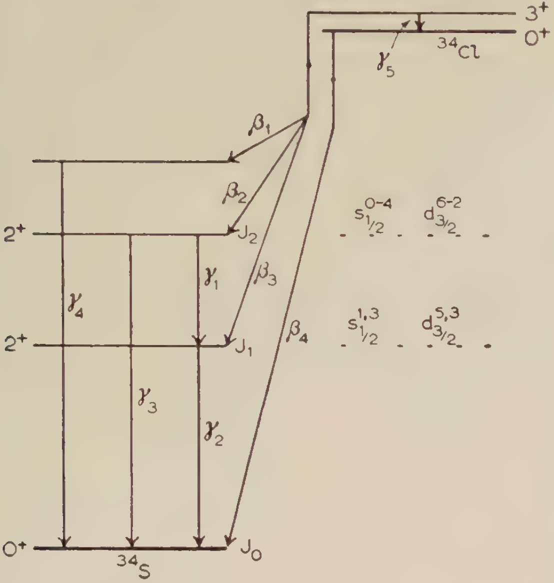

γ	E (Mev)	%	α
1	1·16	15	
2	2·10	39	
3	3·22	7	
4	4·0	0·2	
5	0·145	38	0·14

α is the conversion coefficient

β	$E_{\max}$ (Mev)	%	log ft
1	0·53	0·1	> 5·6
2	1·33	26	4·82
3	2·48	28	6·08
4	4·50	46	3·50

The decay scheme of ^{34}Cl to ^{34}S. The shell model assignments to the second and first excited states of ^{34}S are included. References to this decay scheme are given in I.

As pointed out by Bishop and Yorba (1955) all the necessary information about the polarization of a selected gamma-ray may be expressed by stating the intensities $W(\frac{1}{2}\pi, \frac{1}{2}\pi)$ and $W(\frac{1}{2}\pi, 0)$ in the linear polarizations parallel and perpendicular respectively, to the plane containing the cascade gamma-rays and we call $p = W(\frac{1}{2}\pi, \frac{1}{2}\pi)/W(\frac{1}{2}\pi, 0)$ the maximum degree of plane polarization.

To analyse this polarization, the polarimeter relies on Compton scattering. Gamma radiation incident on the polarimeter tends to be scattered in the plane perpendicular to its electric vector. This can be seen from the differential cross section given by the Klein–Nishina formula for scattering of an incident quantum of energy k_0 through an angle δ with an angle ψ between the direction of polarization of the incident gamma ray and the plane of scattering

$$\frac{d\sigma}{d\Omega} = \frac{e^4}{2m^2C^4}\frac{k^2}{k_0{}^2}\left[\frac{k}{k_0} + \frac{k_0}{k} - 2\sin^2\delta\cos^2\psi\right].$$

Here k is the energy of the scattered quantum

$$k = \frac{k_0}{1 + (k_0/mC^2)(1 - \cos\delta)}.$$

The number of gamma-rays scattered into the horizontal plane, defined by the two gamma-rays of the cascade, will be given by

$$N_H\,d\Omega = H\,d\Omega = W(\tfrac{1}{2}\pi, \tfrac{1}{2}\pi) \times d\sigma_{\psi=0} + W(\tfrac{1}{2}\pi, 0) \times d\sigma_{\psi=\frac{1}{2}\pi}$$

and similarly the number in the vertical plane will be

$$N_V\,d\Omega = V\,d\Omega = W(\tfrac{1}{2}\pi, \tfrac{1}{2}\pi) \times d\sigma_{\psi=\frac{1}{2}\pi} + W(\tfrac{1}{2}\pi, 0) \times d\sigma_{\psi=0}.$$

The ratio $R = d\sigma_{\psi=\frac{1}{2}\pi}/d\sigma_{\psi=0}$ is a measure of the analysing efficiency and it follows that $H/V = (p+R)/(1+pR)$. R depends on both the geometry of the polarimeter and the energy of the gamma-ray (Metzger and Deutsch 1950), while p depends only on the theoretical correlation. For quanta of energy of 1·2 MeV, R has its maximum value for a scattering angle $\delta = 77°$.

§ 3. APPARATUS

The apparatus for the polarization–direction measurements was based upon the angular correlation apparatus described in I. For the polarization studies one of the simple sodium iodide detectors was replaced by an analyser for plane polarized radiation based on the polarimeters used by Metzger and Deutsch and by Bishop and Yorba.

Fig. 2

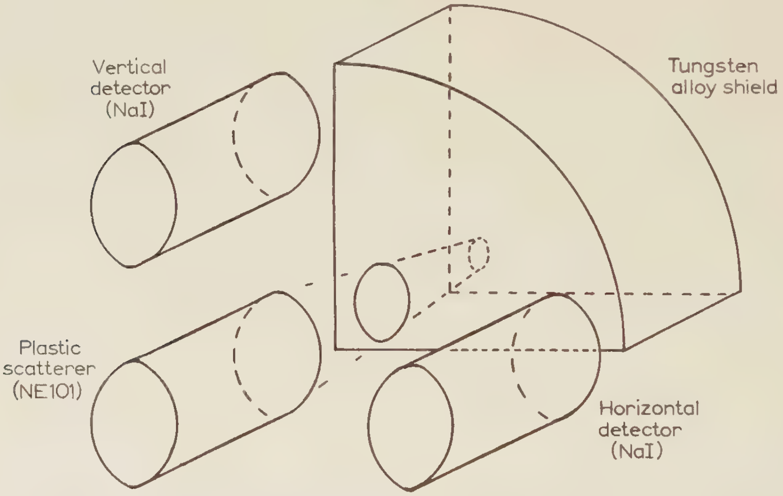

Schematic view of polarimeter showing the arrangement of the detectors and the shield.

The polarimeter is shown in fig. 2. Radiation scattered from the plastic scintillator may enter either of the two side detectors (one horizontal and the other vertical) which are well shielded by 3 in. of tungsten alloy (density 18 g cm^{-3}) from the direct radiation. The plastic scintillator (NE101), $1\frac{1}{2}$ in. in diameter and 2 in. long was attached to a 9514 photomultiplier. The side detectors were standard $1\frac{1}{2}$ in. diameter and 1 in. long NaI(Tl) crystals mounted on 6260 photomultipliers and positioned parallel to the scatterer as shown in the figure.

To form the horizontal triple coincidence output, *H*, one gamma ray of the cascade was detected by the directional counter and the other was scattered in the plastic scintillator. The outputs of these two detectors formed the fast–slow system (of resolving time 10^{-8} sec) discussed in the preceding paper (I). The output from this combination was then placed in slow coincidence with the single counts from the horizontal detector.

Fig. 3

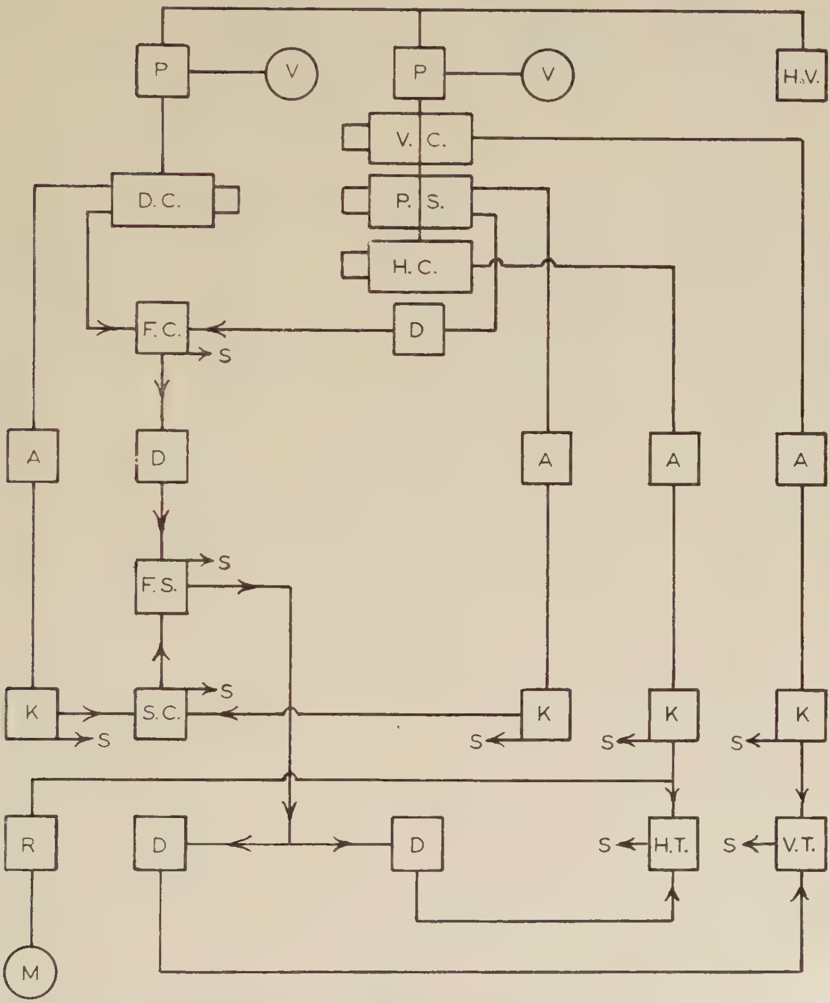

Block diagram of the electronics. The meaning of the symbols used is as follows: A = linear amplifier; D = delay; D.C. = directional counter; F.C. = fast coincidence; F.S. = fast-slow coincidence; H.C. = horizontal counter; H.T. = horizontal triples; H.V. = high voltage supply; K = kicksorter; M = ammeter; P = potentiometer; P.S. = plastic scintillator; R = ratemeter; S = scaler; S.C. = slow coincidence; V = voltmeter; V.C. = vertical counter; V.T. = vertical triples.

Similarly the vertical triple coincidences, V, were formed by having the fast–slow output in coincidence with the vertical detector independently of the horizontal one. The resolving time of all slow units was 10^{-6} sec.

Fig. 4

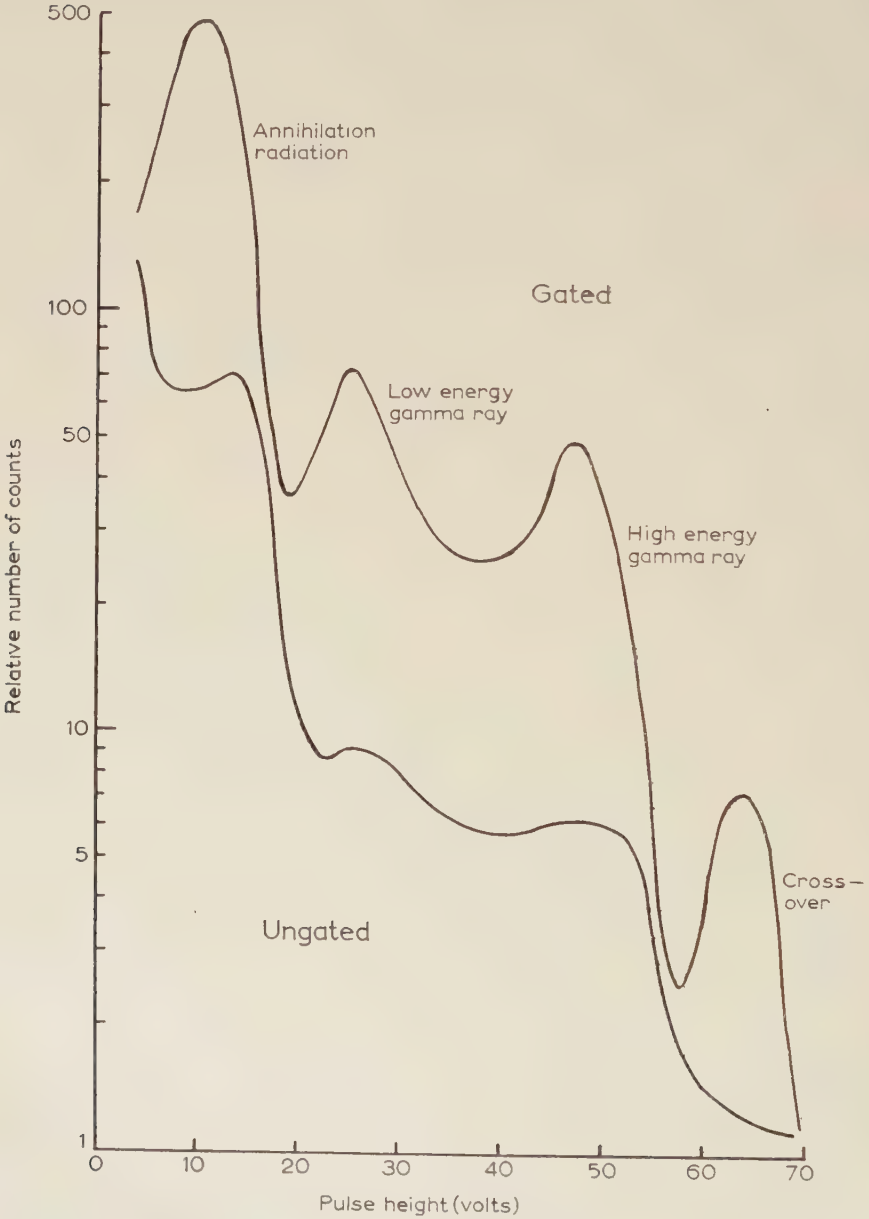

Spectra of ^{34}S in the plastic scintillator. The top curve shows the output gated by that from a side counter. The bottom curve is ungated.

Provision for making random runs was made by switching a delay into one of the fast arms. A block diagram of these pulse height selection and coincidence circuits is shown in fig. 3.

Energy selection of the gamma ray detected in the polarimeter was achieved by the method of Bishop and Yorba. The spectrum in the plastic scintillator was gated by the scattered gamma ray pulses from the side counter being considered. As the scattering angle is relatively well defined, the scattered quantum has a defined energy and the gated spectrum in the plastic resembles that in a Compton spectrometer. Figure 4 shows both the gated and ungated spectrum of ^{34}S in the plastic. Despite the large amount of annihilation radiation present it is possible to select the 1·16 and 2·10 MEV radiation from ^{34}S quite well by this method.

§ 4. OBSERVATIONS

As in the angular correlation experiment, I, ^{34m}Cl† was formed according to the reaction $^{32}\mathrm{S}+{}^{4}\mathrm{He}\rightarrow{}^{34m}\mathrm{Cl}+p+n$ by bombarding a natural sulphur target with an external beam of 40 MEV He^{2+} ions from the Nuffield cyclotron. The target which was about 2 mm thick, adhered to a copper backing and was covered during bombardment by a thin tantalum foil (0·0003 in.) cooled by an air blast. Bombardments of 0·5 μA for 20 min. provided sources of convenient strength. No additional activities comparable in intensity with that of the Cl activity were observed after the lapse of a few minutes from the end of bombardment and therefore it was possible to use the bombarded sulphur directly as the source without chemical extraction of the Cl activity. The sulphur was scraped from the target and placed in a thin walled (0·002 in.) brass cylinder 1/16 in. in diameter and $\frac{3}{8}$ in. long, extending from a 2 B.A. threaded brass rod.

As the half life of ^{34m}Cl is $32\frac{1}{2}$ min a new source was prepared every half hour and the initial source strength was adjusted to 0·2 mc before sealing and placing in the target holder centred between the directional counter and the polarimeter. This initial activity was measured by a ratemeter attached to one of the side counters. Such a source gave a real to random ratio of 6 to 1.

The pulse height analysers of both the directional counter and the polarimeter were set to cover the energy range 0·7 to 2·5 MEV. These settings were decided by preliminary runs which indicated that as the detection process involved triple coincidences, the overall efficiency was so low that both gamma rays had to be included in each detector. This does not destroy the advantage of energy selection in the polarimeter because the 2 to 1 ratio of the energy of the gamma rays in the cascade (see fig. 1) causes the efficiency, η_1, for detecting the low energy gamma ray in the polarimeter and high energy gamma ray in the directional counter to be much greater than that for the reverse measurement, η_2.

---

† The '*m*' means we are referring to the isomeric level.

These efficiencies were determined by using a planimeter to measure the relative areas of the gamma ray profiles on the spectra obtained in the polarimeter and in the directional counter. It was found that $\eta_1 = 9\eta_2$.

Observations were made in the positions $\theta = \frac{1}{2}\pi$ and $\theta = \pi$. In the first p has its maximum value. As the gamma rays do not define any plane when $\theta = \pi$, H should be equal to V and so the actual counting rates obtained can be used to normalize the $\theta = \frac{1}{2}\pi$ runs. As the mean energy of the gamma ray entering the polarimeter is $1/10 \times 2{\cdot}10 + 9/10 \times 1{\cdot}16$ or 1·26 MeV which is also the mean energy of the gamma rays in the ^{60}Ni cascade, the latter was used for the normalization runs.

In the $\theta = \frac{1}{2}\pi$ position 10 000 triple coincidences were recorded at an average rate of 2 counts a minute. In the $\theta = \pi$ position, higher counting rates were easily attained with the ^{60}Ni and 40 000 triple coincidences were recorded at an average rate of 15 counts a minute. No changes were required to the energy settings for the ^{60}Ni runs. The only changes were to the source and the angle setting of the directional counter.

The result obtained was

$$H/V = (H/V)_{\pi/2}/(H/V)_{\pi} = 0{\cdot}842 \pm 0{\cdot}023$$

where the quoted error is the standard deviation obtained only from the actual counts used. The advantage obtained in using simultaneous detection of H and V is that with the easy normalization using ^{60}Ni, the number of cyclotron bombardments needed to obtain this accuracy was halved. During the course of the experiment about 100 targets were bombarded.

The polarimeter was calibrated by using the gamma ray cascades in ^{60}Ni and ^{106}Pd with the following results

$$R = 1{\cdot}88 \pm 0{\cdot}12 \text{ at } 1{\cdot}25 \text{ MeV}$$

and

$$R = 2{\cdot}40 \pm 0{\cdot}09 \text{ at } 0{\cdot}57 \text{ MeV}.$$

The predictions of the Klein–Nishina formula for point geometry are 2·40 and 4·55 respectively. A preliminary run on the gamma ray cascade in ^{88}Sr gave satisfactory agreement with theory.

§ 5. THEORETICAL ANALYSIS

The theoretical analysis of the polarization correlation with the first gamma ray mixed has been given by Biedenharn and Rose as

$$W(\theta, \phi) = \eta_1 W_1(\theta, \phi) + \eta_2 W_2(\theta, \phi)$$

where now $W_1(\theta, \phi)$ is the polarization correlation when the polarization of the mixed radiation is measured and $W_2(\theta, \phi)$ when the polarization of the pure radiation is measured. Now $W_1(\theta, \phi)$ can be reduced to the form

$$W_1(\theta, \phi) = \omega_1 + \delta^2\omega_{11} + 2\delta\omega_{111}$$

where δ^2 is the mixing ratio and ω_1 and ω_{11} are the correlation functions for the pure cascades and ω_{111} is the interference term. If invariance under time reversal is valid, δ is real. The functions may be written

$$\omega_1 = 1/(2J_1+1)(-1)^{J_0+J_2-2J_1}\sum_{\nu} Z_1(L_1J_1L_1J_1;\, J_2\nu)$$
$$\times Z_1(L_2J_1L_2J_1;\, J_0\nu)\mathscr{P}_\nu(L_1L_1;\, \theta\phi)$$
$$\omega_{11} = 1/(2J_1+1)(-1)^{J_0+J_2-2J_1}\sum_{\nu} Z_1(L'_1J_1L'_1J_1;\, J_2\nu)$$
$$\times Z_1(L_2J_1L_2J_1;\, J_0\nu)\mathscr{P}_\nu(L'_1L'_1;\, \theta\phi)$$

and

$$\omega_{111} = 1/(2J_1+1)(-1)^{J_0+J_2-2J_1}\sum_{\nu} Z_1(L_1J_1L'_1J_1;\, J_2\nu)$$
$$\times Z_1(L_2J_1L_2J_1;\, J_0\nu)\mathscr{P}_\nu(L_1L'_1;\, \theta\phi).$$

The Z_1 coefficients have been tabulated in a convenient form by Sharp *et al.* (1954). The function $\mathscr{P}_\nu$ is the equivalent for the polarization correlation of the Legendre polynomial in standard angular correlation theory and is given by Biedenharn and Rose as

$$\mathscr{P}_\nu(LL;\, \theta\phi) = P_\nu(\cos\theta) + (-1)^{\sigma(L)}$$
$$\times \frac{(\nu-2)!}{(\nu+2)!}\,\frac{2\nu(\nu+1)L(L+1)}{\nu(\nu+1)-2L(L+1)}\cos 2\phi P_\nu^2(\cos\theta)$$

where $\sigma(L)$ is the intrinsic parity of the multipole (0 for electric and 1 for magnetic). The function $\mathscr{P}_\nu$ for the interference term is given in this formulation by

$$\mathscr{P}_\nu(LL';\, \theta\phi) = P_\nu(\cos\theta) + (-1)^{\sigma(L')}\frac{(\nu-2)!}{(\nu+2)!}$$
$$\times (L'-L)(L'+L+1)\cos 2\phi P_\nu^2(\cos\theta).$$

For $W_2(\theta, \phi)$ where the polarization of the pure radiation is measured, the only change to the above is that all the $\mathscr{P}_\nu$ are replaced by $\mathscr{P}_\nu(L_2L_2;\, \theta\phi)$.

Thus from these formulae the value of $p = W(\frac{1}{2}\pi, \frac{1}{2}\pi)/W(\frac{1}{2}\pi, 0)$ can be calculated for a given spin sequence and mixing parameter (cf. § 2).

§ 6. COMPARISON WITH EXPERIMENT

Before the correlation above can be compared with the experiment, the corrections for solid angle have to be applied to the theoretical value of p. The procedure given by Rose (1953) was considered sufficiently accurate for this experiment. The attenuation factors as given by Rose were evaluated as $Q_0 = 1$, $Q_2 = 0{\cdot}89$ and $Q_4 = 0{\cdot}70$†. To apply these factors to the polarization correlation, the associated Legendre polynomials in this correlation were broken up into a series of Legendre polynomials.

$$P_2^2(\cos\theta) = 2 - 2P_2(\cos\theta)$$
$$P_4^2(\cos\theta) = 2 + 10P_2(\cos\theta) - 12P_4(\cos\theta).$$

---

† If an angular correlation function is $A_0 + A_2P_2(\cos\theta) + A_4P_4(\cos\theta)$ and this is attenuated to $A_0 + A'_2P_2(\cos\theta) + A'_4P_4(\cos\theta)$ then $Q_0 = 1$, $Q_2 = A'_2/A_2$ and $Q_4 = A'_4/A_4$.

With the small but significant efficiency of each detector for the abundant annihilation radiation resulting from the annihilation of the positrons there is obviously a small isotropic contribution to the correlation. This was determined experimentally as in I. The efficiency of the polarimeter and directional counter for this radiation was measured by setting one on the annihilation peak and leaving the other unaltered. The rise in counting rate at $\theta=\pi$ then gives the efficiency of the unaltered detector. The isotropic component was estimated as 16 ± 1% in $W(\theta, \phi)$.

Table 1

J_2	J_1	J_0	δ'	$(H/V)'$	δ	H/V	Mixture type	
1^+	1^+	0^+	−2·094	1·37	−0·477	1·37	M1	E2
1^-	1^-	0^+	−2·094	1·42	−0·477	1·44	M1	E2
1^+	1^-	0^+	−2·094	0·73	−0·477	0·73	E1	M2
1^-	1^+	0^+	−2·094	0·70	−0·477	0·69	E1	M2
$\mathbf{2^+}$	$\mathbf{1^+}$	$\mathbf{0^+}$	**7·73**	**0·82**	0·451	0·97	**M1**	**E2**
$\mathbf{2^-}$	$\mathbf{1^-}$	$\mathbf{0^+}$	**7·73**	**0·87**	0·451	1·03	**M1**	**E2**
2^+	1^-	0^+	7·73	1·22	0·451	1·03	E1	M2
2^-	1^+	0^+	7·73	1·15	0·451	0·97	E1	M2
$\mathbf{3^+}$	$\mathbf{1^-}$	$\mathbf{0^+}$	**−13·12**	**0·83**	0·710	1·03	**M2**	**E3**
3^-	1^+	0^+	−13·12	0·78	0·710	0·97	M2	E3
3^+	1^+	0^+	−13·12	1·21	0·710	0·97	E2	M3
3^-	1^-	0^+	−13·12	1·28	0·710	1·03	E2	M3
$\mathbf{2^+}$	$\mathbf{2^+}$	$\mathbf{0^+}$	**0·126**	**0·82**	—	—	**M1**	**E2**
$\mathbf{2^-}$	$\mathbf{2^-}$	$\mathbf{0^+}$	**0·126**	**0·87**	—	—	**M1**	**E2**
2^+	2^-	0^+	0·126	1·22	—	—	E1	M2
2^-	2^+	0^+	0·126	1·15	—	—	E1	M2
3^+	2^+	0^+	−0·767	1·19	—	—	M1	E2
3^-	2^-	0^+	−0·767	1·24	—	—	M1	E2
$\mathbf{3^+}$	$\mathbf{2^-}$	$\mathbf{0^+}$	**−0·767**	**0·84**	—	—	**E1**	**M2**
$\mathbf{3^-}$	$\mathbf{2^+}$	$\mathbf{0^+}$	**−0·767**	**0·81**	—	—	**E1**	**M2**
3^-	3^-	0^+	−0·055	0·72	—	—	M1	E2
3^+	3^+	0^+	−0·055	0·75	—	—	M1	E2
3^-	3^+	0^+	−0·055	0·31	—	—	E1	M2
3^+	3^-	0^+	−0·055	0·36	—	—	E1	M2

This table lists all the levels schemes consistent with the angular correlation experiment (I). The value of H/V listed is to be compared to the experimental value of 0·842 ± 0·023.

In I the spins of the states of ^{34}S allowed by the directional correlation experiment are tabulated, together with suggested values of the mixing parameter, δ for the first transition. The corresponding values expected for the ratio H/V (cf. § 2) are found from the theoretical prediction of p corrected as above and from the experimentally determined R (cf. § 4). These values are given for all possible parity combinations with the selected spin sequences in table 1. The cascades which seem consistent with the observed H/V of 0·842 ± 0·023, i.e. which lie between the values 0·89 and 0·80 are in heavy type in table 1. To obtain the values for the cascades 3, 2, 0 which gave no real solutions for δ when the value of $A_2 = 0{\cdot}332$ was used, the value $A_2 = 0{\cdot}300$ which is one standard deviation away, was used. The mixing ratio used for 2, 2, 0 is a mean of that obtained by Handler and Richardson (1·7%) and in I (1·4%). The mixture considered in the table is always that between the lowest order multipoles allowed by the spin and parity values.

§ 7. Discussion

In the arguments presented in I for assigning the spin sequence 2^+, 2^+, 0^+ to the levels of ^{34}S, it was assumed that the beta decay of ^{34m}Cl(3^+) to the first and second excited state of ^{34}S was allowed. The *ft*-value for the decay to the first excited state is however just consistent with first forbidden decay and the schemes allowed by the polarization experiment have been examined with this possibility in view as well.

Table 2

J_2	J_1	J_0	Beta decay to J_2	Beta decay to J_1
2^+	1^+	0^+	Allowed	2nd forbidden
2^-	1^-	0^+	1st forbidden	1st forbidden
2^+	2^+	0^+	Allowed	Allowed
2^-	2^-	0^+	1st forbidden	1st forbidden
3^+	1^-	0^+	Allowed	1st forbidden
3^+	2^-	0^+	Allowed	1st forbidden
3^-	2^+	0^+	1st forbidden	Allowed

In this table the beta decay from the 3^+ level in ^{34m}Cl to each level has been classified for each parity and spin assignment allowed by this experiment. Experimentally, it is known that the decay to J_2 is allowed and that to J_1 is either allowed or 1st forbidden.

The evidence is summarized in table 2. It is known experimentally (see fig. 1) that the ratio of the intensity of the crossover to the first gamma ray is 7/15. In table 3 are presented the theoretical values (Moszkowski) for the mixing ratio and the above intensity ratio as well as the experimental values.

It seems reasonable to assume on the evidence presented in tables 2 and 3 that the only acceptable cascade is 2^+, 2^+, 0^+. This sequence requires only the assumption of slight mixing $(1\frac{1}{2} \pm \frac{1}{2})\%$ to bring experimental and theoretical correlations into agreement. Both the mixing and relative intensity of the crossover seem favourable. Beta decay to the 2^+ levels from the 3^+ level in ^{34m}Cl would be an allowed Gamow–Teller transition agreeing with the *ft* values. Both the 2^+ assignments are in reasonable agreement with even–even nuclei systematics. In view of this evidence we must conclude that the slight difference between the observed and calculated values of A_4 (see I) is not significant.

Morinaga and Bleuler (1956) have assigned the *jj*-coupling shell model schemes to the levels in ^{34}S, as shown on fig. 1, from the beta decay rates to these levels from ^{34}P and ^{34}Cl. The scheme given applies to the 2 protons and 4 neutrons outside the $d_{5/2}$ shell which closes at ^{28}Si, and these particles will then be in the $s_{1/2}$ or $d_{3/2}$ state. The second excited state, and the 3^+ isomeric level in ^{34}Cl are assumed to have either four $s_{1/2}$ and two $d_{3/2}$ particles or six $d_{3/2}$ particles, whereas the first excited state and the ^{34}P ground state, should consist of one to three $s_{1/2}$ particles and five to three $d_{3/2}$ particles. If the M1 transition between the second and first excited state were due solely to the transition of a single particle, then as it would be $d_{3/2} \rightarrow s_{1/2}$ or $s_{1/2} \rightarrow d_{3/2}$ it would be 'l-forbidden' (Mayer and Jensen 1955, or Moszkowski 1955).

Table 3

J_2 J_1 J_0	δ^2	Mixture type	Theoretical mixing	Cross-over	Theoretical ratio
2^+ 1^+ 0^+	$6{\cdot}0 \times 10^1$	M1 E2	$7{\cdot}6 \times 10^{-4}$	E2	$1{\cdot}6 \times 10^{-1}$
2^- 1^- 0^+	$6{\cdot}0 \times 10^1$	M1 E2	$7{\cdot}6 \times 10^{-4}$	M2	$1{\cdot}1 \times 10^{-2}$
2^+ 2^+ 0^+	$1{\cdot}6 \times 10^{-2}$	M1 E2	$7{\cdot}6 \times 10^{-4}$	E2	$1{\cdot}6 \times 10^{-1}$
2^- 2^- 0^+	$1{\cdot}6 \times 10^{-2}$	M1 E2	$7{\cdot}6 \times 10^{-4}$	M2	$1{\cdot}1 \times 10^{-2}$
3^+ 1^- 0^+	$1{\cdot}7 \times 10^{-2}$	M2 E3	$2{\cdot}1 \times 10^{-4}$	M3	$3{\cdot}4 \times 10^{-2}$
3^+ 2^- 0^+	$5{\cdot}9 \times 10^{-1}$	E1 M2	$1{\cdot}0 \times 10^{-6}$	M3	$3{\cdot}3 \times 10^{-8}$
3^- 2^+ 0^+	$5{\cdot}9 \times 10^{-1}$	E1 M2	$1{\cdot}0 \times 10^{-6}$	E3	$1{\cdot}9 \times 10^{-7}$

In this table the experimental mixing ratio δ^2 (the ratio of the intensity of the higher order multipole to the lower) is given in column 2. This is to be compared to the theoretical single particle estimate in column 4. Column 6 gives the theoretical value for the ratio of the crossover intensity to that of the lower order multipole. The experimental value for this ratio is 7/15 (see fig. 1).

As the mixing ratio is 20 times larger than the single particle estimate and the crossover intensity is 3 times larger than expected on this model for $2^+ 2^+ 0^+$ (see table 3), we find that we can explain these values as shell model phenomena by introducing the l-forbiddeness as discussed above. The alternative description furnished by the Bohr and Mottelson model is that there will be collective enhancement of the E2 radiation from the second excited state. The values quoted above seem reasonable either as an estimate of the reduction in the dipole matrix element or as an estimate of the collective quadrupole matrix element. On the whole, as the evidence for the shell model classification of the states seems quite sound it would seem as though the mixing experienced in ^{34}S is a shell model phenomenon rather than a collective one.

ACKNOWLEDGMENTS

We wish to thank Professor W. E. Burcham for his continued interest in this project. The authors are also grateful for private communications with G. R. Bishop and C. F. Coleman concerning details of their own polarimeters. We would also like to acknowledge the assistance of J. Lowe with the measurements.

REFERENCES

BIEDENHARN, L. C., and ROSE, M. E., 1953, *Rev. mod. Phys.*, **25,** 749.
BISHOP, G. R., and YORBA, J. P., 1955, *Phys. Rev.*, **98,** 89.
FISHER, P. S., and SHUTE, G. G., 1957, *Phil. Mag.*, **2,** 1255.
HANDLER, H. E., and RICHARDSON, J. R., 1956, *Phys. Rev.*, **102,** 833.
MAYER, M. G., and JENSEN, J. H. D., 1955, *Elementary Theory of Nuclear Shell Structure* (New York : John Wiley), p. 209.
METZGER, F., and DEUTSCH, M., 1950, *Phys. Rev.*, **78,** 551.
MORINAGA, H., and BLEULER, E., 1956, *Phys. Rev.*, **103,** 1423.
MOSZKOWSKI, S. A., 1955, *Beta and Gamma Ray Spectroscopy* ed. by K. Siegbahn (Amsterdam : North Holland Publishing Co.), p. 385, equation 54,
ROSE, M. E., 1953, *Phys. Rev.*, **91,** 610.
SHARP, W. T., KENNEDY, J. M., SEARS, B. J., and HOYLE, M. G., 1954, *A.E.C.L. Report* No. 97, C.R.T. 556.

The Effect of Stacking Fault Energy on Low Temperature Creep in Pure Metals†

By P. R. Thornton and P. B. Hirsch
Crystallographic Laboratory, Cavendish Laboratory, Cambridge

[Received April 1, 1958 ; and in revised form April 16, 1958]

Abstract

Experimental results obtained by studying the low temperature creep behaviour before and after a small stress change are interpreted in terms of barriers due to intersecting dislocations. Using the data available on the temperature dependence of the flow stress in conjunction with these experimental results, estimates of jog energies are derived and compared with values obtained from flow stress data alone. Relative dislocation widths for various metals are also deduced. From the theoretical analysis relating dislocation width to stacking fault energy, tentative values are suggested for the stacking fault energies of Au, Ag, Al, Ni, Pb, Zn, Cd, Co and Pt, relative to that of Cu. These values are in reasonable agreement with previous estimates where available, thus confirming the hypothesis that low temperature creep is controlled by the proposed mechanism.

The significance of these results is discussed in terms of the exhaustion and work hardening theories of low temperature creep. It is shown that the experimental observation that the apparent activation energy is insensitive to stress and pre-strain can be explained quite naturally on theories based on stress-aided activation and that it does not invalidate such theories.

§ 1. Introduction

The temperature dependence of the flow stress and transient creep in f.c.c. and h.p.c. metal crystals have been interpreted in terms of a process of dislocations cutting through a 'forest' of intersecting dislocations (Cottrell 1953, Seeger 1954, Friedel 1956). Seeger has developed an expression which can be applied to both the flow stress and the creep data, and which involves the jog energy and the width of a dislocation as parameters. The present paper describes experiments designed to determine the jog energies and relative dislocation widths in a number of metals. Values of stacking fault energies can be deduced from these results, and the general agreement obtained between these results and previous estimates confirms the correctness of the proposed mechanism.

§ 2. Theory

The application of rate process theory to a dislocation model for creep gives the creep rate $\dot{\epsilon}$ as:

$$\dot{\epsilon} = NAb\nu_0 \exp(-U/kT) \qquad (1)$$

---

† Communicated by the Authors.

where N is the number of dislocation elements per unit volume contributing to creep, A the area swept out by a dislocation element after thermal activation, b the Burgers vector, ν_0 an atomic frequency and U an apparent activation energy. Experimental studies of the variation of creep rate with time indicate that $\dot{\epsilon}$ may be expressed as:

$$\dot{\epsilon}=C/t^n \qquad . \ . \ . \ . \ . \ . \ . \ . \ . \ . \ . \quad (2)$$

with the parameters C and n depending on the test temperature, the applied stress, the defects present in the metal and their distribution. It has been shown experimentally that for many polycrystalline metals the form of (2) applicable to low temperatures is:

$$\dot{\epsilon}\simeq C/t \qquad . \ . \ . \ . \ . \ . \ . \ . \ . \ . \ . \quad (3)$$

(Smith 1948, Wyatt 1953, Olds 1954). In the region where (3) is obeyed, i.e. in logarithmic creep, it follows from (1) and (3) that:

$$U=kT\log \nu t \qquad . \ . \ . \ . \ . \ . \ . \ . \ . \ . \quad (4)$$

where $\nu=NAb\nu_0/C.$

In recent years U has been measured directly by comparing creep rates before and after a small abrupt change in temperature (Sherby *et al.* 1957, Landon *et al.* 1957, Lytton *et al.* 1957,† Haeszner and Krause 1957). U is found to be insensitive to stress and pre-strain at a particular temperature. The significance of these results will be discussed in § 5, but it should be stated in passing that the present authors believe that no experimental evidence exists which conflicts with theories of low temperature creep based upon stress-aided activation. Before U can be expressed in terms of the applied stress a realistic model for the barriers impeding flow in low temperature creep must be chosen.

Experimental studies of the flow stress as a function of temperature have been interpreted, in the low temperature region, in terms of barriers due to intersecting dislocations (Cottrell 1953, Seeger 1954, Friedel 1956). The barriers operative in low temperature creep are also thought to be these 'forest' dislocations. In f.c.c. and h.c.p. metals the dislocations lying in close packed planes are dissociated into partial dislocations with a stacking fault ribbon between them. (Cottrell 1953, Read 1953). Before such dislocations can cross each other the stacking fault ribbon must become constricted at the point of intersection. Part of the energy U_0 required for the process of intersection is due to the energy of the constrictions and part is due to the energy of jogs or kinks produced as a result of the intersection. In the presence of an opposing internal stress and an applied stress the activation energy, U, will be equal to U_0 minus the work done by the difference of the applied and internal stresses in moving the dislocations across each other, so that

---

† These papers by Dorn and his coworkers will be referred to in future as Dorn *et al.* (1957 a, b and c).

$$U=U_0-l_f.b.D.(\tau-\tau_g). \quad \ldots \ldots \quad (5)$$

where l_f is the average distance between 'forest' dislocations, D, the activation distance, i.e. the distance travelled by the moving dislocation in surmounting the barrier, τ the average resolved shear stress in the slip direction, τ_g the average opposing internal shear stress resolved in the slip direction and v $(=l_f bD)$ is called the activation volume.

In the absence of a more complete analysis of the crossing mechanism the process of intersection is thought to be as shown in fig. 1; fig. 1 (*a*) shows the dislocation ribbons when they are just touching, figs. 1 (*b*) and (*c*) show the configurations obtained by increasing the applied stress. Consideration of such diagrams indicates that

Fig. 1

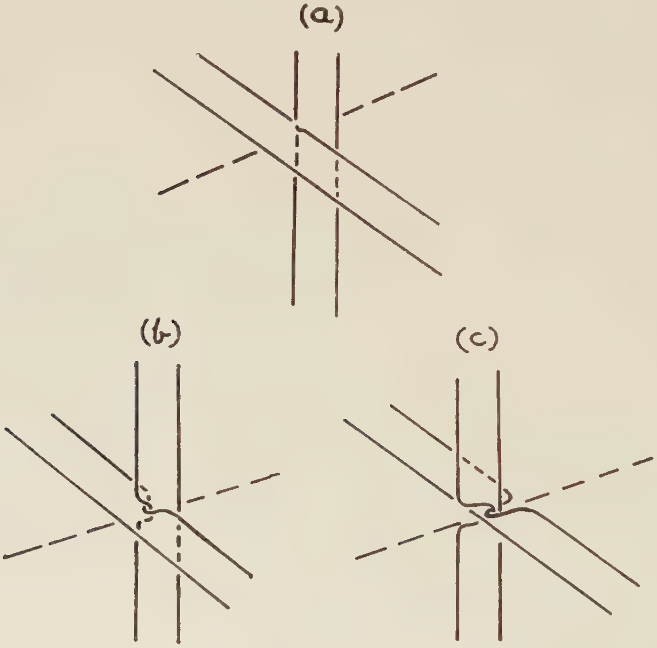

Intersection of two dislocations showing the increasing degree of constriction at the intersection as two extended dislocations are forced together by an applied stress.

$$D \simeq d_1+d_2,$$

where d_1 and d_2 are the effective widths of the two dislocations (see Appendix (A)).

From (4) and (5) we obtain:

$$kT \log \nu t = U_0 - v(\tau - \tau_g). \quad \ldots \ldots \quad (6)$$

Suppose that the applied stress τ is changed by a small amount $\Delta\tau$ at a constant temperature; then

$$kT \Delta \log \nu t = -v \Delta\tau. \quad \ldots \ldots \quad (7)$$

provided the stress change is small, so that v and τ_g may be regarded as constant. Multiplying (7) by τ gives

$$v\tau = -kT\tau\Delta(\log \nu t)/\Delta\tau. \quad \ldots \ldots \quad (8a)$$

If the applied tensile stress is σ, the fractional change in the resolved shear stress ($\Delta\tau/\tau$) may be equated to the fractional change in the applied tensile stress ($\Delta\sigma/\sigma$). Equation (8*a*) becomes

$$v\tau = -kT\Delta(\log \nu t)\sigma/\Delta\sigma. \quad \ldots \ldots \quad (8b)$$

Hence by changing the applied stress slightly during a creep test, the quantity $v\tau$ can be studied. Experiments designed to give relative values of D for different metals and to test the basic mechanism of logarithmic creep are described in the following section. Such experiments were first performed by Wyatt (1953) on polycrystalline copper and discussed by Cottrell (1953) in terms of barriers due to intersecting dislocations.

§ 3. Increment Tests on Polycrystalline Pure Metals

3.1. *Experimental Method*

Bright-drawn wires of pure metals (Johnson, Matthey) were heat-treated to obtain recrystallization with a small grain size. Electropolished creep specimens of diameter approximately 0·5 mm and gauge length 5 cm were prepared and loaded into self-aligning friction grips on a constant stress creep machine. The stress constancy was obtained by use of a linear spring. Apart from the controlled change in stress, the specimens were crept under conditions of constant stress. The strain sensitivity was 2×10^{-5}. Temperature control, in these short time tests, was obtained by use of constant temperature baths; liquid nitrogen, solid CO_2 in acetone and ice/water mixture. A stirred water bath in a large Dewar vessel was satisfactory at room temperature. The temperature remained constant to within $\pm 0{\cdot}25$°c for several hours. Figure 2 indicates the experimental procedure.

Each specimen was crept at a low stress σ for five to ten minutes and the creep curve recorded photographically. A small change $\Delta\sigma$ was made and the creep behaviour recorded for a further ten minutes. This procedure was repeated at a series of increasing stresses throughout the range of logarithmic creep. Each specimen gave a value of $v\tau$ at each stress level used. Successive specimens were crept at the same stresses but with increments of different magnitude. $\Delta \log \nu t$ was obtained from a plot of strain against log time on which the curve subsequent to the increment is moved along the axis of $\log t$ until its slope is equal to that of the initial curve (see fig. 3).

3.2. *Experimental Results*

Figure 4 shows the experimental results for Au, while table 1 summarises the results obtained to date.

In each case $v\tau$ was insensitive to stress, pre-strain and, with one exception, independent of the size of increment or decrement used. This

Fig. 2

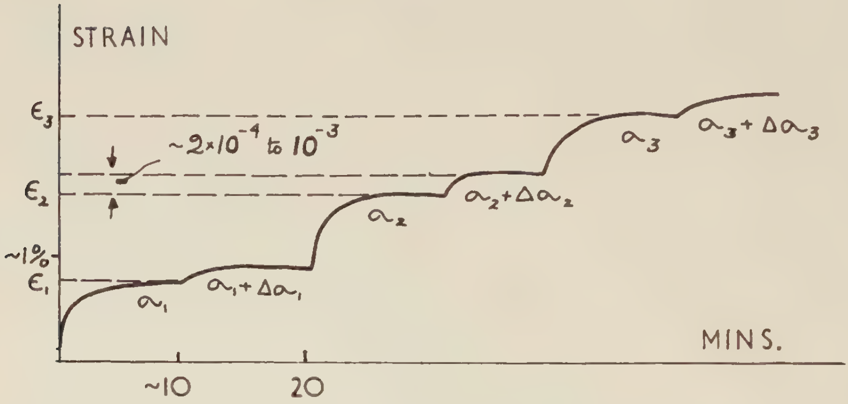

Illustration of the creep tests performed on one specimen.

Fig. 3

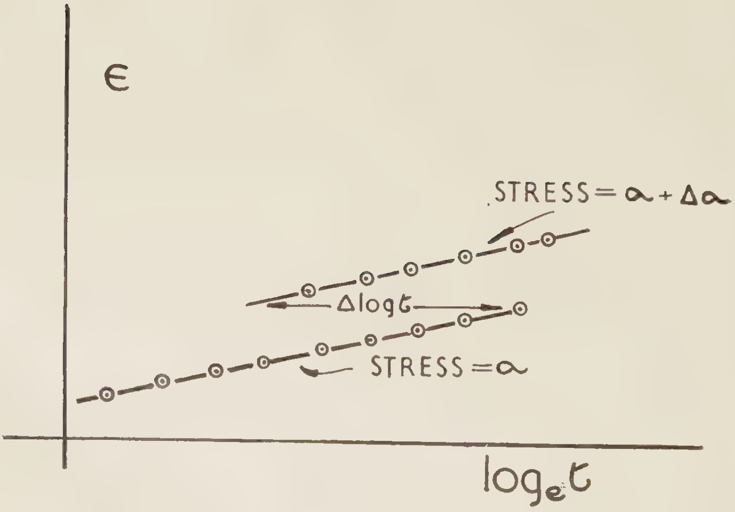

Method of obtaining $\Delta \log t$.

Fig. 4

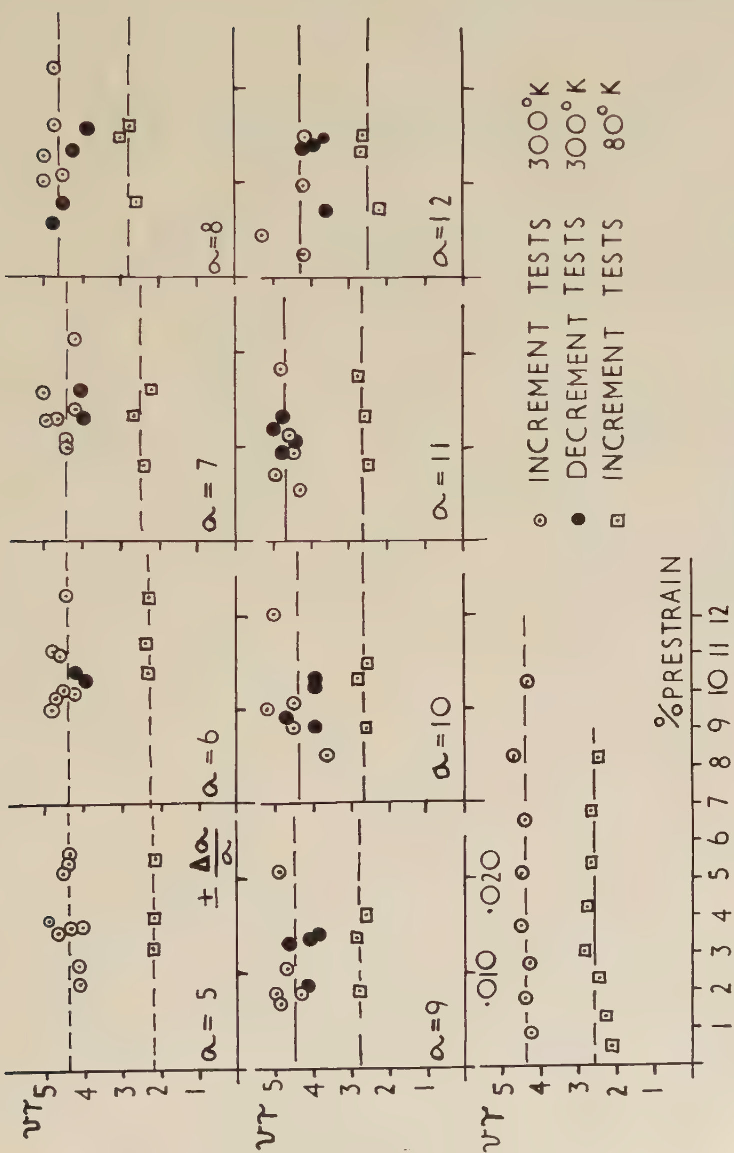

Experimental values of $(v\tau)$ in (ev) for polycrystalline Au.

exception was Ni in which the value of $v\tau$ increased significantly with increment at the lower stresses used. The reason for this difference is not understood. In this case the curve of $v\tau$ against $\Delta\sigma/\sigma$ was extrapolated to $\Delta\sigma/\sigma=0$ and the value of $v\tau$ so obtained quoted in table 1. In the case of Cu and Au where measurements were carried out at several temperatures a dependence of $v\tau$ on temperature was found.

Table 1. Values of $v\tau$ from Creep Increment Tests on Polycrystalline Pure Metals

Metal	Temp. (°K)	$v\tau$ (ev)	Stress-levels used (kg mm^2)	No. of specimens used
Cu	300	$5{\cdot}0\pm0{\cdot}5$	6 to 18	10
Cu	80	$4{\cdot}2\pm0{\cdot}4$	8 to 20	4
Au	300	$4{\cdot}4\pm0{\cdot}3$	5 to 12	10
Au	80	$2{\cdot}7\pm0{\cdot}3$	5 to 12	2
Pt	300	$9{\cdot}0\pm1{\cdot}0$	8 to 15	2
Ni	300	$6{\cdot}7\pm0{\cdot}6$	14 to 28	9
Co	300	$5{\cdot}6\pm0{\cdot}5$	35 to 70	9
Ag	300	$4{\cdot}5\pm0{\cdot}5$	6 to 13	10
Zn	80	$1{\cdot}0\pm0{\cdot}2$	3 to 6	2
Al	80	$0{\cdot}9\pm0{\cdot}2$	2 to 5	2
Pb	80	$1{\cdot}3\pm0{\cdot}5$	1 to 3	1
Cd†	80	$1{\cdot}4\pm0{\cdot}3$	single cryst. $\tau=0{\cdot}3$	1

† Taken from Glen (1956)

§ 4. DISCUSSION OF RESULTS

4.1. *Dislocation Distributions*

Equation (6) may be written

$$U_0+v\tau_g=v\tau+U=v\tau+kT\log\nu t. \quad . \quad . \quad . \quad . \quad . \quad (9)$$

The results of Dorn and his coworkers show that U is insensitive to stress and pre-strain (see § 5 for full discussion) and the present results indicate that $v\tau$ is also independent of stress and pre-strain. It follows from (9) that $v\tau_g$ is likewise independent of strain, since U_0 is a constant.

We may write

$$\tau_g = \alpha Gb/l_g \quad . \quad . \quad . \quad . \quad . \quad . \quad . \quad . \quad . \quad . \quad (10)$$

where α is a constant which may depend on the geometry of the dislocation arrangement, l_g is a dislocation length or separation corresponding to the dislocations responsible for τ_g, and G is a shear modulus. Hence

$$v\tau_g = bDl_f\tau_g = \alpha Gb^2Dl_f/l_g. \quad . \quad . \quad . \quad . \quad . \quad . \quad . \quad (11)$$

On current theories of work-hardening of f.c.c. metals (Seeger *et al.* 1957), l_g is considered to be the average distance between dislocations or groups of dislocations on the primary slip system. (These dislocations will be referred to as the 'primary' dislocations.) This distance l_g is therefore not necessarily the same as l_f, the distance between 'forest' dislocations. It appears from the strain independence of $v\tau_g$ however that $\alpha l_f/l_g$ is a constant. A similar result has also been deduced by previous workers from flow stress measurements (see below). The interpretation of this result is not clear. If the dislocation arrangement remains similar during the deformation, but changes only in scale, α will be constant, and on this interpretation the constancy of $\alpha l_f/l_g$ implies that the density of 'forest' dislocations increases proportionately to that of the 'primary' dislocations with increasing deformation. (This will be referred to as the 'Cottrell–Stokes' law.) It is possible however that τ_g represents the long range stress due to the same 'forest' dislocations as are responsible for l_f in which case l_g may be equal to l_f. In the absence of a proper analysis of the interaction between intersecting dislocations it is not possible to decide between these and other possibilities. However, whatever the correct explanation may be, since $\alpha l_f/l_g$ is constant, we may write

$$v\tau_g = \alpha_g Gb^2D \quad . \quad . \quad . \quad . \quad . \quad . \quad . \quad . \quad . \quad . \quad (12)$$

where α_g is a constant (for further discussion see § 6).

4.2. *Relationship of the Present Results to Measurements of the Temperature Dependence of the Flow Stress*

The flow stress of a metal is considered to be the sum of two contributions: a temperature independent part due to the internal stress τ_g and a temperature dependent part due to 'forest' dislocations. Using Seeger's theory of the temperature dependence of the flow stress (Seeger 1954) and neglecting Friedel's modification (Friedel 1956), the flow stress is given by

$$\tau/\tau_g = 1 + U_0/v\tau_g + (kT/v\tau_g)\ln(\dot{\epsilon}/NAb\nu_0) \quad . \quad . \quad . \quad (13a)$$

for $T < T_c$ where $T_c = U_0/k\log(\dot{\epsilon}/NAb\nu_0)$ and

$$\tau = \tau_g \text{ for } T \geqslant T_c. \quad . \quad . \quad . \quad . \quad . \quad . \quad . \quad . \quad (13b)$$

This is indicated in fig. 5.

By measuring the relative flow stress at a series of temperatures Adams and Cottrell (1955) and Cottrell and Stokes (1955) showed that in single crystals of both copper and aluminium τ/τ_g is independent of the strain. It follows from (13 *a*) that $v\tau_g$ is constant, as pointed out above. Cottrell and Stokes (1955) also found the same value of τ/τ_g for polycrystals as for single crystals. In the following sections it will be assumed that this result is true for all other metals.

4.3. *The Energy for Jog Formation*

From the temperature dependence of the flow stress it is possible to obtain values of $U_0/v\tau_g$; putting $T=0°\text{K}$ in (13 *a*) leads to the expression:

$$\tau_0/\tau_g=1+U_0/v\tau_g. \qquad (14)$$

By rearranging (6) we obtain

$$v\tau_g(U_0/v\tau_g+1)=v\tau+kT\log\nu t. \qquad (15)$$

The frequency term ν can be determined for Al, Cu and Ni from the results of Dorn *et al.* (see § 5). The value obtained ($10^x\ \text{sec}^{-1}$ where $x=10{\cdot}5\pm1{\cdot}5$) is roughly the same for all three metals. This value is assumed for the other metals studied; it is unlikely to be greatly in error and since $kT\log\nu t$ is small compared to $v\tau$ the uncertainty in ν is not important here. Using (14) and (15) values of both U_0 and $v\tau_g$ can be derived. Unfortunately flow stress measurements are not yet available for all the metals studied. The available values are listed in table 2. Values derived from sparse data are indicated by an asterisk. The values of $U_0/v\tau_g$ for the low stacking fault energy metals (Cu, Au and probably Ni) are somewhat uncertain for two reasons: (1) τ_g is taken to be the value of τ in the temperature range 400 to 600°K, where apparently τ has little, if any, dependence on temperature; however, the true value of τ_g may be a little lower

Fig. 5

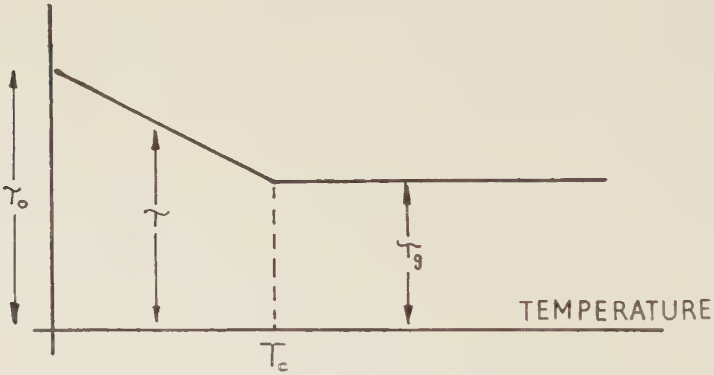

Temperature dependence of the flow stress shown schematically.

(Seeger 1955a). (2) The curve of τ *vs* T is more complex for Cu than is shown in fig. 5 (Adams and Cottrell 1955); an average extrapolation of this curve to $T=0°\text{K}$ gives the value quoted in table 2. The possible errors in the values of both $v\tau$ and of $U_0/v\tau_g$ lead to uncertainties in the values of U_0 and $v\tau_g$, indicated in tables 3 and 4. In table 3 values of U_0 are compared and found to be in reasonable agreement with approximate values given by Friedel (1956), whose values were derived from (13*a*) by making plausible assumptions for $Nab\nu_0$ and inserting the experimentally determined value of T_c. A further comparison may be made with a theoretical estimate as follows. A study of the crossing process shows that in addition to two constrictions, two lengths $\sim b_1$ and b_2 of dislocation line must be formed (b_1 and b_2) are the Burgers vectors of the intersecting

Table 2. Values of $(1+U_0/v\tau_g)$ from Flow Stress Measurements

Metal	$1+U_0/v\tau_g$	Source
Cu	$1{\cdot}2 \pm 0{\cdot}08$	Adams and Cottrell (1955)
Au	$1{\cdot}35 \pm 0{\cdot}1$	Seeger (1954), data of Andrade and Henderson
Ni	$1{\cdot}5 \pm 0{\cdot}13$	Seeger (1954), data of Andrade and Henderson
Ni	$1{\cdot}20 \pm 0{\cdot}05$	Haasen (1958)†
Cd	$3{\cdot}8 \pm 0{\cdot}2$	Seeger (1954), data of Boas and Schmid
Pb	$2{\cdot}4 \pm 0{\cdot}4$	Lander and Howard‡ (1936)
Zn	$2{\cdot}5 \pm 0{\cdot}2$	Seeger (1954), data of Schmid and Fahrenhorst
Al	1·40	Cottrell and Stokes (1955)
	2·5	Seeger (1954), data of‡ Rosi and Mathewson
Co	(1·2)	Assumed
Pt	(1·35)	Assumed
Ag	(1·2)	Assumed

† Data kindly supplied by Dr. Haasen prior to publication.
‡ Limited data.

dislocations). These will be kinks or jogs depending on the orientation and Burgers vectors of the dislocations considered (Cottrell 1953). The total increase in dislocation length is, to a first approximation, the same for all possible orientations and Burgers vectors. The total energy will therefore vary with orientation only through the energy of formation of the constrictions, which may depend somewhat strongly on orientation. Thus the values of U_0 derived above probably represent the energy required to form constrictions in two dislocations of average orientation, plus the energy to form, for example, two jogs, i.e. U_0 is nearly twice the energy to form a constricted jog in a dislocation of average orientation. Thus the experimental values quoted in table 3 can be compared directly with the theoretical values obtained by Friedel (Friedel 1956).

Table 3. Estimates of U_0 obtained from: (i) Combination of Creep and Flow Stress Data, (ii) Flow Stress Data alone, (iii) Friedel's Calculation

Metal	Temp. (°K)	U_0 (ev) From creep and flow stress data	U_0 (ev) From flow stress data	U_0 (ev) Calculated
Cu	300	1·0 ± 0·5	0·7	2·6
	80	0·7 ± 0·35	0·7	1·9
Au	300	1·3 ± 0·5	0·8	2·1
	80	0·8 ± 0·35	0·8	1·1
Ni	300	1·5 ± 0·6	0·8	2·9
Cd	80	1·1 ± 0·3	0·8	0·3
Zn	80	0·7 ± 0·25	0·6	0·3
Al	80	0·5 ± 0·35	0·3	0·2
Pb	80	0·85 ± 0·50	0·3	0·25

If the values of the dislocation widths given in § 4.4 of this paper are used in Friedel's equation, the estimates listed in the final column of table 3 are obtained. In general these calculated values are of the same order of magnitude as those determined experimentally. It should be emphasized that these experimental values of the jog energy $\frac{1}{2}U_0$ are of the order of $\frac{1}{2}$ to 1 ev.

4.4. *Interpretation of* $v\tau_g$

Using the values of tables 1 and 2 estimates of $v\tau_g$ are obtained and are shown in table 4. For Co, Pt and Ag values of $1 + U_0/v\tau_g$ are not available.

Comparison of the plastic behaviour of these metals with Cu, Ni and Au suggests the values which are given in brackets in table 2 and which will be assumed in the subsequent discussion. In § 4.1, it was shown that

$$v\tau_g = \alpha_g G b^2 D = \alpha_g G b^2 (d_1 + d_2) \quad . \quad . \quad . \quad . \quad . \quad . \quad (16)$$

where d_1 and d_2 are the effective widths of the two dislocations. In Appendix (A) it is shown that the volume average ($\bar{D}$) of the activation distance can be expressed in terms of the width (d) of a dislocation line which makes an angle of 45° with its Burgers vector. Assuming that in f.c.c. metals both dislocations lie in close-packed planes and are therefore extended,

$$\bar{D}_{\text{f.c.c.}} = 2d.$$

Table 4. Values of (*a*) $v\tau_g$ obtained from Creep and Flow Stress Data (*b*) Relative Dislocation Widths (N) and Estimates of Stacking-Fault Energy (γ)

Metal	Temp. (°K)	$v\tau_g$ (ev)	$G \times 10^{-11}$ (dynes, cm^2)	$N_{\text{exp'tal}}$	Most probable values and limits of stacking fault energy (γ) (ergs/cm^2)
Cu	300	$4\cdot95 \pm 0\cdot8$	4·5	8·5†	40†
Cu	80	$3\cdot5 \pm 0\cdot55$	4·6	$6\cdot1 \pm 1\cdot9$	$45 < 57 < 80$
Au	300	$3\cdot85 \pm 0\cdot6$	2·7	$7\cdot9 \pm 2\cdot4$	$24 < 33 < 47$
Au	80	$2\cdot15 \pm 0\cdot3$	2·8	$3\cdot9 \pm 1\cdot2$	$50 < 65 < 90$
Ni	300	$5\cdot6 \pm 0\cdot7$	7·8	$6\cdot3 \pm 2\cdot0$	$64 < 95 < 140$
Cd	80	$0\cdot41 \pm 0\cdot11$	2·0	$1\cdot1 \pm 0\cdot5$	> 130
Pb	80	$0\cdot6 \pm 0\cdot3$	0·75	$2\cdot5 \pm 1\cdot3$	$25 < 50 < 140$
Zn	80	$0\cdot48 \pm 0\cdot14$	3·9	$1\cdot0 \pm 0\cdot45$	> 250
Al	80	$0\cdot61 \pm 0\cdot25$	2·7	$0\cdot7 \pm 0\cdot4$	> 200
Co	300	$5\cdot3 \pm 1\cdot0$	5·20	$18\cdot5 \pm 6\cdot9$	$22 < 26 < 36$
Pt	300	$7\cdot25 \pm 1\cdot4$	6·2	$7\cdot6 \pm 2\cdot7$	$56 < 69 < 110$
Ag	300	$3\cdot8 \pm 0\cdot8$	2·9	$7\cdot2 \pm 2\cdot6$	$26 < 35 < 58$

† Assumed. The uncertainties quoted represent the probable experimental error ; no estimate of the uncertainty due to the approximation used in the analysis relating dislocation width and stacking fault energy has been included in the limits shown for γ.

In h.c.p. metals the forest dislocations are assumed to lie in pyramidal and prismatic planes and are assumed to be unextended, whence

$$\bar{D}_{\text{h.c.p.}} = d+b.$$

Defining $N=d/b$ we obtain from eqn. (16)

$$v\tau_g/Gb^3=\alpha_g\,2N \quad \text{(f.c.c. metals)} \quad . \quad . \quad . \quad . \quad . \quad (17\,a)$$

while

$$v\tau_g/Gb^3=\alpha_g(N+1) \quad \text{(h.c.p. metals).} \quad . \quad . \quad . \quad (17\,b)$$

In § 4.1 it was shown experimentally that α_g is a constant independent of pre-strain. The constancy of $v\tau_g$ with respect to pre-strain indicated that α_g is independent at least of the scale of the dislocation distribution. If the assumption is now made that α_g is independent of the geometry of the dislocation distribution and of the temperature, relative values of N for different metals can be calculated from the given experimental data. Such values of N are shown in table 4, where a value of $N=8{\cdot}5$ has been assumed for Cu at room temperature†. This assumption is based on calculations due to Seeger and Schoeck (1953) who showed that the widths may be considerably different for dislocations in the screw and edge orientations. Assuming a value of 40 ergs/cm² for the stacking fault energy, these authors obtain for Cu $N_{\text{edge}}=12$ and $N_{\text{screw}}=5$. If these values are accepted, a reasonable estimate for a dislocation of average orientation in Cu is $N=8{\cdot}5$; while no great accuracy can be claimed for dislocation widths derived in this manner, these values are generally in agreement with estimates derived from theoretical considerations, work-hardening characteristics and twin boundary energies. This agreement lends support to the view that the assumed mechanism for logarithmic creep is correct.

It is of interest to calculate the magnitude of α_g from eqn. (17 a). Inserting the values applicable to Cu at room temperature, α_g is found to be approximately 0·1. If τ_g is due to the internal stress of the 'primary' dislocations, it would seem reasonable to expect α (in eqn. (10)) to be about $1/2\pi$; hence it follows from eqn. (12) that $l_g \sim l_f$. Thus it appears on this interpretation that in the regions where the activation is occurring the densities of dislocations on the primary and secondary system are approximately equal. If the dislocations on the primary system occur in piled-up groups, as expected for example on Seeger's theory of work-hardening (Seeger *et al.* 1957), $l_p \sim nl_f$, where l_p is the spacing between groups and n is the number of dislocations per pile-up. In this case the density of dislocations of the secondary system is $\sim n$ times that of the primary system, a rather unlikely result. It seems that there is at present no satisfactory explanation of this experimental result (see however § 6).

4.5 *Stacking Fault Energies*

Estimates of the stacking fault energies (γ) can be obtained from the observed values of the dislocation widths.

---

† In these calculations we have used average shear moduli for f.c.c. metals and $1/s_{44}$ for hexagonal metals.

Seeger and Schoeck (1953) and Seeger (1955 a) have carried out detailed calculations of dislocation widths as a function of the stacking fault energy and elastic constants. The calculations are based on the Peierls model of a dislocation and take the crystal anisotropy fully into account. Full numerical calculations have been completed only for Cu, Co, Ni and Al; however estimates of the dislocation widths as a function of stacking fault energy in the other metals studied can be obtained from the analysis of Seeger and Schoeck by an approximate method. The approximation involved concerns the parameter χ (see Seeger and Schoeck) for which the isotropic value is taken, instead of the value obtained by full consideration of the anisotropy. An estimate of the error introduced by this approximation was made by comparing the values obtained by the approximate method for Co, Cu, Ni and Al with those obtained by Seeger and Schoeck using the full analysis. The maximum difference was found† to be 20%. In table 4 we have shown for each metal the value of the stacking fault energy which has to be assumed to obtain agreement between experimental and calculated estimates of the dislocation widths. Taking into account the errors in the experiments (which are reflected in the limits of stacking fault energy given in table 4) and the uncertainties in the calculations, these values can be considered to be in satisfactory agreement with previous estimates where available. Thus Cu, Ag and Au all appear to have similar low stacking fault energies, as expected from theoretical considerations (Seeger 1955 a, b).

The value of 95 ergs/cm^2 for Ni is in good agreement with the value of 90 ergs/cm^2 estimated by Haasen (1958) from an interpretation of the temperature dependence of the onset of stage III of the work-hardening curve for single crystals. The comparatively small (but rather inaccurately determined) value for Pb was at first sight surprising, but is confirmed by the fact that observations in this laboratory indicate that annealing twins occur rather more frequently in Pb than in Al, which is a typical metal of high stacking fault energy. For Al, Zn and Cd only lower limits could be determined, but it is clear that these metals have high stacking fault energies. The value for Co appears to be rather higher than expected from data on the martensitic transformation (Seeger 1955 a), but it is quite possible that the constant α_g, assumed to be the same for all metals, may in fact have a different value for the hexagonal metals.

A further consequence of assuming α_g to be independent of temperature is the apparent dependence of dislocation width on temperature in Au and Cu (see table 4). It is possible that this dependence is due to a significant entropy contribution to the free energy of an extended dislocation. This contribution has hitherto been neglected. Both the entropy due to the stacking fault and that due to the partial dislocations should be taken into account. Assuming isotropic elasticity, the approximate width of an extended dislocation is given by

---

† In these calculations values of the shear moduli called G_{fr} by Seeger and Schoeck have been used, except for Pt for which the value for the polycrystalline metal had to be assumed. These values are not the same as those shown in table 4, which are used to derive N from $v\tau_g$.

$$d = \frac{gb_1^2}{2\pi K'} \left\{ \gamma_0 - \left(S\gamma + \frac{\partial S_d}{\partial d} \right) T \right\} \quad . \quad . \quad . \quad . \quad . \quad . \quad (18)$$

where K' is a function of Poisson's ratio, b_1 is the Burgers vector of the partial dislocation, γ_0 and S_γ are the energy and entropy of a stacking fault, and $\partial S_d/\partial d$ represents the rate at which the entropy of the two partial dislocations (S_d) varies with their separation (d). It is not clear at present which of the two entropy contributions would be the more important. However, it is expected that for large d, S_γ is important, while for very small d, $\partial S_d/\partial d$ may make the larger contribution. Since the Debye temperatures for both Au and Cu lie between the temperatures at which creep measurements were made, $(S_\gamma + \partial S_d/\partial d)$ is probably temperature dependent. However, the average value of $(S_\gamma + \partial S_d/\partial d)$ between 80 and 300°K is found to be 0·114 ergs/cm²/°K for Au and 0·0544 ergs/cm²/°K for Cu. These values are somewhat larger than the value of S_γ for Co of 0·0228 ergs/cm²/°K estimated from the martensitic transformation. It is hoped that experiments at present being carried out on the temperature dependence of $v\tau_g$ for Co will lead to a clarification of this point.

§ 5. THE RELATIONSHIP BETWEEN THE PROPOSED INTERPRETATION AND FORMAL THEORIES

The discussion in the preceding sections deals with the interpretation of the activation energy for logarithmic creep in terms of the 'forest' hardening. This interpretation taken by itself does not lead to a prediction of the dependence of creep rate on time. Two formal theories have been put forward in explanation of logarithmic creep. (*a*) The exhaustion theory (Mott and Nabarro 1948, Smith 1948, Cottrell 1953, Mott 1953); (*b*) The 'work-hardening' theory, (Orowan 1947, Mott 1953, Seeger 1954).

On the former theory, the metal is thought to contain dislocation barriers of different heights and during the course of creep, the dislocation elements hindered by low barriers move first. If no replenishment occurs they become exhausted with a resultant increase in activation energy with time. The theory leads to logarithmic creep with an activation energy given by

$$U = kT \log \nu_0 t$$

where ν_0 is the atomic frequency.

On the work hardening theory, the activation energy is taken as proportional to the creep strain, whence

$$U = kT \log \nu t$$

with

$$\nu = \nu_0 (Nbl^2 B\theta)/kT\sigma_0$$

where N is the number of elements per unit volume, l the average distance between forest dislocations, B the jog energy, θ the strain hardening coefficient and σ_0 the applied stress.

The two theories are similar in the sense that for both there is an activation energy characteristic of any given time during the creep curve, and that this activation energy increases gradually with time, in one case because the elements of lower activation energy become exhausted, in the other because the internal stress increases gradually and therefore the activation energy, which is assumed stress dependent, also increases with time.

On the exhaustion theory, the activation energy is independent of stress and pre-strain and since $\nu_0 \sim 10^{12}\,\mathrm{sec}^{-1}$ (as the activation is expected to take place in a small volume around the constriction, see (§ 2), the variation with time will be small, possibly too small to detect even in a long time creep test (see below). On the work-hardening theory, it is not possible to determine whether ν should be strain dependent or not. Inserting reasonable values for the parameters, ν is again found to be large, and U is therefore insensitive to time.

Dorn and his collaborators (1957 a, b, c) have found the apparent activation energy U by direct measurement. These workers claim that U is independent of pre-strain, stress, time and creep strain. With regard to the dependence of U on time and creep strain, it should be emphasized that such a dependence is very difficult to detect experimentally. For consider the case in which the maximum creep rate measurable is $\dot{\epsilon}_1$, while the minimum observable creep-rate is $\dot{\epsilon}_2$. Let the times at which these rates occur be t_1 and t_2, while the corresponding activation energies are U and $U+\Delta U$. From eqn. (1) we obtain

$$\log(\dot{\epsilon}_1/\dot{\epsilon}_2) = \Delta U/kT,$$

where ΔU is the change in activation energy necessary to account for the change in creep rate observed. A study of the results of Dorn *et al.* (1957 a) shows that these workers used $\dot{\epsilon}_1/\dot{\epsilon}_2 \sim 10^2$. Thus the expected change ΔU is approximately $5kT$, which, judging from the experimental error, would be very difficult to detect. A detectable change in U, say $12kT$, involves measurement of $\dot{\epsilon}_1/\dot{\epsilon}_2$ up to 10^5. Since t_2/t_1 would be 10^5, tests over periods much longer than hitherto are required. Hence the claim of Dorn *et al.* that the apparent absence of a dependence of U on time or creep strain invalidates the present theories of logarithmic creep cannot be accepted. In fact it is possible that the results of Dorn *et al.* (1957 a) shown in table 5 do indeed indicate a dependence of U on time, although it is not clear whether the trend is significant. Values of ν obtained by using eqn. (4) are also shown; the average value of $\nu \sim 10^{10\cdot5 \pm 1\cdot0}$ is in good agreement with the predictions of the creep theories above.

With regard to the dependence of U on applied stress or pre-strain, it is clear that similar arguments apply. Whatever the dislocation distribution, the activation energy for those dislocations contributing to creep at a given temperature is essentially constant over the range of time or creep rates so far considered. In terms of eqn. (5) for U, this means that the quantity $v(\tau-\tau_g)$ must be constant, independent of pre-strain or stress. This quantity has a very simple physical interpretation. Consider the dislocation loop held back by two intersecting 'forest' dislocations as shown in fig. 6. The equilibrium form of the dislocation loop is given by

$$\tau-\tau_g=Gb/2R=(Gb/l_f)\sin\alpha_0\sim Gb\alpha_0/l_f. \qquad (19a)$$

if α_0 is small, where R is the radius of curvature of the dislocations and α_0 the angle indicated. Hence, for f.c.c. metals,

$$v(\tau-\tau_g)=Gb^3 2N\alpha_0. \qquad (19b)$$

It follows from the above arguments that irrespective of the absolute values of the applied stress, internal stress, and density of 'forest' dislocations, only those dislocations for which all these factors combine to give a value of α_0, say α_c, appropriate for creep at the particular temperature, will contribute to creep. Dislocations with angles α_0 greater than α_c will effectively have taken part in the instantaneous extension, those with $\alpha_0<\alpha_c$ have no chance of moving in a measurable time. Inserting experimental values in eqn. (5) α_c is found to be $\sim 0{\cdot}5$ degrees for Cu at 80°K and 6·0 degrees for Al at the same temperature. (It should be noted here that α_c is the additional angle corresponding to the excess of the applied stress τ over the internal stress τ_g; if the major part of τ_g is essentially due to local elastic interaction between the mutually intersecting dislocations, the 'primary' dislocation may be bowed out considerably to overcome this local elastic interaction; the additional curvature corresponding to α_c will then be relatively small.)

Table 5. Dependence of Activation Energy on time for Polycrystalline Al at 78·8°K (Dorn 1957 a)

Time to Temp. change (sec.)	Total strain	U (Kcal/mole)	$\mathrm{Log}_{10}\nu$	$\nu(\mathrm{sec}^{-1})$
600	0·18	4·56	10·2	$10^{10\cdot5\pm1\cdot0}$
600	0·20	4·40	9·7	
1 500	0·21	5·02	10·9	
3 600	0·22	4·88	10·0	
4 500	0·23	5·27	11·3	
10 800	0·24	4·72	9·5	

It should perhaps be emphasized here that the experimental results discussed in § 4 show that $v\tau$ and $v\tau_g$ separately remain constant during creep and are independent of stress and pre-strain. On the formal creep theories only the difference of these quantities is expected to be constant; the constancy of $v\tau_g$ is therefore an additional result which is not understood but which presumably has its origin in the geometry of the deformation (see however § 6).

Dorn and his coworkers have also determined U as a function of temperature for Cu, Ni and Al. Their results on polycrystals are shown in fig. 7 together with the results obtained by Haeszner and Krause on work-hardened Al. In the low temperature region (below $\frac{1}{2}T_m$, where T_m is the melting temperature) a rough proportionality to kT is observed at the lowest temperatures as expected from the formal theories of logarithmic creep with deviations from linearity near $\frac{1}{2}T_m$. These departures are possibly due to impurity, particularly in the case of Ni, as a similar but more pronounced effect has been observed in an aluminium alloy containing 3·2 atm % of Mg in α solid solution (Dorn *et al.* 1957 c). Also, if a stress aided activation is considered, the activation energy will depend on the elastic moduli. In a change of temperature test the difference in creep rate observed is caused by the difference in probability of a thermal fluctuation and by a change in activation energy due to the temperature dependence of the elastic constants. Therefore the value of U derived from

Fig. 6

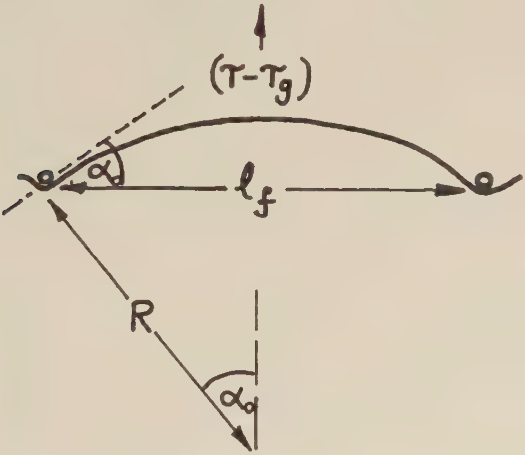

Equilibrium form of a dislocation loop under an effective stress $(\tau-\tau_g)$.

$$\frac{U}{k} = -\log\frac{\dot{\epsilon}_1}{\dot{\epsilon}_2}/\Delta\left(\frac{1}{T}\right) \qquad . \quad . \quad . \quad . \quad . \quad . \quad . \qquad (20)$$

Fig. 7

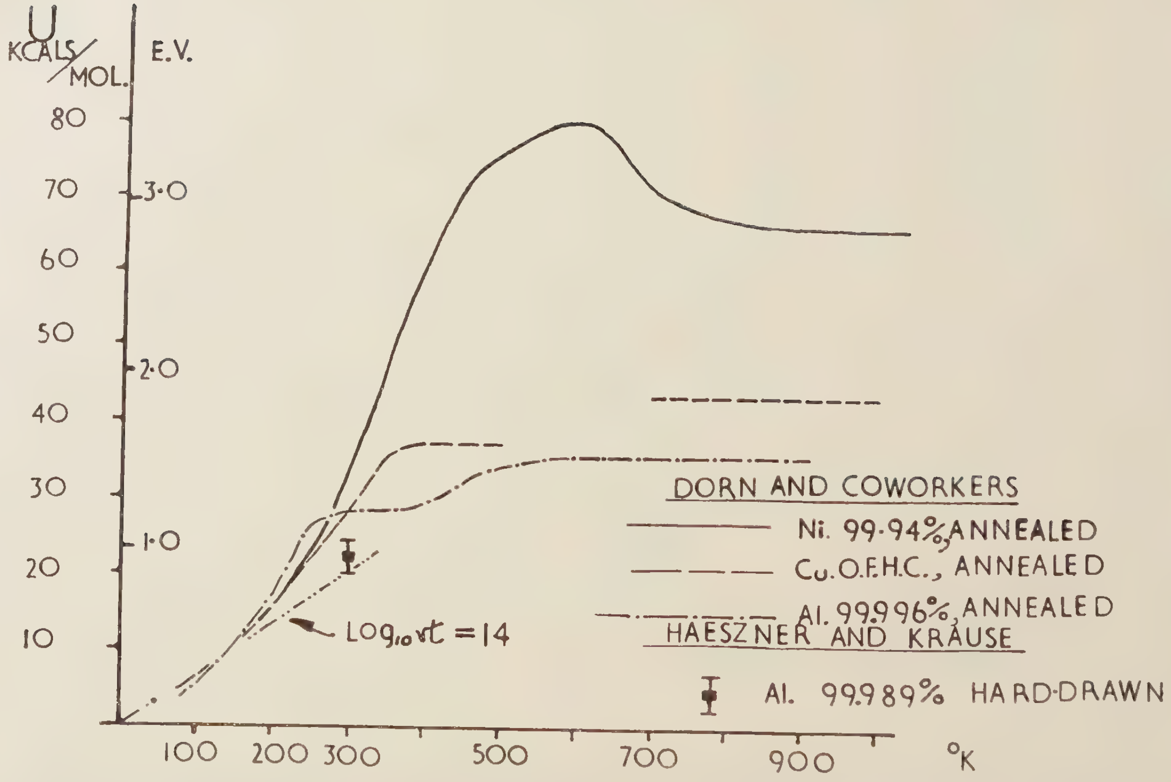

The apparent activation energy for creep as a function of temperature for polycrystalline Cu, Ni and Al.

should be corrected to take into account this second contribution. Basinski (1957) has indicated the necessary correction for Al. It is small at 80°K but at room temperature it substantially reduces the value of U obtained from eqn. (20). It is considered that the low temperature values (*circa* 100°K) are little in error and from these values we have determined a value of $\nu \sim 10^{11 \pm 1 \cdot 5}\,\mathrm{sec}^{-1}$ (see fig. 7).

It appears then that, contrary to the view expressed by Dorn *et al.* the two formal theories mentioned above both lead to an interpretation of all the existing data on low temperature creep of polycrystalline metals. It is not possible at present to distinguish experimentally between the two; the experimentally determined value of $\nu(\sim 10^{11}\,\mathrm{sec}^{-1})$ can be accounted for on either of the two theories.

§ 6. Conclusions

Experimental results on low temperature creep have been interpreted in terms of barriers due to intersecting 'forest' dislocations. Such an interpretation leads to reasonable dislocation widths, jog energies and stacking fault energies, and is consistent with the current interpretation of the temperature dependence of the flow stress. The hypothesis that logarithmic creep is controlled by the proposed mechanism appears to be correct. It is also shown that the current theories of logarithmic creep account for all the experimental facts and that the experiments of Dorn and his co-workers fit in well with these theories and the proposed stress-aided activation mechanism.

The interpretation used in this paper shows how dislocation widths, jog energies and stacking fault energies can be derived by combining measurements of logarithmic creep and flow stress. At present flow stress data are not sufficiently extensive to enable accurate values to be deduced except in a few cases. More detailed flow stress and increment tests are required, and it is likely that the numerical values presented in this paper may have to be revised. Hence the numerical estimates should be considered as tentative.

From a theoretical point of view the process of intersection of dislocations also requires further detailed attention. It is usually assumed that the internal stress τ_g is due to the dislocations on the 'primary' system (see Seeger 1954). The experiments indicate that on this interpretation the density of dislocations on the 'forest' systems is proportional and at least equal if not greater than the density of dislocations on the 'primary' system. It is therefore essential to consider the elastic interaction between the moving dislocations and the 'forest' dislocations. This elastic interaction can be very large, for example in cases where Cottrell–Lomer locks are formed, and in fact larger than for dislocations on parallel slip planes, as intersecting dislocations can actually touch. The present authors would like to suggest, that contrary to the views held by Seeger *et al.* (1957), the 'internal stress' τ_g is due mainly to the elastic interaction between the 'primary' and 'forest' dislocations. On this interpretation the activation volume v and the 'internal stress' τ_g depend both on l_f, the distance between 'forest' dislocations, and the 'Cottrell–Stokes law' follows. The constant α_g will then depend simply on the distribution of the 'forest' dislocations. It is not unreasonable to suppose that the distribution of 'forest' dislocations is more or less random and similar for all metals, at least for those with the same crystal structure. This is the basic idea which we believe justifies the assumption made in this paper that α_g has the same value for all metals. It should be emphasized that these ideas are at present tentative; they are presented here in order to show how this assumption of constancy of α_g might be supported. It is hoped to discuss this model for the flow stress of a metal in another paper.

The experiments also suggest that the stacking fault energy may vary considerably with temperature. If true, this must be taken into account if the variations of mechanical properties with temperature are to be explained satisfactorily. It is hoped that further increment tests which are to be carried out in this laboratory on single and polycrystals, and which are to extend over wider ranges of stress, time and temperature than hitherto explored, will help to answer some of these and other questions.

ACKNOWLEDGMENTS

Our thanks are due to Professor N. F. Mott, F.R.S., and Dr. W. H. Taylor for much help and encouragement, and to Drs. C. J. Ball and D. Turnbull for many useful discussions. The experiments were begun as a result of a stimulating course of lectures given by Dr. A. Seeger, with whom we have enjoyed many discussions. One of us (P. R. T.) acknowledges receipt of a maintenance grant from the Admiralty.

APPENDIX A

Introduction

For a given pair of dislocations, D is equal to the sum of effective widths d_1 and d_2 of the gliding and 'forest' dislocations, i.e. the sum of the widths of each dislocation resolved in a direction perpendicular to the moving dislocation line. Now $d_1 = d_1^0$, and $d_2 = d_2^0 \times$ some angular function, where d_1^0 and d_2^0 are the widths of the two dislocation ribbons. Then $D = d_1 + d_2 = d_1^0 + d_2^0 \times$ angular function. The quantities d_1^0 and d_2^0 depend on the relative orientation of the dislocations to their Burgers vectors, while the angular function depends on the relative orientation of the two dislocations. The average value ($\bar{D}$) of D in a crystal of normal size will be the average value of D for all possible orientations and possible Burgers vector pairs.

Value of $\bar{D}$ for f.c.c. Metals

If the isotropic approximation is valid the variation of dislocation width with orientation for dislocations lying in close packed planes is given by:

$$d(\psi)=d(1-K\cos 2\psi)$$

where $K=2\nu/(2-\nu)$, ψ is the angle between the dislocation line and its Burgers vector, d is the width of a dislocation line inclined at $\frac{1}{4}\pi$ to its Burgers vector and ν is Poisson's ratio (Read 1953). In terms of the quantities defined in fig. (8)

$$d_1{}^0=d(\theta)=d\{1-K\cos 2(\theta-\theta_0)\},$$

$$d_2{}^0=d(\phi)=d\{1-K\cos 2(\phi-\phi_0)\},$$

and

$$d_1=d(\theta),\ d_2=d(\phi)\sin\theta/\sin\phi.$$

Fig. 8

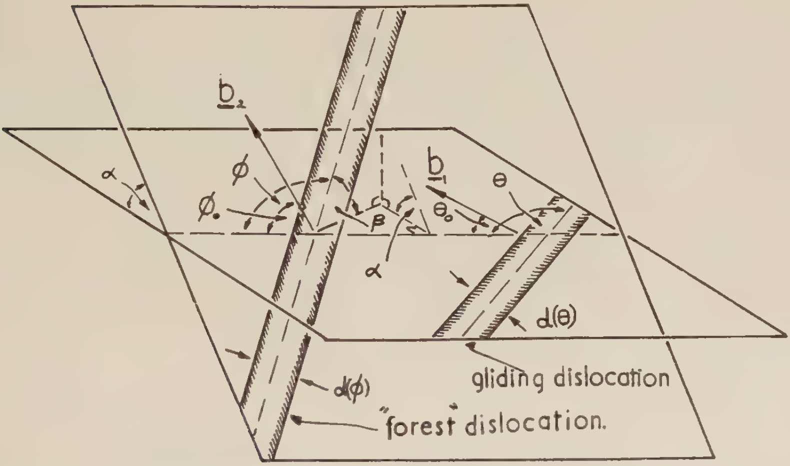

Intersection of two extended dislocations. Illustration of the angles used to define the orientation of a 'forest' dislocation relative to that of the 'primary' dislocation.

If the 'forest' dislocation lies in a close packed plane then

$$\bar{D}=\frac{1}{n}\sum_n\int_\theta\int_\phi D(\theta\phi)\,p(\theta,\phi)\,d\phi\,d\theta\Bigg/\int_\theta\int_\phi p(\theta,\phi)\,d\phi\,d\theta$$

where the summation is over all possible Burgers vector pairs, n is the total number of such pairs and $p(\theta,\phi)\,d\phi\,d\theta$ is the relative probability of an interaction between dislocations of this relative orientation occurring.

Thus $p(\theta, \phi)$ is the 'relative cross section' of a 'forest' dislocation whose orientation relative to the gliding dislocation is defined by θ and ϕ. The 'forest' dislocations have an average length l_f, and over a volume large compared to l_f^3 all possible orientations relative to the gliding dislocation may be assumed. The length of a 'forest' dislocation of orientation defined by θ and ϕ resolved parallel to the normal of the primary slip plane is

$$l_f \sin \beta = l_f \sin \phi \sin \alpha.$$

The 'relative cross section' of such a dislocation is $l_f \sin \phi \sin \alpha / l_f \sin \alpha = \sin \phi$. Therefore

$$\bar{D} = \frac{1}{n} \sum_n \frac{\int_0^\pi \int_0^\pi [d\{1 - K \cos 2(\theta - \theta_0)\} \sin \phi + d\{1 - K \cos 2(\phi - \phi_0) \sin \theta\}] \, d\phi \, d\theta}{\underset{= 2d}{\int_0^\pi \int_0^\pi \sin \phi \, d\phi \, d\theta}}$$

$$= \frac{1}{n} \sum_n 2d.$$

Hence $\bar{D}_{\text{f.c.c.}} = 2d \equiv 2Nb$.

Value of $\bar{D}$ for h.c.p. Metals

In metals with a hexagonal close packed structure it is assumed that the 'forest' dislocations of importance in this context are those in pyramidal or prismatic planes with Burgers vectors for example corresponding to close packed directions in the basal planes of the type $[1\bar{2}10]$. Such 'forest' dislocations are thought to be unextended. Therefore,

$$d_1 = d(\theta) \text{ while } d_2 = b \sin \theta / \sin \phi.$$

By repeating the calculation of the preceding paragraph with

$$D(\theta, \phi) = d(\theta) + b \sin \theta / \sin \phi$$

the expression $\bar{D}_{\text{h.c.p.}} = d + b \equiv (N+1)b$ is obtained.

REFERENCES

Adams, M. A., and Cottrell, A. H., 1955, *Phil. Mag.*, **46,** 1187.

Basinski, Z., 1957, *Acta Met.*, **5,** 684.

Cottrell, A. H., 1953, *Dislocations and plastic flow in crystals* (Oxford: Clarendon Press).

Cottrell, A. H., and Stokes, R. J., 1955, *Proc. roy. Soc.* A, **233,** 17.

Friedel, J., 1956, *Les dislocations* (Paris: Gauthier-Villars).

Glen, J. W., 1956, *Phil. Mag.*, **47,** 400.

Haasen, P., 1958, *Phil. Mag.*, **3,** 384.

Haeszner, F., and Krause, M., 1957, *J. Metals*, **9,** 1299.

Lander, C. H., and Howard, J. V., 1936, *Proc. roy. Soc.* A, **156,** 411.

Landon, P. R., Lytton, J. L., Shepard, L. A., and Dorn, J. E., 1957, *Inst. of Engineering Research Report*, Series 103, University of California, No. 2.

Lytton, J. L., Shepard, L. A., and Dorn, J. E., 1957. *Inst. of Engineering Research Report*, Series 103, University of California, No. 1.

Mott, N. F., 1953, *Phil. Mag.*, **44,** 742.

MOTT, N. F., and NABARRO, F. R. N., 1948, *Report on the Conference on Strength of Solids* (London : Physical Society).

OLDS, G. C. E., 1954, *Proc. phys. Soc. Lond.* B, **67**, 832.

OROWAN, E., 1947, *J. W. Scot. Iron St. Inst.*, **54**, 45.

READ, W. T., 1953, *Dislocations in Crystals* (New York : McGraw-Hill).

SEEGER, A., 1954, *Z. Naturf.*, **9**, 870 ; 1955 a, *Handbuch der Physik*, Band Vii, Tl. 1 ; 1955 b, *Phil. Mag.*, **46**, 1194.

SEEGER, A., DIEHL, J., MADER, S., and REBSTOCK, H., 1957, *Phil. Mag.*, **2**, 323.

SEEGER, A., and SCHOECK, G., 1953, *Acta Met.*, **1**, 519.

SHERBY, O. D., LYTTON, J. L., and DORN, J. E., 1957, *Acta Met.*, **5**, 219.

SMITH, C. L., 1948, *Proc. phys. Soc. Lond.*, **61**, 201.

WYATT, O. H., 1953, *Proc. phys. Soc. Lond.* B, **66**, 459.

Optical Constants, Heat Capacity and the Fermi Surface†

By M. H. Cohen

Institute for the Study of Metals, University of Chicago‡
and Cavendish Laboratory, University of Cambridge

[Received January 21, 1958 ; and in revised form March 24, 1958]

Abstract

Thermal and optical effective masses are defined and expressions for them obtained for metals with arbitrary Fermi surfaces. The ratio of these two effective masses is shown to depend on the shape of the Fermi surface. It follows from experimental values of the optical constants and the electronic heat capacity that the Fermi surface is not spherical in Cu, Ag and Au and that it contacts the surface of the first Brillouin zone to an appreciable degree in Cu and Ag. Similar evidence indicates a non-spherical Fermi surface in Li, Na and K. A simplification of the theory of the optical constants of metals is given which fits the experimental data for Na, K, Rb and Cs satisfactorily. Values of the plasma frequencies and widths of the plasma resonances of the alkali metals are calculated.

§ 1. Introduction

The electronic heat capacity of a metal is related to its band structure and Fermi surface in a comparatively simple manner. The same is true for the optical constants when relaxation effects can be ignored. Accurate measurements of the heat capacity (Corak *et al.* 1955, Rayne 1956 a, b) and of the optical constants (Schulz 1954, 1957) have recently been carried out for Cu, Ag and Au. Data are also available for the Alkali metals (Parkinson and Quarrington 1955, Roberts 1957, Wood and Lukens 1938, Ives and Briggs 1936, 1937 a, b). In this paper, we attempt to ascertain just what information about the band structure or Fermi surface can be obtained from comparison of the results of the optical and thermal experiments. This aim is readily achieved for the noble metals. For the alkali metals, however, it is first necessary to make a detailed analysis of the experimental values of the optical constants (Ives and Briggs 1936, 1937 a, b), and this, in turn, requires a suitable simplification of the general theory of the optical constants of metals. The analysis of the optical constants also leads to values of the plasma frequency and the width of the plasma resonance for the alkali metals.

§ 2. Thermal Effective Mass

The electronic heat capacity of a metal is γT, where (Seitz 1940, p. 151)

$$\gamma = \tfrac{1}{3}\pi^2 k^2 n(\epsilon_F) ; \qquad (1)$$

---

† Communicated by the Author. Guggenheim Fellow, 1957–58.

‡ Permanent Address.

here

$$n(\epsilon_F)=(2/(2\pi)^3)\int dS_F|\partial\epsilon/\partial\boldsymbol{k}|^{-1} \qquad . \quad . \quad . \quad . \quad . \quad . \quad (2)$$

is the density of states at the Fermi energy, ϵ_F. By noting that $\boldsymbol{v}=\hbar^{-1}\partial\epsilon/\partial\boldsymbol{k}$ is the velocity of an electron, $n(\epsilon_F)$ may be written as

$$n(\epsilon_F)=[2/(2\pi)^3\hbar]S_F\langle 1/v\rangle_F, \qquad . \quad . \quad . \quad . \quad . \quad . \quad (3)$$

where S_F is the area of the Fermi surface and

$$\langle 1/v\rangle_F=S_F^{-1}\int dS_F(1/v). \qquad . \quad . \quad . \quad . \quad . \quad . \quad (4)$$

It is customary and convenient to present experimental values of γ in terms of an effective mass. We *define* as the thermal effective mass m_t of the conduction electrons

$$m_t/m=\gamma/\gamma(\text{free}), \qquad . \quad . \quad . \quad . \quad . \quad . \quad . \quad . \quad (5)$$

where γ(free) is the value of γ for free electrons of the same density as those in the metal. Available experimental values of the thermal masses of the monovalent metals are listed in table 1. The expression for m_t which follows from eqn. (1), (3), (4) and (5) is

$$m_t=\hbar k_F(S_F/S_F{}^0)\langle 1/v\rangle_F, \qquad . \quad . \quad . \quad . \quad . \quad . \quad . \quad (6)$$

where $S_F{}^0$ is the area the Fermi surface would have if it were spherical. The radius of this hypothetical Fermi sphere is k_F, $S_F{}^0=4\pi k_F{}^2$, and the volume such that it holds the correct number of electrons per atom.

§ 3. OPTICAL EFFECTIVE MASS

The dielectric constant of a cubic metal with an infinite relaxation time is (Seitz 1940, pp. 649–651)

$$D=D'-iD'', \qquad . \quad . \quad . \quad . \quad . \quad . \quad . \quad . \quad . \quad (7)$$

where

$$D'=1-\left(\frac{\omega_a}{\omega}\right)^2+4\pi e^2\sum_s\frac{2}{(2\pi)^3}\int d^3\boldsymbol{k}\sum_r\left(\frac{1}{m^*}\right)_{rs}\frac{1}{\omega^2-\omega_{rs}{}^2} \qquad . \quad . \quad (8)$$

and

$$D''=\frac{2\pi^2e^2}{\omega}\sum_s\frac{2}{(2\pi)^3}\int d^3\boldsymbol{k}\sum_r\left|\left(\frac{1}{m^*}\right)_{rs}\right|\delta(\omega-\omega_{rs}) \qquad . \quad . \quad . \quad (9)$$

for light of angular frequency ω. The second term in (8) is the contribution to D' of the acceleration of the conduction electrons by the electric field. The usual expression for $\omega_2{}^2$ is

$$\omega_a{}^2=4\pi N_ce^2/m_a, \qquad . \quad . \quad . \quad . \quad . \quad . \quad . \quad . \quad (10)$$

where N_c is the number of conduction electrons per unit volume and $m_a{}^{-1}$ is the average inverse effective mass of the conduction electrons,

$$m_a{}^{-1}=(4\pi^3N_c\hbar^2)^{-1}\int d^3\boldsymbol{k}\tfrac{1}{3}\nabla_{\boldsymbol{k}}{}^2\epsilon. \qquad . \quad . \quad . \quad . \quad . \quad . \quad (11)$$

The integration in (11) is over the occupied region of the conduction band. An expression for m_a more useful for our present purposes follows from

(11) by partial integration,

$$m_a = \hbar k_F (S_F^0/S_F) v_F^{-1}, \qquad . \quad . \quad . \quad . \quad . \quad . \quad . \quad (12)$$

where v_F is the average velocity at the Fermi surface. The third term in (8) is the contribution to D' of the atomic polarizability as modified in the metal. In both this term and in D'', the sum over r includes all states of wave number $\boldsymbol{k}$ which are occupied, the $\boldsymbol{k}$-integration is over the occupied region of the sth band, and the sum over s includes all partially or fully occupied bands. That is, we have $\epsilon_r > \epsilon_F$ and $\epsilon_s \leqslant \epsilon_F$ in both (8) and (9). The quantity $(1/m^*)_{rs}$ is the contribution of the rth band to the effective mass of an electron in the sth band,

$$\left(\frac{1}{m^*}\right)_s = \hbar^{-2} \nabla_{\boldsymbol{k}}^2 \epsilon_s = \frac{1}{m} + \sum_n{}' \left(\frac{1}{m^*}\right)_{ns}, \qquad . \quad . \quad . \quad (13)$$

where the summation is over all bands except the sth. The explicit expression for $(1/m^*)_{ns}$ is

$$\left(\frac{1}{m^*}\right)_{ns} = \frac{2\boldsymbol{P}_{sn} \cdot \boldsymbol{P}_{ns}}{3m^2(\epsilon_s - \epsilon_n)}, \qquad . \quad . \quad . \quad . \quad . \quad . \quad . \quad (14)$$

where

$$\boldsymbol{P}_{ns} = -i(u_{\boldsymbol{k}n}, \hbar \nabla u_{\boldsymbol{k}s}). \quad . \quad . \quad . \quad . \quad . \quad . \quad . \quad . \quad (15)$$

In eqn. (15), $u_{\boldsymbol{k}n}$ and $u_{\boldsymbol{k}s}$ are the periodic parts of the Bloch functions $\psi_{\boldsymbol{k}n}$ and $\psi_{\boldsymbol{k}c}$. They are normalized to unity over a unit cell, the domain of integration for $\boldsymbol{P}_{ns}$. Finally, we note that D'' arises entirely from the absorption of light via interband transitions which occur when ω equals any ω_{rs}, $\hbar\omega_{rs} = \epsilon_r - \epsilon_s$. Local field corrections are not included in (8) and (9).

At frequencies sufficiently less than the interband absorption edge, ω^2 much less than any ω_{rs}^2, eqn. (8) simplifies to

$$D' = 1 + 4\pi N \alpha_T - (\omega_a/\omega)^2, \qquad . \quad . \quad . \quad . \quad . \quad . \quad . \quad (16)$$

where

$$\alpha_T = \frac{e^2}{N} \sum_s \frac{2}{(2\pi)^3} \int d^3\boldsymbol{k} \sum_r \left(\frac{1}{m^*}\right)_{sr} \frac{1}{\omega_{rs}^2}. \qquad . \quad . \quad . \quad . \quad (17)$$

Here N^{-1} is the volume of the unit cell and α_T is the total atomic polarizability. Local field corrections are not important if α_T is sufficiently small. We see that in this limit, D' has the simple form $A - B/\omega^2$ as a function of ω.

It is possible that the dependence of D' on $\omega = A - B/\omega^2$ even when ω exceeds the minimum value of ω_{rs}. Let us consider the case where interband excitation of conduction electrons takes place and not that of core electrons. Define $\omega^*(\boldsymbol{k})$ as the minimum optical excitation energy for a conduction electron of wave number $\boldsymbol{k}$ and band index c. Suppose, now, that the spread of values of $[\omega^*(\boldsymbol{k})]^2$ is very large, its maximum much greater than ω^2 and its minimum much less for the pertinent range of ω. Let us replace the energy denominator $(\omega^2 - \omega_{rc}^2)$ by ω^2 for all $\omega_{rc}^2 < \omega^2$ and by $-\omega_{rc}^2$ for all $\omega_{rc} > \omega^2$. This approximation is good if those $\boldsymbol{k}$ for which $\omega^* \simeq \omega$ give a relatively small contribution to D', as occurs when ω^* has a wide spread of values. We obtain in this way

$$D' = 1 + 4\pi N\alpha_0 + 4\pi e^2 \frac{2}{(2\pi)^3}\int d^3\boldsymbol{k} \sum_{\substack{r \\ \omega_{rc}<\omega}} \left(\frac{1}{m^*}\right)_{cr} \frac{1}{\omega_{rc}{}^2}$$
$$- \frac{\omega_a{}^2}{\omega^2} + \frac{4\pi e^2}{\omega^2}\frac{2}{(2\pi)^3}\int d^3\boldsymbol{k} \sum_{\substack{r \\ \omega_{rc}<\omega}} \left(\frac{1}{m^*}\right)_{rc}, \quad . \quad . \quad . \quad (18)$$

where α_0 is the contribution of the core bands to α_p. When the spread in values of ω^* is sufficiently large, the third term in eqn. (18) depends only slightly on ω, and the fifth term depends on ω nearly as ω^{-2}. The real part of the dielectric constant is again of the form $A - B/\omega^2$,

$$D' = 1 + 4\pi N\alpha_1 - (\omega_b/\omega)^2 \,. \quad . \quad . \quad . \quad . \quad . \quad . \quad (19)$$

The definitions of α_1 and ω_b become apparent upon comparison of (18) and (19). We note further that α_1 is greater than the core polarizability α_0.

Table 1. Experimental Values of Thermal and Optical Effective Masses

Metal	m_t/m	m_0/m	$m_0 \leq m_a$
Cu	$1{\cdot}38 \pm 0{\cdot}01$	$1{\cdot}45 \pm 0{\cdot}06$	$=$
Ag	$0{\cdot}96 \pm 0{\cdot}01$	$0{\cdot}97 \pm 0{\cdot}04$	$=$
Au	$1{\cdot}16 \pm 0{\cdot}02$	$0{\cdot}98 \pm 0{\cdot}04$	$=$
Li	2·32	0·98	$<$
Na	1·6 (*a*), 1·22 (*b*)	$1{\cdot}01 \pm 0{\cdot}02$	$<$
K	1·1	$1{\cdot}08 \pm 0{\cdot}02$	$<$
Rb	—	$1{\cdot}08 \pm 0{\cdot}03$	$<$
Cs	—	$1{\cdot}02 \pm 0{\cdot}02$	$<$

(*a*) Parkinson and Quarrington (1955).
(*b*) Roberts (1957).

We have just shown that D' is of the form $A - B/\omega^2$ if (1) ω is sufficiently smaller than the minimum frequency at which interband absorption occurs or if (2) interband absorption occurs, but the absorption frequencies are spread over a sufficiently wide range. In these two cases, it is possible to define an optical effective mass m_0

$$m_0/m = \omega_p{}^2(\text{free})/B, \quad . \quad . \quad . \quad . \quad . \quad . \quad . \quad . \quad (20)$$

where

$$\omega_p{}^2(\text{free}) = 4\pi N_c e^2/m \quad . \quad . \quad . \quad . \quad . \quad . \quad . \quad . \quad (21)$$

is the plasma frequency of free electron at the density of the conduction electrons. In case (1), m_0 is identical to m_a. In case (2), however, it is only possible to say that m_0 is less than m_a. The fifth term in eqn. (18) has the effect of removing the contributions of those states for which $\omega_{rc} < \omega$ from m_a as it appears in $\omega_a{}^2$ (eqn. (10)). Since these levels lie above the conduction band, their contribution must increase the effective mass, or the removal of their contribution decrease it, according to the sum rule (eqns. (13) and (14)). We conclude, therefore, that

$$m_0 \leq m_a \quad . \quad . \quad . \quad . \quad . \quad . \quad . \quad . \quad . \quad . \quad (22)$$

is true if the conditions for cases (1) or (2) are met.

Experimental values of the optical masses of the monovalent metals are given in table 1. The values for Cu, Ag, and Au are taken from the infra-red measurements of Schulz (1954, 1957) at wavelengths well beyond the absorption edge and hence relate to case (1), $m_0 = m_a$. On the other hand, the values for the alkali metals relate to case (2), $m_0 < m_a$. The value for Li follows from the ultra violet-transparency results of Wood and Lukens (1938) after a correction for the core polarizability is made. The values for the remaining alkali metals are derived from a least squares fit of the data of Ives and Briggs (1936, 1937 a, b) to the form $A - B/\omega^2$ for D', as discussed in § 5.

§ 4. SHAPE OF THE FERMI SURFACE

We now show that certain gross features of the Fermi surface can be derived from measurements of the thermal and optical effective masses. We obtain

$$m_t/m_a = (S_F/S_F^0)^2 v_F \langle 1/v \rangle_F \quad . \quad . \quad . \quad . \quad . \quad . \quad (23)$$

for the ratio of thermal to average effective mass by combining eqns. (6) and (12). The quantities v_F and $\langle 1/v \rangle_F$ are both proportional to integrals of functions of wave number over the Fermi surface. The Schwarz inequality applies to the integral of the product of two such functions, a and b; that is,

$$\left[\int dS_F ab \right]^2 \leqslant \int dS_F a^2 \int dS_F b^2 . \quad . \quad . \quad . \quad . \quad . \quad (24)$$

holds for any two functions defined on the Fermi surface. The equality pertains only to the case a proportional to b. If we substitute $v^{1/2}$ for a and $v^{-1/2}$ for b in eqn. (24), we obtain

$$v_F \langle 1/v \rangle_F \geqslant 1, \quad . \quad . \quad . \quad . \quad . \quad . \quad . \quad . \quad . \quad (25)$$

which is merely the relation between the harmonic and arithmetic mean. By recalling that $m_a \geqslant m_0$ (eqn. (22)) and using eqn. (25), we see that

$$m_t/m_0 \geqslant m_t/m_a \geqslant (S_F/S_F^0)^2 . \quad . \quad . \quad . \quad . \quad . \quad . \quad . \quad (26)$$

The seond equality in (26) holds only if v is constant. Then the Fermi surface is spherical, and $m_t = m_a$.

Let us now restrict ourselves to the monovalent metals, in which the Fermi surface is most probably singly connected. If the Fermi surface does not intersect, or contact, the surface of the first Brillouin zone (BZ), it follows that $S_F \geqslant S_F^0$ and

$$m_t/m_0 \geqslant m_t/m_a \geqslant 1 \quad \text{(no contact)}. \quad . \quad . \quad . \quad . \quad . \quad . \quad (27)$$

The second equality in (27) holds only if the Fermi surface is spherical. Thus, the thermal mass exceeds the optical mass for a non-spherical Fermi surface which does not contact the faces of the BZ.

If the Fermi surface does intersect the faces of the BZ, the intersected area is not a part of the Fermi surface because the states there have energies lower than the Fermi energy. If the area of contact is large enough to compensate for the departures from a sphere elsewhere in the zone and for the excess of $v_F \langle 1/v \rangle_F$ over unity, then m_t/m_a can be less than unity. Certainly an experimental value of m_t/m_a significantly less than unity must indicate contact. Our conclusions for the various cases of contact and no contact are summarized in table 2.

Table 2. Interpretation of Values of m_t/m_a

Experimental result	Interpretation
$m_t/m_a > 1$	Anisotropic Fermi surface and little if any contact.
$m_t/m_a \simeq 1$	Nearly spherical Fermi surface or anisotropy with appreciable contact.
$m_t/m_a < 1$	Considerable area of contact.

To clarify the preceding statements about the effect of contact consider a Fermi sphere of radius R separated by h from the surface of the BZ. Suppose that contact with the zone boundary is provided by a cylindrical collar of radius r, as in fig. 1. If r and h are much smaller than R, then

Fig. 1

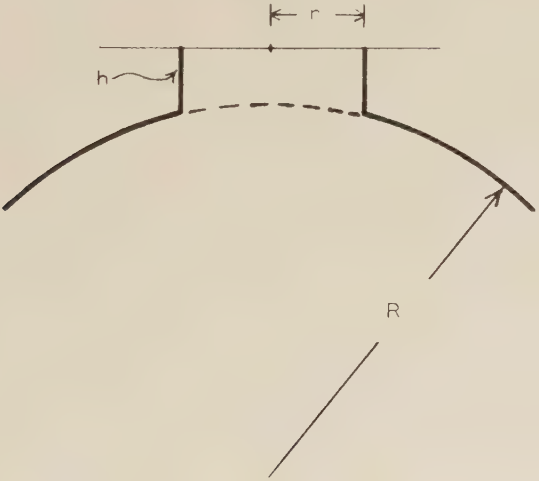

A simple example of contact of the Fermi surface with a zone boundary.

the change in R is required to keep the volume constant may be neglected in calculating the area. Thus S_{F} is given by

$$S_{\mathrm{F}} = S_{\mathrm{F}}^0 + 2\pi rh - \pi r^2. \qquad (28)$$

We see that S_{F} increases until $r = h$ and then decreases as r increases. When r equals $2h$, S_{F} equals S_{F}^0. We designate this situation as the case of critical contact. The area of contact must in general exceed the critical area before m_t becomes less than m_a in order to overcome the effects of departures from the sphere elsewhere and the excess of $v_F\langle 1/v\rangle_F$ over unity. On the other hand, eqn. (28) probably leads to an over-estimate of the critical radius.

The Fermi spheres of the monovalent metals do approach close enough for our simplified description of the contact process to be applicable ($h/R = 0{\cdot}11$ for face-centred cubic and $0{\cdot}13$ for body-centred cubic). If we compare the experimental values of m_a and m_t for the noble metals (table 1) in the light of the results given in table 2, we arrive at the following conclusions. The critical area of contact is appreciably exceeded in Cu. Either the contact is probably about critical in Ag, or the Fermi surface is nearly spherical. Finally, there is little if any contact in Au but decided anisotropy.

Pippard (1957) has obtained a value for the radius of contact from the interpretation of his anomalous skin effect measurements in the following way. He first found a closed Fermi surface which gave the correct variation of surface resistance with orientation. When the volume enclosed was adjusted to hold one electron per atom, the surface was found to project beyond the zone face. The Fermi surface was then slightly deformed so that it fitted into the zone. The deformation argued for by Pippard leads to a radius of contact 0·7 of our critical radius, which is in good agreement with our rough estimate. Previous arguments for contact, or near contact, in Cu were based on the ordinary transport properties (Klemens 1954, Jones 1955, Chambers 1956) for which the theory is in a rather less satisfactory state than for the optical, thermal, and anomalous skin effects and in which the anisotropy of the Fermi surface is beclouded by anisotropy of the scattering processes.

There are two difficulties which prevent comparably detailed statements on the shapes of the Fermi surfaces of the alkali metals. First, the optical constants have been measured only in a wavelength range where interband absorption occurs so that $m_0 < m_a$. It may happen that m_t/m_0 exceeds unity while m_t/m_a is less than unity, therefore, a value of m_t/m_0 significantly greater than unity does not preclude either contact with the zone faces or a nearly spherical Fermi surface. Secondly, electronic specific heats have been measured only for Li, Na and K. There is, however, a low temperature phase transformation in Li and Na of martensitic type (Barrett 1955, 1956, Rayne 1954). It is conceivable that gradual transformation could lead to an effective heat capacity of the form $\gamma T + AT^3$ and that measurements taken on heating would yield a spuriously large value of γ. It would be necessary to obtain information on the degree of transformation of the specimen before the specific heat data could be used safely. On the other hand K, Rb and Cs do not show this transformation from body-centred cubic to close-packed structure. It would be of great interest, therefore, to have accurate values of γ and of the optical constants in the infra-red for these three metals. Nevertheless, if one uses the existing specific heat data unquestioningly, the indications are that the Fermi surfaces of Li, Na and K are anisotropic, particularly that of Li.

It is not entirely legitimate to compare the values of m_t with the values of m_0 in table 1 in that the optical data were taken at room temperatures primarily and the thermal data all at helium temperatures. In the absence of suitable low temperature optical measurements, we must rely on band structure calculations of the dependence of effective mass on lattice constant for an estimate of the errors involved. The calculations of Brooks (1953) indicate a negligible change in the effective masses of the alkali metals between room and helium temperatures except possibly for Li. Corresponding calculations for the noble metals are unavailable.

Our considerations have thus far been confined to the one-electron approximation. However, it is now known that electron correlation destroys the equality of m_t and m_0 for the electron gas (Pines 1954, 1955, Gell-Mann 1957, Sawada *et al.* 1957, Brout 1957), which certainly has a spherical Fermi surface. Our previous conclusion that a spherical Fermi surface implies equality of m_t and m_0 is incorrect. On the other hand, our most important conclusion, namely that m_0 exceeds m_t only when the Fermi surface contacts the zone boundary, would be strengthened if the effect of electron correlations were to cause m_t to exceed m_0 for a spherical Fermi surface. It is well established that the long-wavelength plasma frequency is given by eqn. (21) (Bohm and Pines 1953, Pines 1955, Sawada *et al.* 1957, Brout 1957) so that m_0 is the free electron mass m. Gell-Mann (1957) obtains $m/m_t = [1 + 0{\cdot}083 r_s(-\ln r_s - 0{\cdot}203) + \ldots]$ for the leading terms in an exact expansion of m/m_t in r_s, the radius (in units of the Bohr radius) of a sphere holding one electron. Relevant values of r_s may not necessarily lie within the as yet unknown radius of convergence of this series. Nevertheless, we can estimate the effect of the next term on the range of r_s in which m_t/m exceeds unity very roughly as follows. We choose β in Pine's result for m/m_t (Pine's 1955, eqn. (8·3)) so that it agrees with Gell-Mann's exact result at high densities. This requires $\beta = 0{\cdot}816 r_s^{1/2}$ and yields a range of $1{\cdot}2 \lesssim r_s \lesssim 6{\cdot}0$ in which $m_t/m \geqslant 1$. Normal conduction electron densities are such that $1{\cdot}8 \lesssim r_s \lesssim 5{\cdot}6$. Thus, in the absence of more precise results, it seems reasonable that electron correlation tends to cause m_t to exceed m_0. We maintain, therefore, that *a value of m_t less than that of m_0 indicates contact.* This view is supported by our results for copper.

§ 5. Optical Constants and Plasma Frequencies of the Alkali Metals

5.1. *Real Part of the Dielectric Constant*

Ives and Briggs have measured the complex refractive index, $n_c = n - i\kappa$, of sodium (1936), of potassium (1937 a) and of rubidium and caesium (1937 b) as a function of wavelength λ in the range 2536 Å to 5780 Å. They attempted to fit their data by neglecting the atomic polarizability and interband absorption and found good agreement for Na, rough agreement for K, and very poor agreement for Rb and Cs. We have found that the values of

$$D' = n^2 - \kappa^2$$

derived from the measurements of Ives and Briggs can be fitted quite accurately to the form $A - B/\omega^2$. Figure 2 displays the experimental

Fig. 2

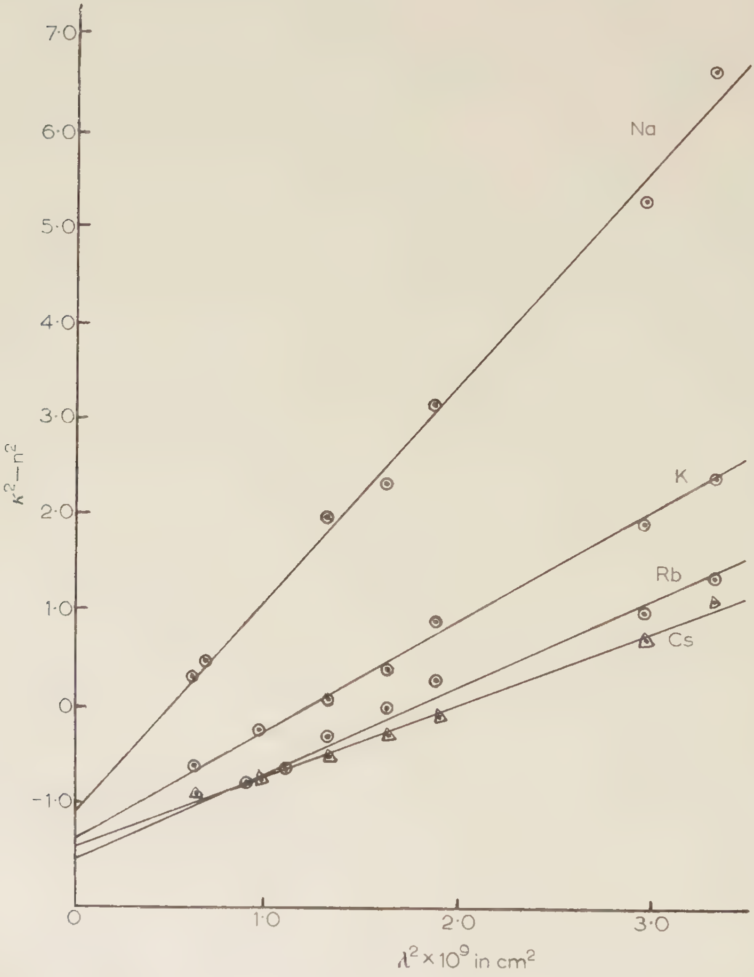

Real part of the dielectric constant versus wavelength squared for Na, K, Rb and Cs. Values of $\kappa^2 - n^2$ calculated from the experimental data of Briggs and Ives (1936, 1937 a, b) are indicated by circles or triangles. The straight lines represent the least squares fit of these values to the equation $\kappa^2 - n^2 = -A + B\lambda^2$. The scatter appears random except possibly for Rb.

values of $n^2-\kappa^2$ *vs* λ^2 together with straight lines representing the least squares fit to the form $-A+[B/(2\pi c)^2]\lambda^2$ obtained by assuming no error in λ. The agreement is excellent except perhaps for Rb, where there are small systematic deviations from the straight line instead of scatter about it. In all cases, the agreement is considerably better for the form $A-B/\omega^2$ for $n^2-\kappa^2$ than for the form $1-B/\omega^2$ for $-\kappa^2$ used by Ives and Briggs so that the deviation of A from unity must be regarded as significant.

We interpret this agreement as indicating that eqn. (19) is valid and that the conduction electron excitation energies are spread over a wide range which includes the working range of Ives and Briggs. The values of $4\pi N\alpha_1$ obtained on this interpretation from the least-squares values of $A-1$ are given in table 3. Values for B have already been presented in table 1 in the form of values for the optical mass. For both quantities the probable errors indicated in the tables are statistical and not experimental.

Table 3. Values of $4\pi N\alpha$

Metal	$4\pi N\alpha_0$ (*a*)	$4\pi N\alpha_1$ (*b*)
Li	0·02	—
Na	0·13	0·10 ± 0·08
K	0·23	0·28 ± 0·05
Rb	0·28	0·50 ± 0·05
Cs	0·38	0·37 ± 0·03

(*a*) TKS values of α (Tessman *et al.* 1953).

(*b*) Present analysis of the data of Ives and Briggs (1936, 1937 a, b).

Values of $4\pi N\alpha_0$ are also included in table 3, for comparison. These were calculated by using the Tessman, Kahn and Shockley (1953), or TKS, values of the polarizabilities of alkali ions in alkali halides for the core polarizability α_0. In principle, α_1 exceeds α_0 by the value of the conduction electron polarizability at these frequencies, which should be relatively small. We should expect, therefore, that the two sets of entries in table 3 agree quite closely except in so far as the core polarizability differs in the metal and in an ionic crystal (changed energy denominators and matrix elements) and in so far as the local field changes the value of A. The two sets of entries do agree to within the statistical error for Na, K, and Cs, a strong confirmation of the present interpretation of the optical constants. In the case of Rb, on the other hand, $4\pi N\alpha_1$ is considerably larger than $4\pi N\alpha_0$. This and the poorer fit for Rb suggest that the conduction–electron excitation energies may not be so widely spread out in Rb as in the other alkali metals.

The value of the optical mass of Li given in table 1 is derived from the wavelength at which the metal becomes transparent (Wood and Lukens 1938) that is, at which $D'=0$. This occurs when

$$\omega^2=\omega_t^2=\omega_b^2/(1+4\pi N\alpha_1), \quad . \quad . \quad . \quad . \quad . \quad . \quad . \quad (29)$$

according to eqn. (19), so that

$$m_0=\frac{\omega_P^2(\text{free})}{\omega_t^2(1+4\pi N\alpha_1)}. \quad . \quad . \quad . \quad . \quad . \quad . \quad . \quad . \quad (30)$$

If we use the TKS value of α_0 for α_1 (see table 3) and the result of Wood and Lukens that $\omega_t=\omega_P$(free), we obtain 0·98 for the value of m_0/m for Li.

Existing calculations of the excitation energies support the contention that the lowest excitation energy varies over a wide range in Na, K and Cs. One can estimate very roughly that the range of λ^* $[=\omega^*/c]$ is 780 Å to 8850 Å in Na (Von der Lage and Bethe 1947, Howarth and Jones 1952, Ham 1955) 1040 Å to 27 000 Å in K (Callaway 1956) and 1300 Å to 16 000 Å in Cs (Callaway and Haase 1957) from energy band calculations. These are to be compared with the experimental range of 2536 Å to 5780 Å (Ives and Briggs 1936, 1937 a, b). Similarly one can estimate that the range of λ^* is 700 Å to 4100 Å for Li (Glasser and Callaway 1958) which is to be compared with the wavelength of transparency of 1550 Å (Wood and Lukens 1938).

5.2. *Imaginary Part of the Dielectric Constant*

The optical absorption of Na, K, Rb and Cs is shown in fig. 3. in the form of $D''=2n\kappa$ *vs* wavelength squared. There are two origins of non-zero values of $2n\kappa$, relaxation effects and interband absorption, and a complete theory must include the anomalous skin effect, as well. Ives and Briggs have already noted that relaxation effects would be far too small to account for the observations, even for Na. The anomalous skin effect is also too small. We are left with interband transitions as the mechanism responsible for the optical absorption of the alkali metals (Butcher 1951).

The optical absorption of these metals increases systematically with atomic number (fig. 3). We can shed light on the origin of this by putting eqn. (9) for D'' into the form

$$D''=-\frac{4\pi^2e^2}{3m^2\hbar^2\omega^2}\sum_r\frac{2}{(2\pi)^3}\int dS_{rc}\boldsymbol{P}_{cr}\cdot\boldsymbol{P}_{rc}(v_{rc})^{-1}. \quad . \quad . \quad . \quad (31)$$

In eqn. (31), we have assumed that only conduction electrons undergo interband transitions, dS_{rc} is an element of the surface in $\boldsymbol{k}$-space on which

$$\epsilon_r(\boldsymbol{k})-\epsilon_c(\boldsymbol{k})=\hbar\omega,$$

and v_{rc} is defined as

$$v_{rc}=\hbar^{-1}|\partial\epsilon_r/\partial\boldsymbol{k}-\partial\epsilon_c/\partial\boldsymbol{k}|.$$

The area in $\boldsymbol{k}$-space on which energy can be conserved, S_{rc}, has an almost geometric significance and should not vary strongly from one metal to the next. The similarity of the optical masses of the four metals suggests that v_{rc} should also not differ widely. Therefore, the variation of $\boldsymbol{P}_{rc}$ with atomic number should be principally responsible for the differences in the optical absorption.

Fig. 3

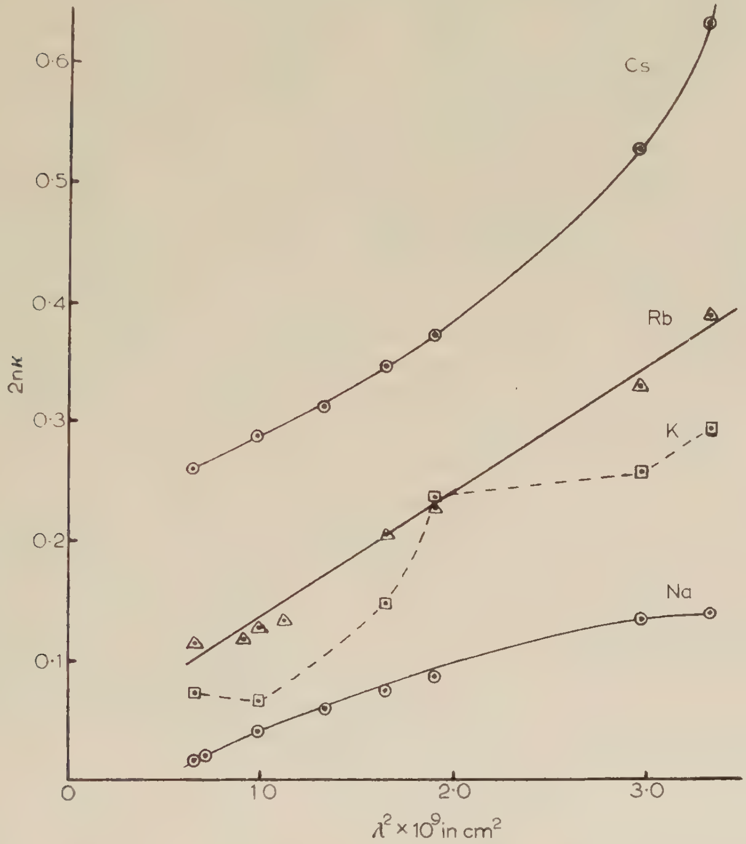

Imaginary part of the dielectric constant versus wavelength squared for Na, K, Rb and Cs. Values of $2n\kappa$ calculated from the experimental data of Briggs and Ives (1936, 1937 a, b) are indicated by circles, squares, or triangles. The lines are of no theoretical significance. Note the extreme scatter for K. The absorption is presumably associated with interband transitions (Butcher 1951).

This indicated increase of $\boldsymbol{P}_{rc}$ with atomic number can be understood by representing the Bloch functions as linear combinations of orthogonalized plane waves (OPW). Each Bloch function is then a linear combination of plane waves and of the atomic orbitals to which the plane waves have been orthogonalized. One expects the matrix elements between the plane-wave parts to be roughly independent of wave number, zero, in fact, if a single OPW is an adequate representation of each Bloch function. Therefore, the matrix element increases with atomic number primarily because of the increased number of atomic orbitals present in the wave function, which couple both with the plane-wave parts and among themselves.

One would expect that P_{rc} is a decreasing function of ω. Indeed, P_{rc} is inversely proportional to ω in the nearly-free-electron approximation. The dependence of v_{rc} on frequency may well be slight; it does not depend on ω in the nearly free electron approximation. The area S_{rc} increases from zero at the absorption edge to a maximum value and then decreases to zero when ω exceeds the maximum value of ϵ_{rc}. One expects, therefore that D'' should increase linearly just beyond the absorption edge, reach a maximum value before S_{rc} reaches its maximum, and finally decrease very approximately as ω^{-2}. The data of Ives and Briggs show the behaviour expected on the high frequency side of the maximum. The rough estimates of the absorption edge given earlier are 4100 Å for Li, 8850 Å for Na, 27 000 Å for K, and 16 000 Å for Cs and are derived from various band-structure calculations. It would be of great interest, both intrinsically and in relation to the band structure calculations, to obtain experimental values for these cut-off wavelengths by extending the observations into the infra-red.

5.3. *Plasma Frequency and Line Width*

Mott (1954) has pointed out that the plasma frequency is the frequency of a spontaneous polarization wave in the metal (Pines 1955). A spontanous oscillation is one for which Maxwell's displacement vector and therefore the dielectric constant vanish (Fröhlich and Pelzer 1955). For the alkali metals D is complex, and so must the plasma frequency be. That is, a plasma oscillation has a finite lifetime through energy loss *via* interband excitation of the conduction electrons.

If we are to find the complex frequency

$$\omega=\omega_p+i\Gamma \qquad (32)$$

which is the root of

$$D=0, \qquad (33)$$

we must know the behaviour of D in the upper half of the complex frequency plane. We do know this for $D'=A-B/\omega^2$ but not for D''. Values of the latter could in principle be obtained by analytic continuation of D'' into the upper half plane. However, it has proved sufficiently accurate to substitute for D'' in eqn. (33) its value at the frequency at which D' vanishes, $\omega_b A^{1/2}$. The resulting values of ω_p and Γ are listed in table 4 together with the ω_p(free) for comparison. Table 4 shows that ω_p(free) exceeds ω_p, a consequence of the departure of m_0 and $1+4\pi N\alpha_1$ from unity, as well as of the finite width, Γ. These results for $\hbar\omega_p$ are to be compared with the earlier ones of Ferrell (1956) and of Pines (1956) based on a less complete analysis.

Table 4. Energies and Widths of the Plasma Resonances

Metal	$\hbar\omega_P$(free) (ev)	$\hbar\omega_P$ (ev)	$\hbar\Gamma$ (ev)
Li	8·01	8·01	—
Na	5·93	5·62	0·01
K	4·32	3·67	0·10
Rb	3·85	3·01	0·13
Cs	3·42	2·91	0·30

REFERENCES

BARRETT, C. S., 1955, *J. Inst. Metals*, **84,** 43 ; 1956, *Acta cryst.*, **9,** 671.

BOHM, D., and PINES, D., 1953, *Phys. Rev.*, **92,** 609.

BROOKS, H., 1953, *Phys. Rev.*, **91,** 1027 and unpublished work quoted by Ham (1955).

BROUT, R., 1957, *Phys. Rev.*, **108,** 515.

BUTCHER, P. N., 1951, *Proc. phys. Soc. Lond.* A, **64,** 765.

CALLAWAY, J., 1956, *Phys. Rev.*, **103,** 1219.

CALLAWAY, J., and HAASE, E. L., 1957, *Phys. Rev.*, **108,** 217.

CHAMBERS, R. G., 1956, *Proc. roy. Soc.* A, **68,** 1191.

CORAK, W. S., GARFUNKEL, M. P., SATTERTHWAITE, C. B., and WEXLER, A., 1955, *Phys. Rev.*, **98,** 1699.

FERRELL, R. A., 1956, *Phys. Rev.*, **101,** 554.

FRÖHLICH, H., and PELZER, H., 1955, *Proc. phys. Soc. Lond.* A, **68,** 525.

GELL-MANN, M., 1957, *Phys. Rev.*, **106,** 369.

GLASSER, M. L., and CALLAWAY, J., 1958, *Phys. Rev.*, **109**, 1541.

HAM, F. S., 1955, *Solid State Phys.*, **1,** 127.

HOWARTH, D. J., and JONES, H., 1952, *Proc. phys. Soc. Lond.* A, **65,** 355.

IVES, H. E., and BRIGGS, H., 1936, *J. opt. Soc. Amer.*, **26,** 238 ; 1937 a, *Ibid.*, **27,** 181 ; 1937 b, *Ibid.*, **27,** 395.

JONES, H., 1955, *Proc. phys. Soc. Lond.* A, **68,** 1191.

KLEMENS, P. G., 1954, *Aust. J. Phys.*, **7,** 70.

VON DER LAGE, H. C., and BETHE, H., 1947, *Phys. Rev.*, **71,** 612.

MOTT, N. F., 1954, *Proceedings of the 10th Solvay Congress* (Brussels: Institut International de Physique Solvay), p. 67.

PARKINSON, D. H., and QUARRINGTON, J. E., 1955, *Proc. phys. Soc. Lond.* A, **68,** 762.

PINES, D., 1954, *Phys. Rev.*, **92,** 626 : 1955, *Solid State Phys.*, **1,** 367 ; 1956, *Rev. mod. Phys.*, **28,** 184.

PIPPARD, A. B., 1957, *Phil. Trans. roy. Soc.* A, **250,** 325.

RAYNE, J. A., 1954, *Phys. Rev.*, **95,** 1428 ; 1956 a, *Proc. phys. Soc. Lond.* B, **69,** 482 ; 1956 b, *Austr. J. Phys.*, **9,** 189.

ROBERTS, L. M., 1957, *Proc. phys. Soc. Lond.* B, **70,** 744.

SAWADA, K., BRUECKNER, K. A., FUKUDA, N., and BROUT, R., 1957, *Phys. Rev.*, **108,** 507.

SCHULZ, L. G., 1954, *J. opt. Soc. Amer.*, **44,** 540 ; 1957, *Advanc. Phys.*, **6,** 102.

SEITZ, F., 1940, *Modern Theory of Solids* (New York : McGraw-Hill).

TESSMAN, J. R., KAHN, A. H., and SHOCKLEY, W., 1953, *Phys. Rev.*, **92,** 980.

WOOD, R. W., and LUKENS, C., 1938, *Phys. Rev.*, **54,** 332.

CORRESPONDENCE

A Method of Detecting an Observer Bias

By R. M. Tennent
Physics Department, University of Leeds

[Received March 23, 1958]

In a recent experiment, electrical pulses derived from a cosmic-ray detector were displayed on a cathode-ray oscilloscope and photographed. The pulse height spectrum was found by projecting the developed images on to squared paper and estimating their heights by eye. In a particular case the pulse magnitudes were estimated to the nearest $\frac{1}{2}$ volt and, as the estimations were difficult to make and fatiguing, it was considered necessary to analyse the measurements in order to determine whether, when making a particular reading, the observer was influenced by the previous reading. The analysis was performed by finding the distribution of runs of a particular reading, that is, the numbers of times the particular reading occurred once only, twice consecutively, three times consecutively etc., as the pulse heights were read from the film.

Consider a set of M readings, of which N are of a particular type x (say). If the probability of obtaining a reading of type x is f, the fraction of such readings present in the total (i.e. N/M) is an estimate of f and approaches f when M is large. In this case, the expected distribution of runs (that is consecutive readings) of x, containing one, two, three etc. x's is given by the terms of the series:

$$Mf(1-f)^2(1+f+f^2+f^3+\ldots). \qquad \ldots \qquad (1)$$

As an example of a distribution of this sort, the runs of even numbers occurring in the first 7500 digits in a table of random numbers (Fisher and Yates 1938) were analysed. Here $N/M=0{\cdot}495$ was taken as the best estimate of f and the observed and expected distributions are shown plotted in fig. 1.

However, when the readings taken from the film referred to above were analysed in the same way it was found that the agreement with theory was poor. For example, the distribution of runs of 2 volt pulses is shown in fig. 2 with the theoretically expected distribution, calculated from eqn. (1), drawn as a full line. Clearly the agreement is poor, (a χ^2 test gives the probability of such a poor fit as less than 0·03).

The observed distribution of 2 volt pulses can be understood if we assume that the probability of the observer's calling a particular pulse a 2 volt pulse depends on the value of the previous pulse. In particular, with the distribution shown, the observer is biased towards recording a 2 volt pulse when the previous pulse recorded was also a 2 volt pulse. As a check, the same readings were analysed again for runs of 2 volt pulses, but taking the readings in an order different from the order of film reading. A distribution was obtained which agreed with that predicted by eqn. (1).

Fig. 1

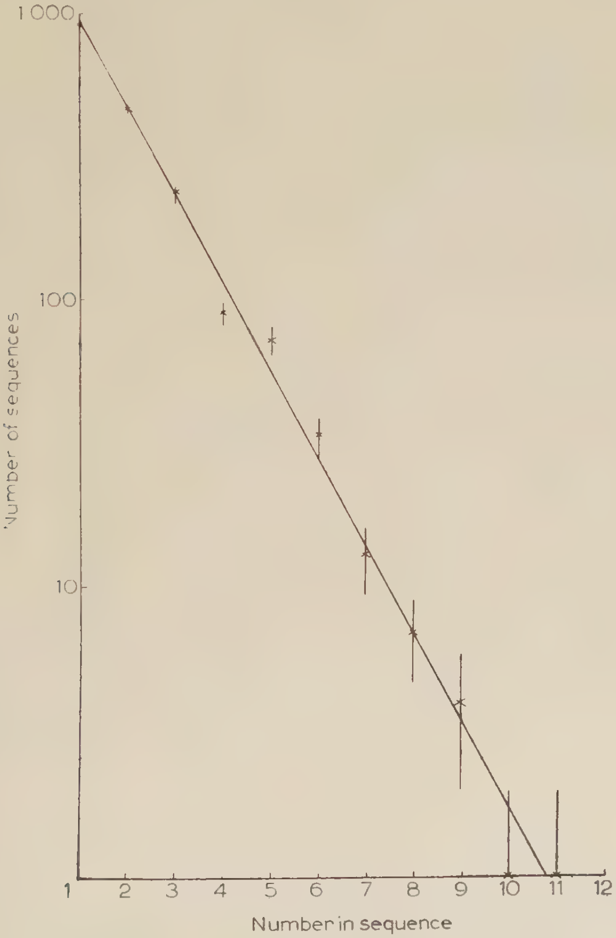

Distribution of sequences of random numbers which are even.

Suppose we now define two probabilities; f_1 is the probability of recording a reading 'x' after a dissimilar ('*not* x') reading and f_2 is the probability of recording a reading 'x' after a similar reading. Neither of these probabilities is equal to the fraction of events which is finally observed, and which we now call f_0 $(=N/M)$. It can be shown that f_1, f_2 and f_0 are related by the equation

$$f_0 = f_1/(1+f_1-f_2)$$

Fig. 2

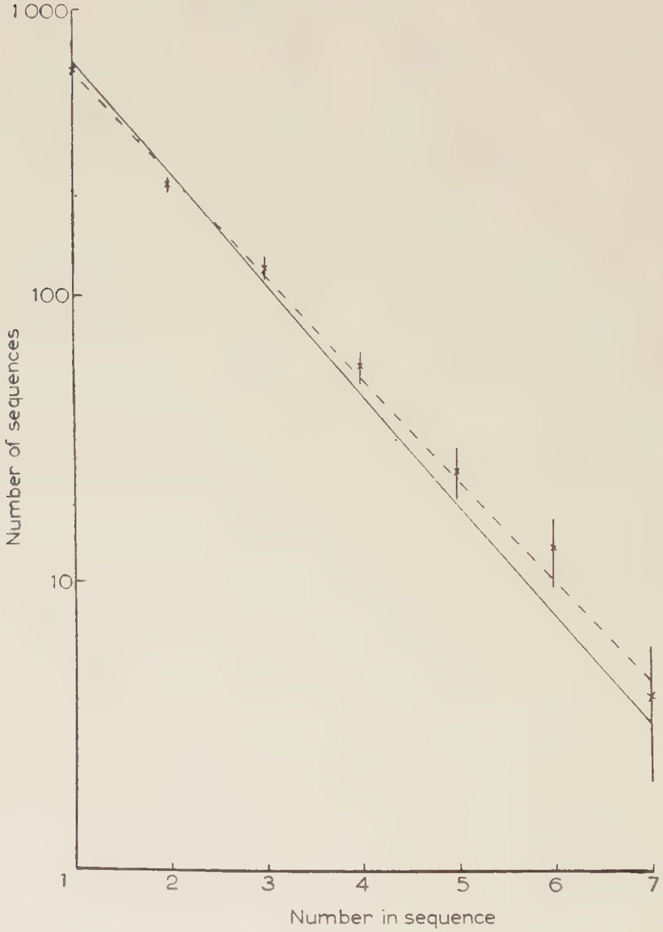

Distribution of sequences of 2 volt pulses compared with theoretical distribution for an unbiased observer (full line) and a biased observer (dotted line).

and the expected distribution of runs of x containing one, two, three etc. x's is given by the terms of the series

$$Mf_0(1-f_2)^2(1+f_2+f_2^2+f_2^3+\text{etc.}\ldots), \quad . \quad . \quad . \quad . \quad . \quad (2)$$

when M is a large number. An estimate of f_2 may be made from the distribution of sequences by measuring the slope of the logarithmic plot, or by using the relation:

$$N(1-f_2)=A, \qquad (3)$$

where A is the total number of runs. In a similar way, an estimate of the probability f_1 may be made remembering that the expected distribution of runs '*not* x' events is similar to eqn. (2) above, with $(1-f_1)$ substituted for f_2; and that the total number of 'x' sequences is equal to the total number of '*not* x' sequences, whence

$$(M-N)f_1=A. \qquad (4)$$

Using this analysis on the results displayed in fig. 2 we have $M=4611$; $N=1907$; $f_0=0{\cdot}414$; $A=1070$. We find, using relations (3) and (4), $f_1=0{\cdot}396$; $f_2=0{\cdot}439$; and the expected distribution is shown as a dotted line on fig. 2. The fit is good, a χ^2 test gives the probability of a worse fit to be 0·7. We conclude then that the distribution obtained can be explained by an observer bias such that the probability of recording a 2 volt pulse is increased when the previously recorded pulse was also a 2 volt pulse.

Having got thus far, the only conclusion possible is that the film should be read again, more slowly, or with some better measuring technique. The method of analysing the results described has revealed an observer bias. However, in some experiments, results of this kind might be useful even though biased since the method of analysis does yield estimates of the two probabilities f_1 and f_2. For instance, neon tube counters (Conversi and Gozzini 1955, Gardener *et al.* 1957) are known to be left in a supersensitive state for some seconds after a discharge has occurred. If during an experiment such a counter were pulsed frequently, the counter would have two probabilities of firing, depending on whether it was in a supersensitive state (following a previous discharge) or in its normal state. Thus an analysis of runs of discharges would show whether the effect was serious in the experiment and, if it was, would enable an estimation of the true probability of discharge to be made.

ACKNOWLEDGMENTS

I am indebted to Dr. B. L. Welch and Mr. G. S. James of the Department of Mathematics, University of Leeds, for a helpful discussion on the final form of this letter.

REFERENCES

CONVERSI, M., and GOZZINI, A., 1955, *Nuovo Cim.*, **2,** 189.

FISHER, R. A., and YATES, F., 1938, *Statistical Tables* (Edinburgh: Oliver and Boyd).

GARDENER, M., KISDNASAMY, S., RÖSSLE, E., and WOLFENDALE, A. W., 1957, *Proc. phys. Soc. Lond.* B, **70,** 687.

The Specific Heats of Gadolinium and Terbium between 0·2°K and 6°K

By N. Kurti and R. S. Safrata†
Clarendon Laboratory, Oxford

[Received June 4, 1958]

The specific heats of most rare earth metals have so far been determined down to 15°K (Griffel *et al.* 1954, 1956, Skochdopole *et al.* 1955, Gerstein *et al.* 1957, Jennings *et al.* 1957) and, in some cases, down to 1·5°K (Parkinson *et al.* 1951). Measurements at lower temperatures seemed to us desirable for two reasons:

(*a*) They might permit a reliable separation of the electronic and spin-wave specific heats,

(*b*) The determination of the hyperfine coupling anomalies might give information about the electronic states in these metals (cf. Heer and Erickson 1957, Arp *et al.* 1957) and about their use for the ferromagnetic nuclear orientation method (Grace *et al.* 1955, 1957, Khutsishvili 1955).

Ingots of gadolinium and of terbium made from Specpure materials and weighing about 20 g each were used in these experiments: we are very grateful to Mr. A. R. Powell, F.R.S., of Johnson, Matthey and Co. for the loan of these samples. The metal ingot, with its heater and carbon resistance thermometer (470 ohm, ½ watt 'Old' Speer resistor, cf. Nicol and Soller 1957) was glued by means of GE 7031 varnish to a crystal of cerium magnesium nitrate weighing 10 g. This assembly was mounted on a thin walled German Silver tube in a damagnetization cryostat, with manganese ammonium sulphate pills serving as thermal shields and getters. Cerium magnesium nitrate is eminently suitable for calorimetry below 1°K since its entropy of magnetization and cooling power is of the same order as that of the more usual cooling agents while its specific heat in zero field is very small (Daniels and Robinson 1953).

Some difficulty was caused by the strong hysteresis heating in the metal when its magnetization dropped appreciably below the saturation value; as a result the specimen actually warmed up as the field was reduced below a few kilogauss during demagnetization. In the case of Gd this difficulty was overcome by carrying out some measurements in a residual external field of 650 G. For Tb, where this heating effect was marked even in high fields, the metal ingot had to be separated geometrically from the cooling salt while remaining in thermal contact with it. The calibration of the thermometer below 1°K, carried out in a separate experiment, was based on the constancy of H/T down to $H=2$ kG during the isentropic demagnetization of cerium magnesium nitrate.

---

† On visit from the Institute of Nuclear Physics, Czechoslovak Academy of Sciences, Prague.

Figure 1 shows the results for Gd. The curve is calculated from the data of Hofmann *et al.* (1956) which, in turn are based on the analysis of the results of Griffel *et al.* (1954). Our experimental results, which are in tolerable agreement with the curve above 4°K, deviate markedly at lower temperatures. The scatter at the higher temperatures cannot be explained by random errors; more experiments are needed to establish whether, as in other rare earth metals, thermal hysteresis is the cause. It is not likely that the excess specific heat is due to oxide or nitride impurities because they would have to be present in a concentration of about 2%, more than ten times the amount one would expect. Since the entropy content of the anomaly, $S/R=0{\cdot}036$, is less than 2% of the total spin entropy $S/R=\ln 8$, and is within the error given by Hofmann *et al.* (1956) for the magnetic entropy computed from experiment, the anomaly could be of magnetic origin. But the possibility of an austenitic transition is not excluded and more accurate measurements of the specific heat and of the temperature dependence of the saturation magnetization would be needed to decide this question.

Fig. 1

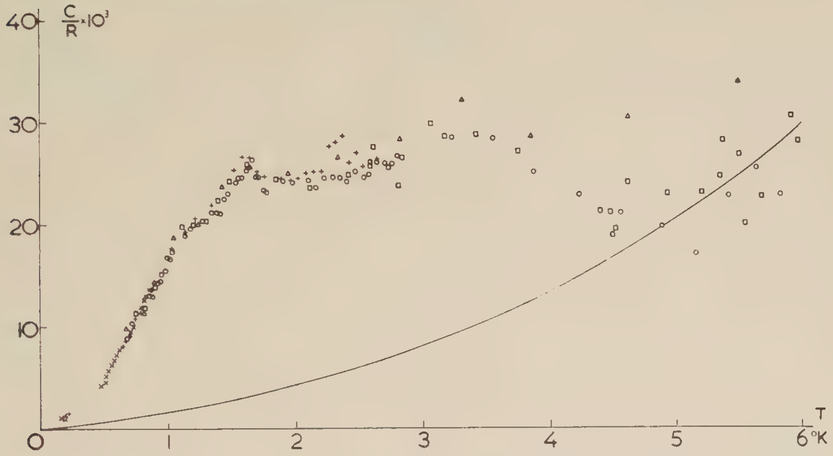

The specific heat of Gd.

○ △ □ Measurements in zero magnetic field.

+ × Measurements in $H=650$ G.

——— $C/R\times 10^3=0{\cdot}8T+0{\cdot}066T^3+0{\cdot}75T^{3/2}$.

There is no anomaly due to hyperfine coupling down to 0·2°K. None would be expected, since the effective field of the 4f electrons at the nucleus should be about the same in the metal as in the salts of Gd^{3+} and in the latter (Low 1956) the nuclear specific heat at 0·2°K would be $C/R\simeq 10^{-5}$

only. An extension of the specific heat measurements to lower temperatures might give information about possible s-electron contribution.

The results for Tb, given in fig 2, show below 1 °K a rapid rise which is likely to be due to hyperfine coupling. The curve represents the sum of the lattice, electronic, spin-wave and nuclear contributions. For the lattice and electronic terms we used the values given by Jennings *et al.* (1957). The spin-wave term was determined from our results between 4 °K and 7 °K, and the nuclear term from our results below 1 °K. The curve fits the experimental data reasonably well except between 1 °K–4 °K where we find an anomaly of the same order and, possibly also of the same origin as in Gd. The nuclear term $CT^2/R = (24 \cdot 8 \pm 1 \cdot 2) \times 10^{-3}$ is slightly smaller than the value $(28 \cdot 2 \pm 0 \cdot 6) \times 10^{-3}$ which paramagnetic resonance measurements by Baker and Bleaney (1955) predict for Tb^{3+} in the ethyl sulphate. Since the electronic moments are fully aligned both in the metal and in the salt, one would expect the same value; the small difference could possibly be accounted for by a slight reduction of the mean value $\langle r^{-3} \rangle$ for the 4f orbits in the metal as compared with the salt. Any s-electron contribution, e.g. by conduction electrons would tend to increase the nuclear term.

Fig. 2

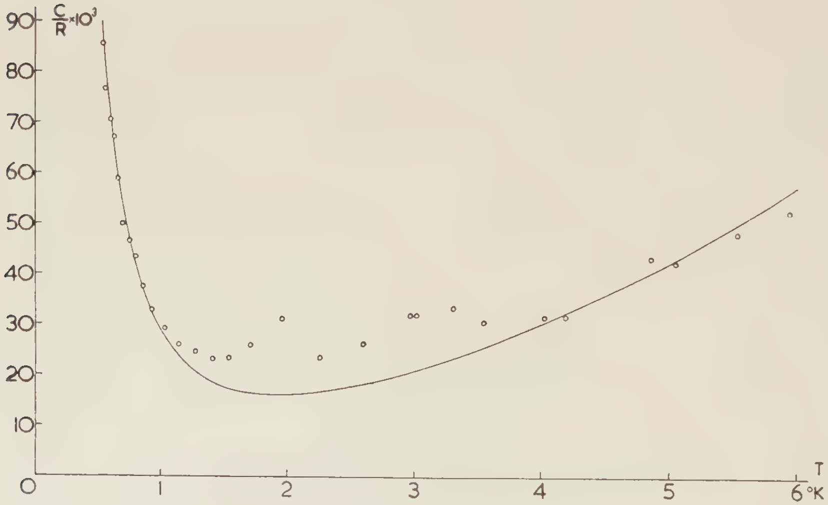

The specific heat of Tb.

——— $C/R \times 10^3 = 25/T^2 + 1 \cdot 2T + 0 \cdot 059T^3 + 2 \cdot 5T^{3/2}$.

Acknowledgments

We are very grateful to Dr. R. J. Elliott for helpful discussions. R. S. S. wishes to thank all concerned for the hospitality extended to him at the Clarendon Laboratory.

References

Arp, V., Kurti, N., and Peterson, R., 1957, *Bull. Amer. phys. Soc.*, **2,** 388.

Baker, J. M., and Bleaney, B., 1955, *Proc. phys. Soc. Lond.* A, **68,** 257.

Daniels, J. M., and Robinson, F. N. H., 1953, *Phil. Mag.*, **44,** 630.

Gerstein, B. C., Griffel, M., Jennings, L. D., Miller, R. E., Skochdopole, R. E., and Spedding, F. H., 1957, *J. chem. Phys.*, **27,** 394.

Grace, M. A., Johnson, C. E., Kurti, N., Scurlock, R. G., and Taylor, R. T., 1955, *Comm. Conf. Basses Temperatures*, p. 263 ; 1957, *Bull. Amer. phys. Soc.*, **2,** 136.

Griffel, M., Skochdopole, R. E., and Spedding, F. H., 1954, *Phys. Rev.*, **93,** 657 ; 1956, *J. chem. Phys.*, **25,** 75.

Heer, C. V., and Erickson, R. A., 1957, *Phys. Rev.*, **108,** 896.

Hofmann, J. A., Paskin, A., Tauer, K. J., and Weiss, R. J., 1956, *J. Phys. Chem. Solids*, **1,** 45.

Jennings, L. D., Stanton, R. M., and Spedding, F. H., 1957, *J. chem. Phys.*, **27,** 909.

Khutsishvili, G. R., 1955, *J. Exptl. Theor. Phys.* (U.S.S.R.), **29,** 894.

Low, W., 1956, *Phys. Rev.*, **103,** 1309.

Nicol, J., and Soller, T., 1957, *Bull. Amer. phys. Soc.*, **2,** 63.

Parkinson, D. H., Simon, F. E., and Spedding, F. H., 1951, *Proc. roy. Soc.* A, **207,** 137.

Skochdopole, R. E., Griffel, M., and Spedding, F. H., 1955, *J. chem. Phys.*, **23,** 2258.

REVIEWS OF BOOKS

Proceedings of the Rehovoth Conference on Nuclear Structure 1957. Edited by H. J. LIPKIN. (Amsterdam: North-Holland Publishing Company.) [Pp. xvi+614.] 45 guilders (90*s*.).

THE value of the formal proceedings of a conference is largely determined by the quality of the review papers and, in this respect, the Rehovoth Conference was well served by a series of contributions which should answer some of the prayers of the non-specialist and clarify the ideas of those more familiar with the subjects under discussion.

The proceedings were devoted equally to nuclear models, electromagnetic effects, parity violation and nuclear spectroscopy experiments and, in the main, they are intelligible and happily free from unnecessary detail. The section on parity violation, which should attract the greatest interest, contains discussions of the theoretical implications and summaries of the confirmatory experimental evidence.

The work is enlivened by the occasional, brief, outstanding description of a special topic—Racah's account of the seniority quantum number springs to mind—and also by the penetrating wit of the humorous Daily Bulletins of the Conference.

In spite of the exceptional speed of publication, the quality of production maintains the high standards of the North-Holland Company. V. J. E.

Surface Chemistry. Theory and Applications. By J. J. BIKERMAN. (Academic Press Inc.) [Pp. x+501.] $15.00

THIS is a second edition of the author's book "Surface Chemistry for Industrial Research" published ten years ago. The author expresses the hope that it will be used for the teaching of surface chemistry in universities as he feels that a unified account of this wide subject is long overdue. The reviewer has found in the book clear and simple accounts of branches of this subject which are perhaps little known to most physicists, such as the principles of foam formation and electro-capillarity. As a book of reference and an introduction to what is known in this wide field of physical chemistry, the book will be very useful indeed. On some subjects, however, it does not go very far or give up to date references. The discussion of surface phenomena and crystal growth, for example, makes no mention of such concepts as dislocations, kink sites and so on, and the section on friction does not mention some of the most recent work. None the less it contains a clearly set out body of information which is not easily available anywhere else. N. F. M.

[The Editors do not hold themselves responsible for the views expressed by their correspondents.]

Fig. 1

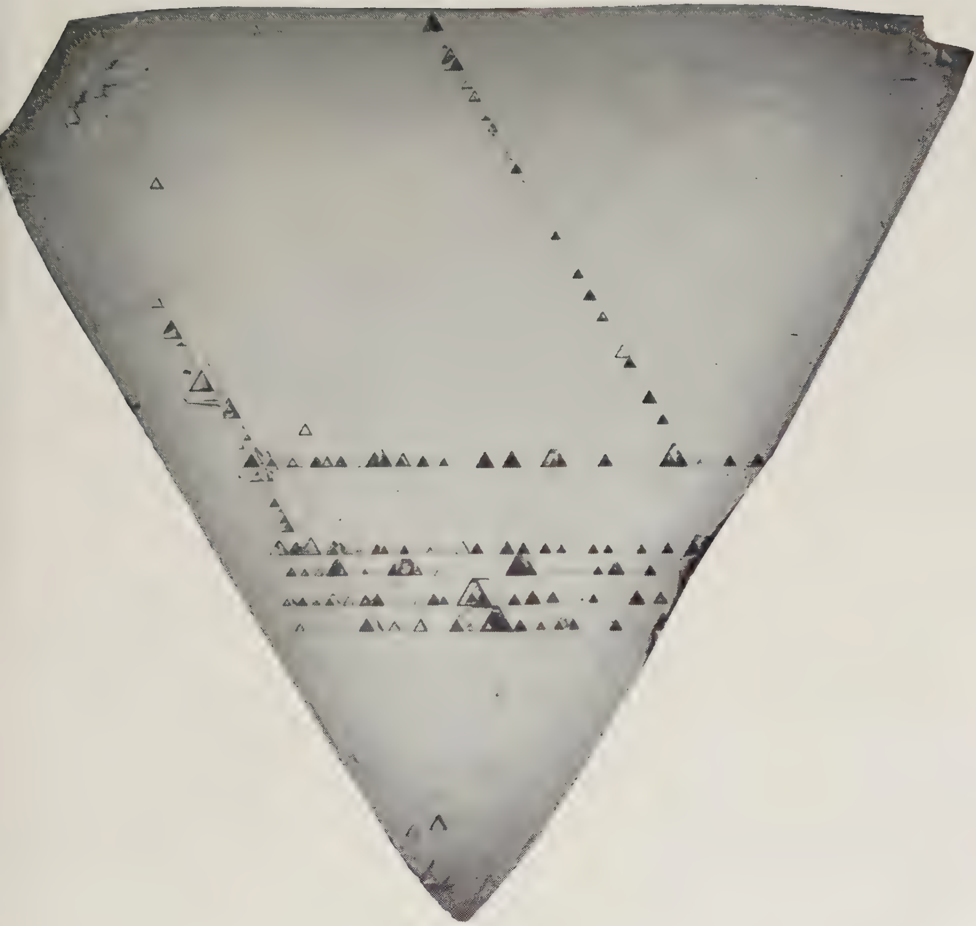

Fig. 2

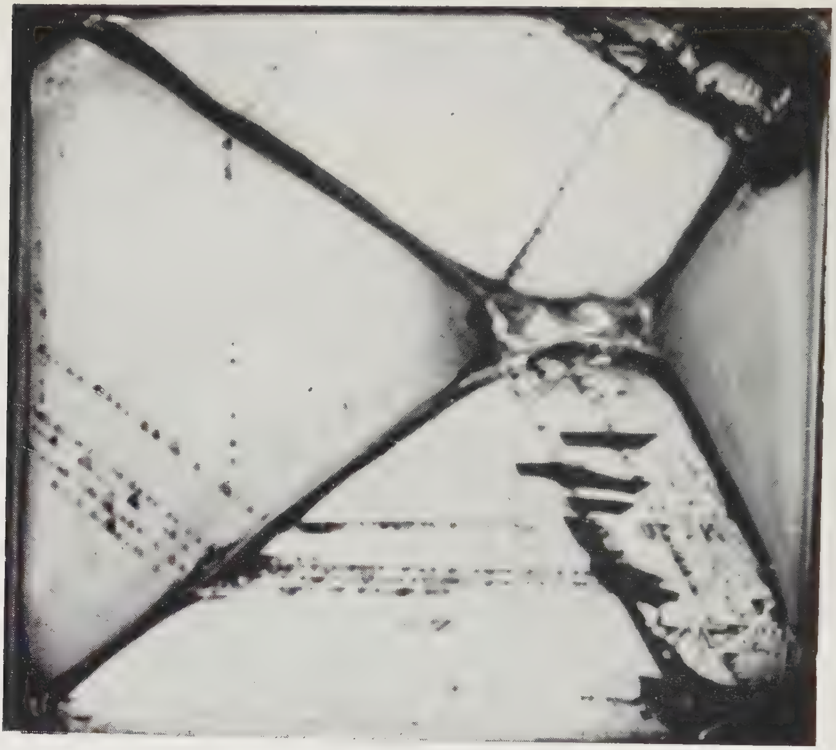

Fig. 3

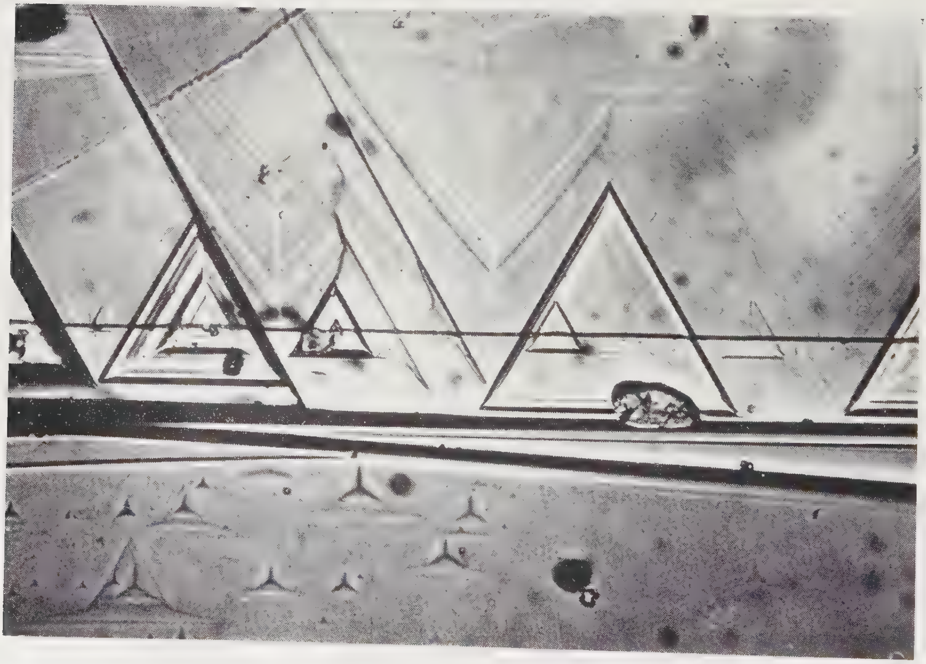

Fig. 4

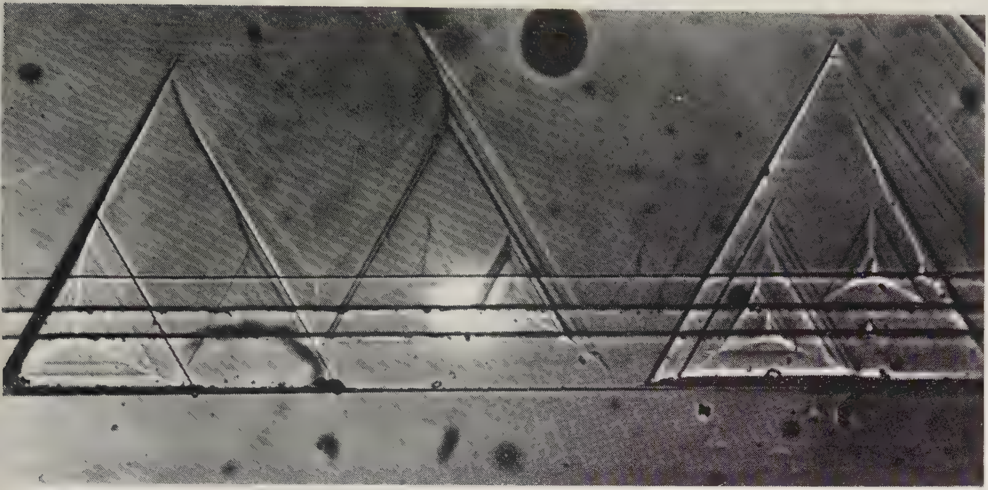

Fig. 5

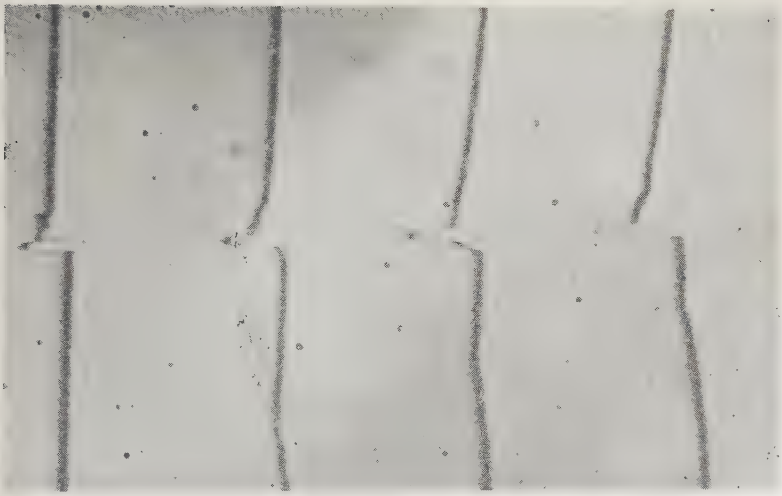

Fig. 6

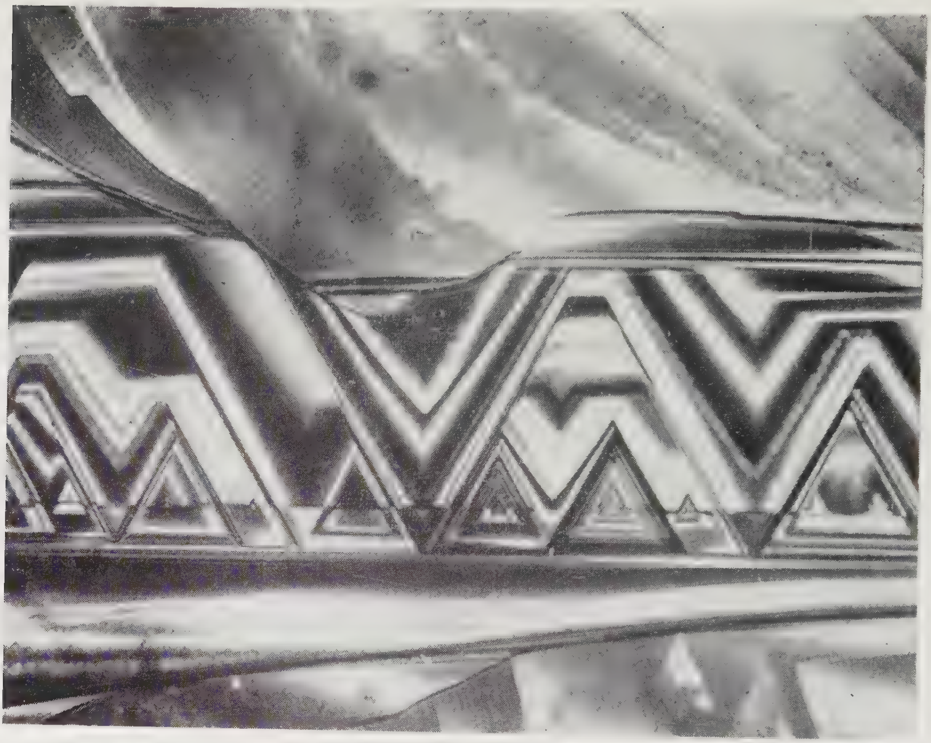

Fig. 7

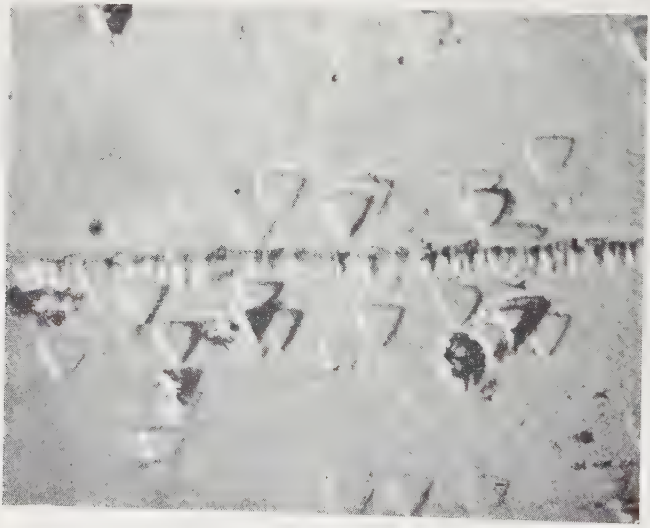

Fig. 8

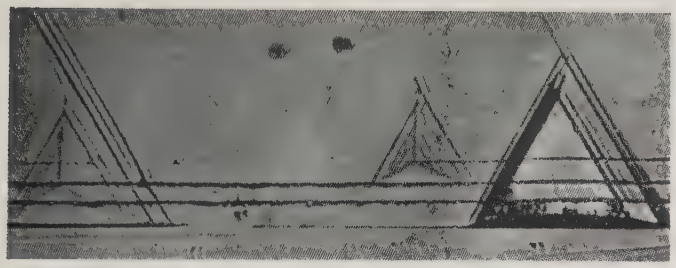

Fig. 9

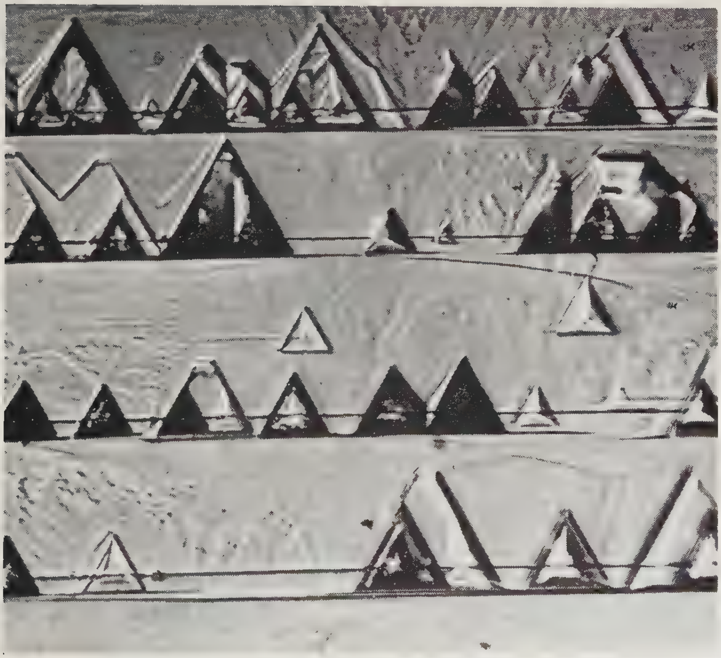

Fig. 2

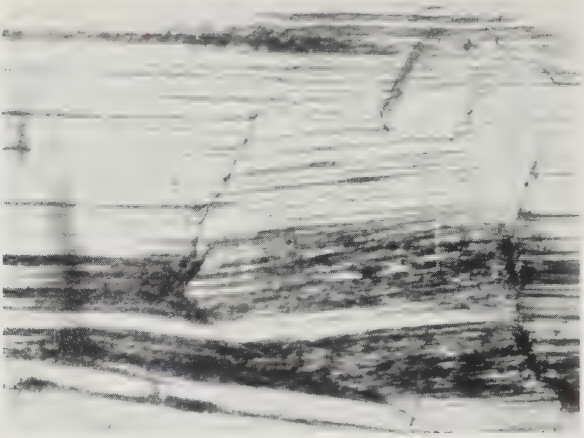

Banding of slip lines, before sectioning. ×200.

Fig. 3

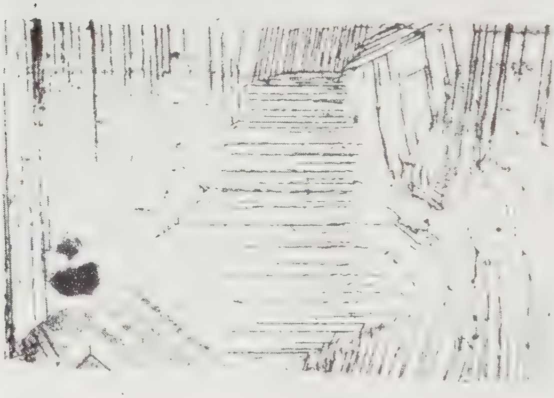

Internal Slip zones, low mag. 11×100.

Fig. 4

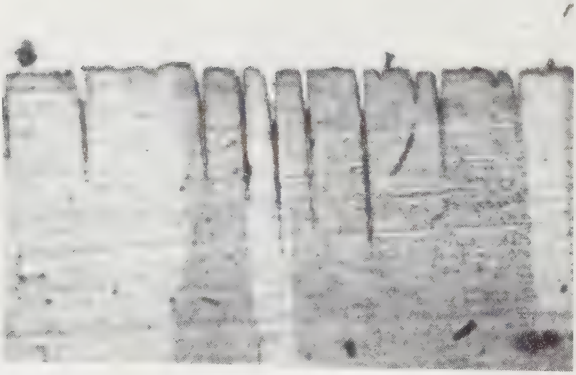

Notch effect, 20×1000.

Fig. 5

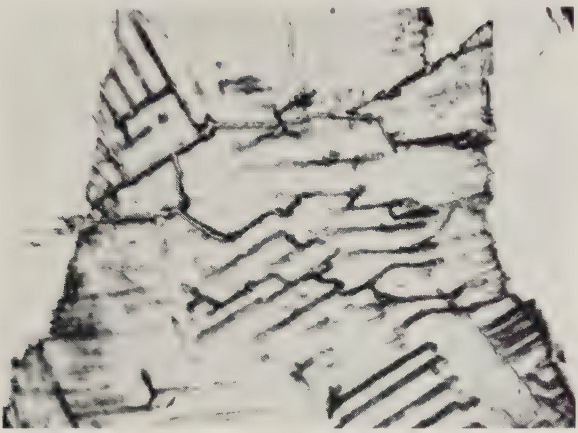

Linking of fissures at fracture stage, tapering section, c. 40 × 500.

Fig. 6

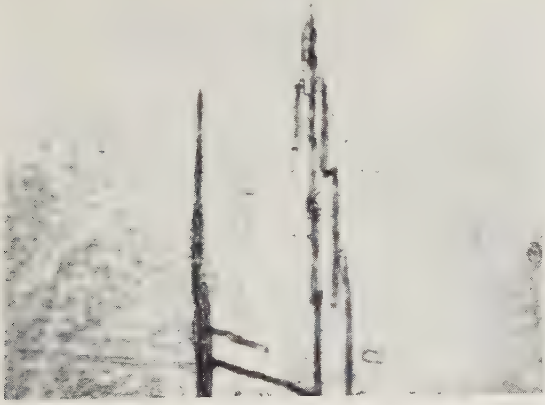

Peak effect, 20 × 500.

Fig. 7

Combined notch and peak effects, 20 × 1000.

Fig. 8

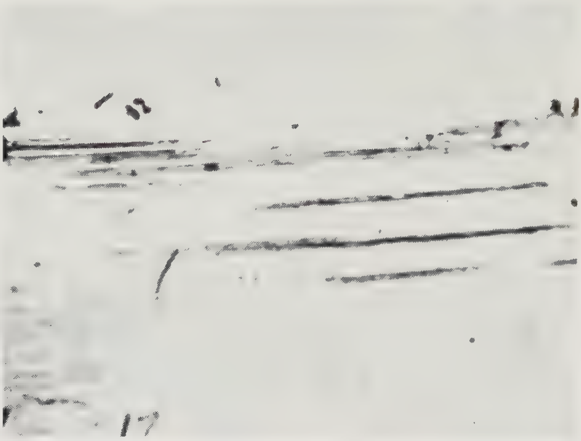

Slip and fissures parallel to surface, 20 × 1000.

Fig. 9

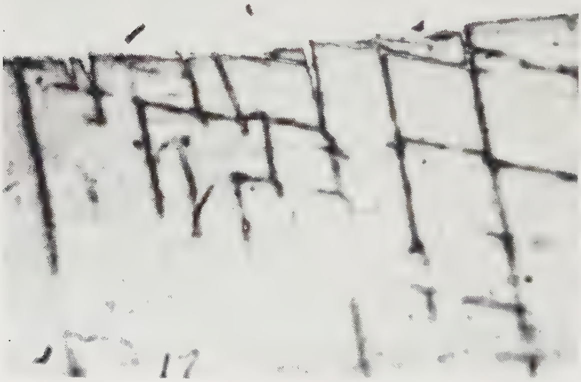

Crossed slip and fissures, 20 × 1000.

Fig. 10

Block movement beginning, 20 × 500.

Fig. 11

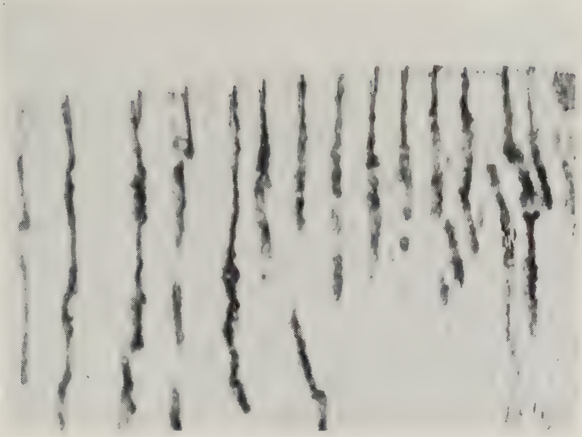

Block movement enhanced, 20 × 500.

Fig. 12

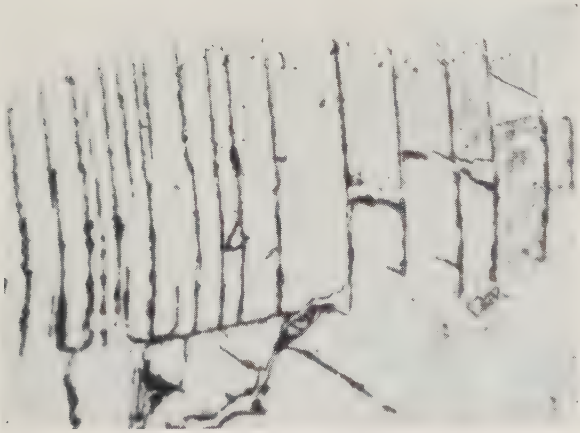

Block movement with disintegration, 20 × 500.

Fig. 13

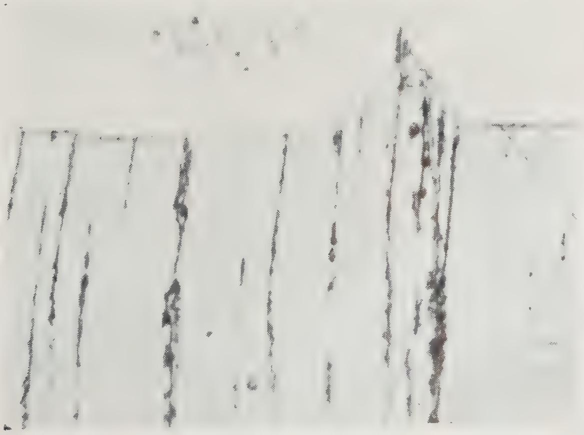

Disintegrating peak, 20 × 500.

Fig. 14

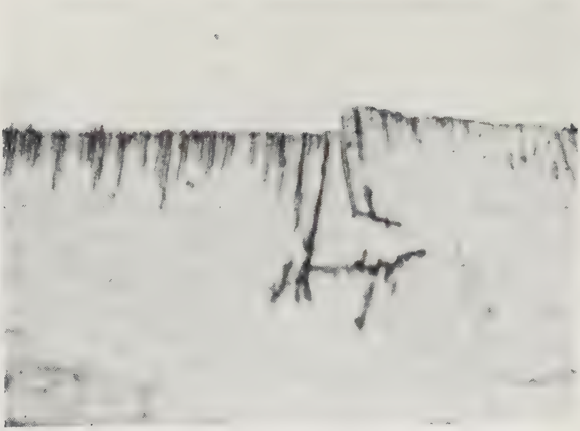

Rearing of grain, 25 × 500.

Fig. 15

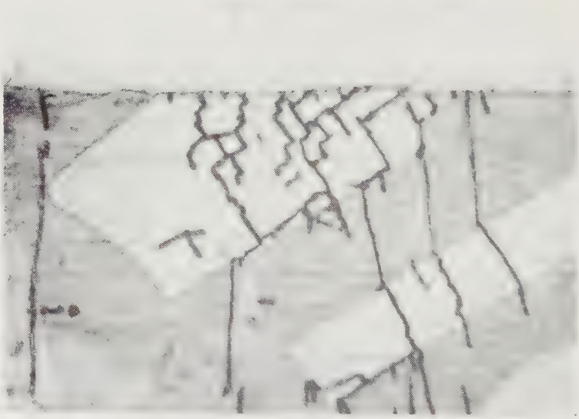

Crazy slip, 25 × 500.

Fig. 16

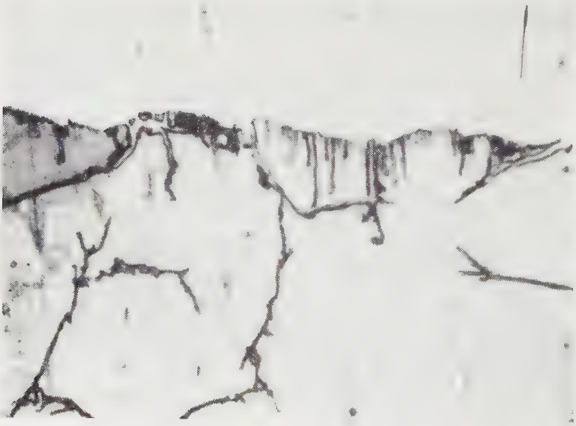

Irregular cracking at large amplitude, 25 × 500.

Fig. 17

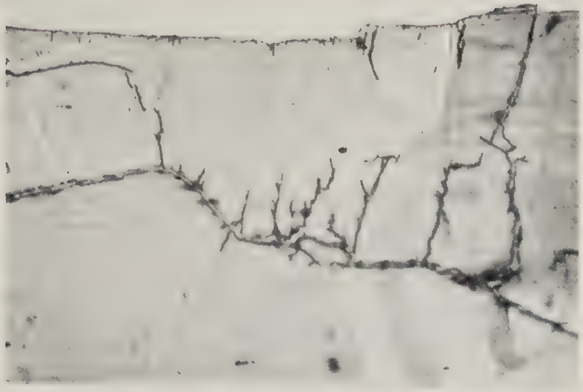

Slip-less cracking at large amplitude, 25 × 500.

Fig. 18

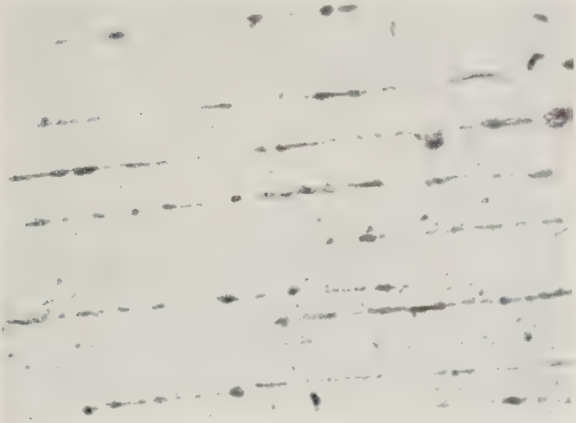

'Balling-up' of slip zones after heating, × 1000.

Fig. 19

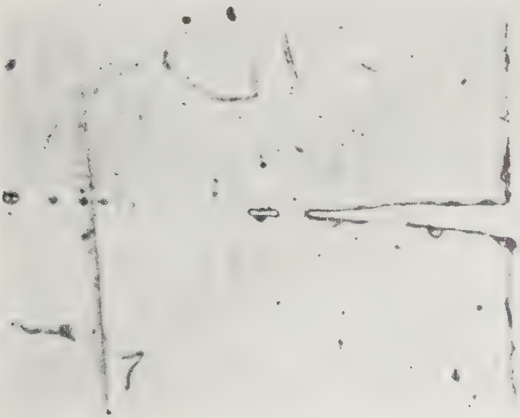

Cavity formation by heating, 20 × 1000.

Fig. 20

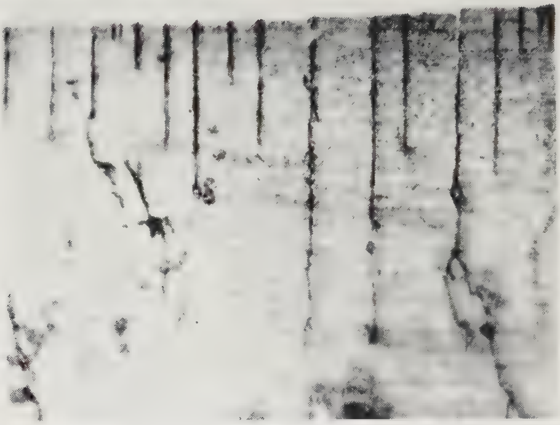

Before and after bending of section, 15 × 500. Slip zones with notch at head open into cracks (which extend into silver plating above).

Fig. 21

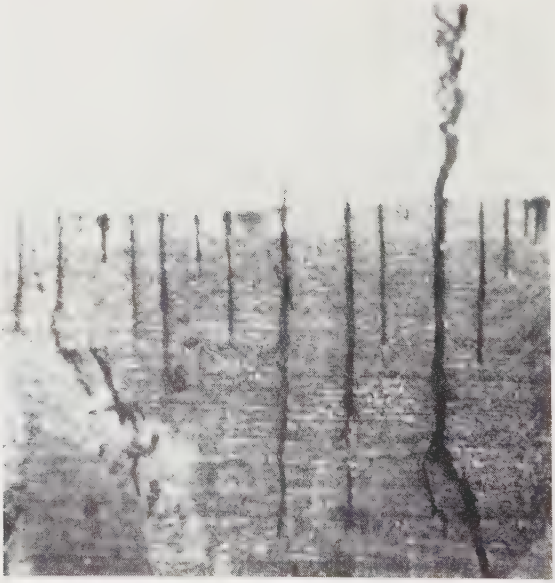

Before and after bending of section, 15 × 500. Slip zones with notch at head open into cracks (which extend into silver plating above).

R. J. STOKES, T. L. JOHNSTON and C. H. LI Phil. Mag. Ser. 8, Vol. 3, Pl. 40.

Fig. 1

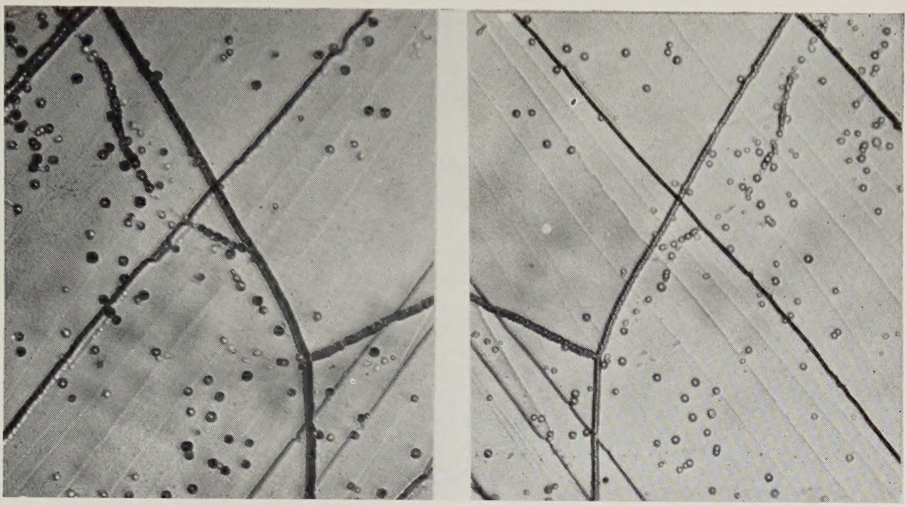

Etch pits on two matching cleavage surfaces (×150).

Fig. 2

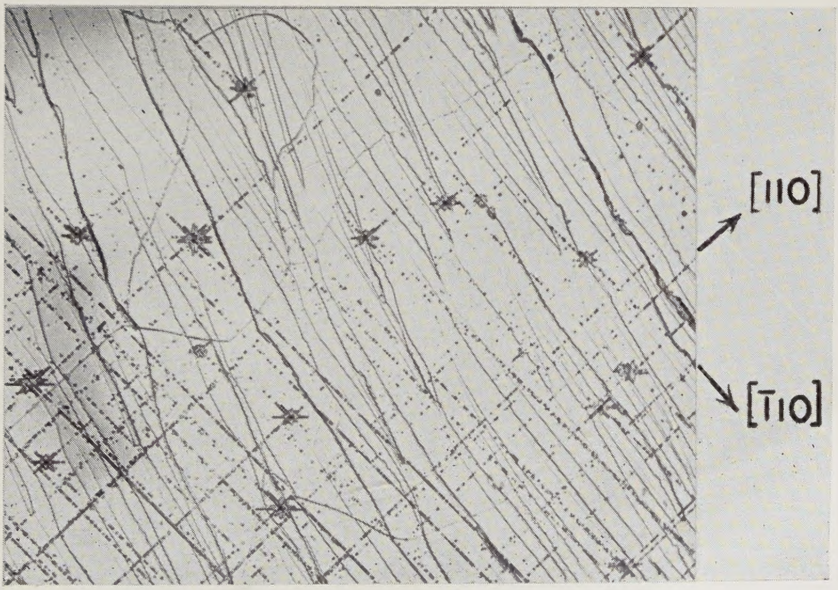

Slip lines originating from ‘ rosettes ’ in a lightly strained magnesium oxide crystal (×50).

Fig. 3

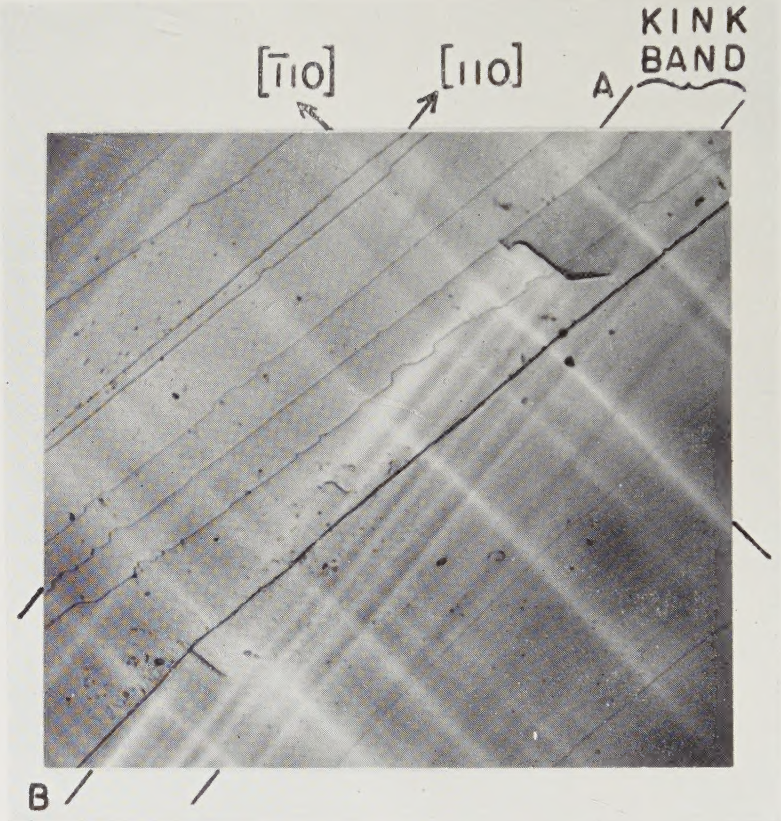

Three secondary cracks lying within a kink band. One tip of each crack is situated along the kink band boundary A–B (polarized illumination ×300).

Fig. 4

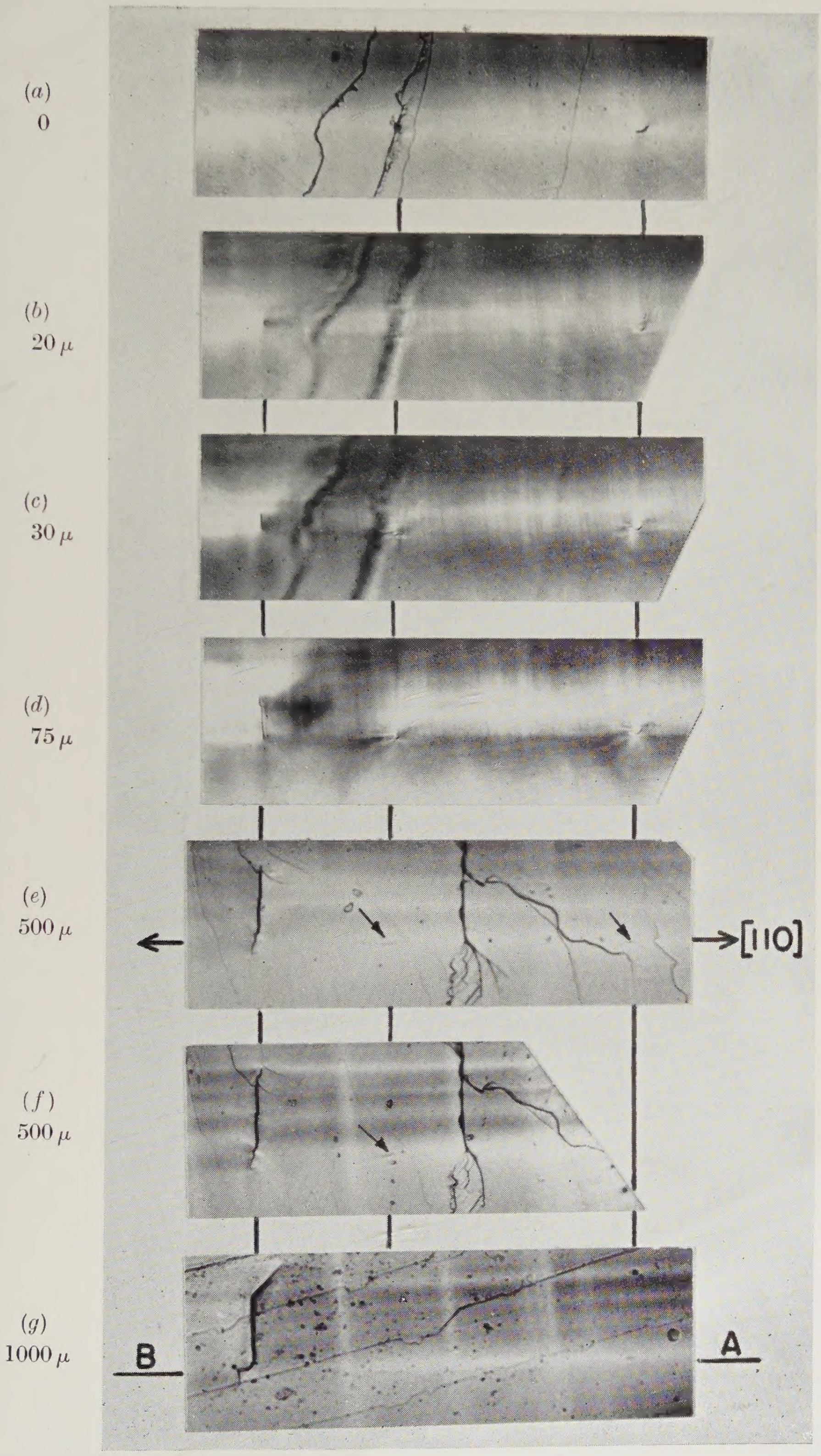

Sequence of photomicrographs taken at different levels beneath the crystal surface. The secondary crack in (*g*) is included in fig. 3 (top, right). Line A–B represents the boundary of the kink band. (*e*) and (*f*) were photographed on internal surfaces cleaved after compression. (*e*) and (*g*) were printed on reversal of the film (polarized illumination ×400).

Fig. 6

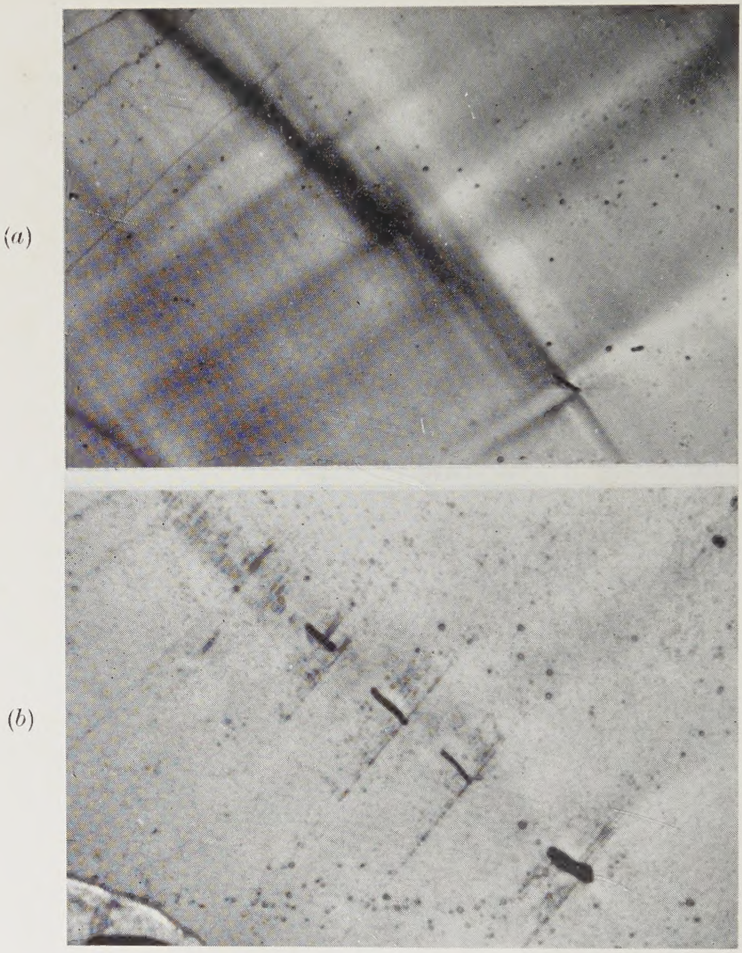

Effect of etching on a kinked region. (*a*) before etching (polarized illumination) : (*b*) after etching (normal illumination ×300).